



D2.1 Characterising Dynamic Multi-Hazard Physical Vulnerability



This project has received funding from the European Union's Horizon Europe research and innovation programme under the grant agreement number 101147385. Views and opinions expressed are however those of the author(s) only and do not necessarily reflect those of the European Union or CINEA. Neither the European Union nor the granting authority can be held responsible for them.

Project Acronym: Minority Report

Project Full Title: Mitigating environmental disruptive events using people-centric predictive digital technologies to improve disaster and climate resilience

Grant Agreement: 101147385

Project Duration: 42 months (01/06/2024 – 30/11/2027)

DELIVERABLE 2.1

Methodology for Characterising Dynamic Multi-Hazard Physical Vulnerability

Work Package: WP2 Risk Assessment, Quantification and Mitigation

Task: T2.1: Characterising Dynamic Multi-Hazard Physical Vulnerability

Document Status: v0.1

File Name: MinorityReport_D2.1_v0.1

Due Date: 31-11-2025 (M18)

Submission Date: 28-11-2025

Lead Beneficiary: UCL

Dissemination Level

Public ☒

Confidential, only for members of the Consortium (including the Commission Services) ☐

Authors List

Leading Author			
First Name	Last Name	Beneficiary	Contact e-mail
Diego	Valdivieso Cascante	UCL	d.cascante@ucl.ac.uk
Co-Authors(s)			
First Name	Last Name	Beneficiary	Contact e-mail
Carmine	Galasso	UCL	c.galasso@ucl.ac.uk
Logan	Brunner	UI	logan.brunner@urbanintelligence.co.nz
Barry	Evans	UoC	barry.evans@canterbury.ac.nz
Lea	Dasallas	UoC	lea.dasallas@canterbury.ac.nz
Theuns	Henning	UoA	t.henning@auckland.ac.nz
Garyfallia	Liappi	UPAT	garyfallia.liappi@upatras.gr
George	Kosmopoulos	UPAT	giokosmopoulos@gmail.com
Polychronis	Economou	UPAT	peconom@upatras.gr

Reviewers List

Reviewers			
First Name	Last Name	Beneficiary	Contact e-mail
Giulia	Barbano	IESRD	giulia.barbano@iesve.com
Luca	Bianconi	STAM	l.bianconi@stamtech.com
Amilcare	Paoletta	LASIA	amilcare.paoletta@lasia.it

Version History

v	Author	Date	Brief Description
0.1	Diego Valdivieso Cascante, Carmine Galasso	10-11-2025	Initial version
0.2	Diego Valdivieso Cascante, Carmine Galasso, Logan Brunner, Barry Evans, Lea Dasallas, Theuns Henning, Garyfallia Liappi, George Kosmopoulos, Polychronis Economou, Luca Bianconi, Amilcare Paoletta, Giulia Barbano	21-11-2025	Complemented by partners and reviewers

1.0	Diego Valdivieso Cascante, Carmine Galasso	25-11-2025	Internally reviewed

Legal Disclaimer

The Minority Report project has received funding from the European Union's Horizon Innovation Action programme under grant agreement No 101147385. The sole responsibility for the content of this publication lies with the authors. It does not necessarily reflect the opinion of the European Climate, Infrastructure and Environment Executive Agency (CINEA) or the European Commission (EC). CINEA or the EC are not responsible for any use that may be made of the information contained therein.

Copyright

Copies of this publication – also of extracts thereof – may only be made with reference to the publisher.

Executive Summary

This deliverable D2.1 presents the methodologies developed under WP2 Task 2.1 for characterising dynamic multi-hazard physical vulnerability of the built environment in support of people centric risk reduction. It introduces a general taxonomy that integrates physical and social dimensions and defines clear processes for scoring, selecting and developing impact models across hazards and geographies. A harmonised asset taxonomy is adopted building on the universal taxonomy for natural hazard and climate risk and resilience assessments from ARUP and the exposure taxonomy maintained by the Global Earthquake Model (GEM). Fourteen attributes such as material lateral load resisting system, height, date of construction or retrofit status, occupancy, structural irregularity, exterior walls, roof and floor systems, and ground floor hydrodynamics enable consistent multi-hazard description and linkage to global fragility and vulnerability repositories, and each asset receives a unique taxonomy string to support interoperability and model selection.

The report then applies these methods in three pilot contexts. In Dublin (Ringsend), Ireland, although timber construction is not yet widespread, its role in sustainable housing and low-carbon development is expected to expand significantly in the coming years. Including a flood vulnerability analysis for timber buildings therefore provides a forward-looking perspective that anticipates future risks and helps embed resilience in emerging construction practices—aligning with climate adaptation priorities, supporting policy compliance, and strengthening the long-term sustainability of Dublin’s built environment. A physics-informed component-based flood performance framework is implemented for timber housing aligned with state-of-the-art international flood load procedures. Fragility is quantified with depth, velocity, and duration as intensity measures. Key findings include low baseline capacity at inundation onset, strong uplift driven float risk and large benefits from targeted mitigation such as strengthening hold-downs and shear wall connections to foundations. Median depths at which continued occupancy and collapse prevention are achieved increase markedly with mitigation though delayed water ingress requires parallel hold-down upgrades to avoid buoyancy amplification. Time dependence is critical because before equalisation depth dominates while after equalisation hydrodynamics matter and velocity can either reduce risk through earlier breach and equalisation or increase it at higher values. Information fidelity studies identify priorities for model accuracy.

In Patras Greece seven representative archetypes are classified using the GEM exposure taxonomy and matched to fragility and vulnerability models through the OpenVulnerability web tool, which ensures consistency between exposure data and selected functions and enables staged multi-hazard modelling that begins with seismic effects and then adds flood effects, thus supporting dynamic multi-hazard vulnerability functions in the WP2. Beyond individual buildings, the Patras pilot also serves as a testbed for system-level analysis: taxonomy-based exposure data for critical services are coupled with a system-dynamics framework to explore how earthquakes, floods, and compound events affect the performance and recovery of interdependent urban infrastructures such as electricity, water supply, digital communications, and key road links.

In Wellington New Zealand flood and wildfire hazards are modelled using the InfoWorks Integrated Catchment Model and the Inferno wildfire model to produce time series hazard maps such as depth and radiant heat flux, which support assessment of mitigation and adaptation at both catchment and property levels including probabilistic ignition estimation based on radiant heat flux. A suite of vulnerability curves drawn from established literature is used to represent different asset classes: residential, commercial, industrial, and institutional buildings, as well as roads and electrical substations. For assets with sufficient attribute data, the closest curve is selected to reflect their construction and use; where information is limited, a range of applicable curves is propagated and the upper bound of damage is used to highlight worst-case impacts.

Across the pilots this report demonstrates a consistent workflow that includes: taxonomy-based asset characterisation, structured scoring and selection of vulnerability/fragility models and targeted model development where gaps exist, laying the foundation for integrated performance-based risk

assessment and prioritised component level mitigation strategies that can be adapted to local data fidelity and stakeholder needs.

Table of Contents

1	Introduction.....	17
1.1	Background.....	17
1.2	Scope and objectives of the deliverable	17
1.3	Structure of the deliverable	18
2	Dynamic Multi-Hazard Physical Vulnerability	19
2.1	Social-Physical Multi-Hazard Vulnerability Taxonomy	19
2.1.1	Introduction	19
2.1.2	Taxonomy description	19
2.2	Scoring, selecting, and developing physical impact models for multi-hazard risk assessment.	31
2.2.1	Introduction and motivation	31
2.2.2	Overview of physical impact models for natural hazards	32
2.2.3	Proposed characterization procedure for physical impact models.....	40
2.2.4	Conclusions	51
2.3	Methodologies of impact and risk models employed in this work.	52
2.3.1	Dublin, Ireland	54
2.3.2	Patras, Greece	65
2.3.3	Wellington, New Zealand	78
3	Physical vulnerability modelling	82
3.1	Dublin, Ireland: Performance-based flood engineering for timber buildings: evaluating structural vulnerability and mitigation strategies.	83
3.1.1	Introduction.....	83
3.1.2	Flood performance assessment	84
3.1.3	Probabilistic Performance Assessment	86
3.1.4	Case study.....	87
3.1.5	Assessing the impact of information fidelity on fragility response	90
3.1.6	Results	92
3.1.7	Conclusions.....	100
3.2	Patras, Greece.....	101
3.2.1	Theoretical background.....	101
3.2.2	Critical infrastructure modelling.....	102
3.2.3	Methodology	102
3.2.4	Simulation and impact analysis	105
3.2.5	Conclusions.....	114

3.3	Wellington, New Zealand	115
3.3.1	Introduction	115
3.3.2	Flood Model.....	115
3.3.3	Wildfire Model.....	119
3.3.4	Conclusions.....	122
4	Conclusions.....	123
5	References.....	123

List of Figures

Figure 1 Proposed Taxonomy for Multi-Hazard, Multi-Resolution Risk Analysis of Communities.	20
Figure 2 Example of result by class.....	23
Figure 3: Example a) vector-valued; b) and state-dependent dual-hazard fragility models. IM: intensity measure; DS: damage state; S: state; H: hazard.	35
Figure 4 Availability of quantitative multi (dual)-hazard physical impact models. Each mark indicates that the literature includes at least one (building or bridge) physical impact model for the considered dual-hazard combination.	39
Figure 5 Proposed methodology to score and select physical impact models for a given asset class.....	41
Figure 9 Ged4ALL attributes for describing buildings (taken from Silva et al., 2022).	54
Figure 10 Ringsend suburb, as defined by the community.....	55
Figure 11 Histograms of attributes for single-family (left) and multi-family (right) residential buildings in Ringsend.....	56
Figure 12 Proposed candidate vulnerability model (based on Huizinga et al., 2011)	64
Figure 13 Patras Pilot Site. The red shaded area represents the borders of the examined site. 66	
Figure 14 Fragility/vulnerability curves for Archetypes a-g.	77
Figure 15. Hazard model domains for Wellington case study.....	78
Figure 16. Sample vulnerability curves used in the Wellington pilot.....	82
Figure 17 Timber house typology: (a) First story plan layout and (b) Representative elevation view of a two-story house.	87
Figure 18 Impact of mitigation measures on the fragility response of archetype light-frame timber houses: (a) one-story baseline, (b) two-story baseline, (c) one-story fully mitigated, and (d) two-story fully mitigated.....	93
Figure 19 Impact of mitigation measures on the fragility response of archetype light-frame timber houses: (a) three-story baseline, (b) four-story baseline, (c) three-story fully mitigated, and (d) four-story fully mitigated.	94
Figure 20 Evaluation of the impact of IMs on the Continued Occupancy performance level response: (a) one-story baseline; (b) four-story baseline; (c) one-story fully mitigated; (d) four-story fully mitigated at the onset of the flood event.....	95

Figure 21 Evaluation of the impact of IMs on the Collapse Prevention performance level response: (a) one-story baseline; (b) four-story baseline; (c) one-story fully mitigated; (d) four-story fully mitigated after water get inside the structure.....	96
Figure 22 Parametric sensitivity of failure probability for the baseline archetype as a function of information fidelity (grouped as in Table 29) at the onset of a flood event with depth 1.0 m and velocity 0.0 m/s: Continued Occupancy, a) one story and b) four story; Collapse Prevention, c) one story and d) four story.....	97
Figure 23 Parametric sensitivity of failure probability for the fully mitigated archetype as a function of information fidelity (grouped as in Table 29) at the onset of a flood event with depth 1.0 m and velocity 0.0 m/s: Continued Occupancy, a) one story and b) four story; Collapse Prevention, c) one story and d) four story.	98
Figure 24 Parametric sensitivity of failure probability for the fully mitigated archetype as a function of information fidelity grouped as in Table 29, evaluated at the Collapse Prevention level for a flood with depth 1.5 m and velocity 0.5 m/s, two minutes after onset: (a) one story, (b) four story.	98
Figure 25 Assessment of the influence of the assumed response distribution on performance levels for the one-story baseline case: (a) as a function of water depth with velocity set to 0.0 m per second, and (b) as a function of flow velocity at a fixed water depth of 0.60 m, both at the onset of the flood event.....	99
Figure 26 Evaluation of the effect of flood water mixture on the Collapse Prevention performance level two minutes after the start of the event for the four story fully mitigated archetype: (a) lightly sedimented hyper concentrated flows; (b) moderately sedimented hyper concentrated flows; (c) moderately sedimented hyper concentrated flows; (d) debris flow like mixtures with very high sediment content.....	100
Figure 27 Integrated building blocks, developed by Canzani (2016).	105
Figure 28 Causal links across CIs.....	105
Figure 29 Scenario 1 - running operations.....	108
Figure 30 Scenario 1 - service levels.....	109
Figure 31 Scenario 2 - running operations.....	109
Figure 32 Scenario 2 - service levels.	110
Figure 33 Scenario 3 - running operations.....	110
Figure 34 Scenario 3 - service levels.	111
Figure 35 Scenario 4 - running operations.....	111
Figure 36 Scenario 4 - service levels.	112

Figure 37 Scenario 5 - running operations.....	112
Figure 38 Scenario 5- Service levels.....	112
Figure 39 Recovery Time (Running Operations) per Critical Infrastructure under Energy disruption scenarios.	113
Figure 40 Recovery Time (Running Operations) per Critical Infrastructure under Energy disruption scenarios.	113
Figure 41. Rainfall profile with historical and climate projected rainfall intensities for Wellington City.....	117
Figure 42. Coastal tide fluctuations with climate projected sea level rise projection for Wellington City.....	117
Figure 43 Infoworks ICM stormwater network and building void data	118
Figure 44 Sample flood depth output using Infoworks ICM	119
Figure 45 Example scenario of 6-hour wildfire spread and corresponding RHF values experienced at the property level.	121
Figure 46 Example fragility curve derived from First Street Foundation (2023)	122
Figure 47 Example application of fragility curve to define ignition probability based off max RHF values.	122

List of Tables

Table 1 Definition of the resolution and typical scale.....	22
Table 2 Physical Vulnerability Taxonomy	24
Table 3 Data needs per risk	29
Table 4 GED4ALL attributes for buildings exposed to different hazards. OSM: OpenStreetMap; R: required; O: optional; EQ: earthquake; FL: flood; DF: debris flow; TS: tsunami; LA: landslide; FI: Fire; WI: wind; VA: volcanic ash.	42
Table 5 GED4ALL attributes for bridges exposed to different hazards. Notation as per Table 4. 43	
Table 6 Model screening criteria: minimum thresholds for acceptance [<i>Nds</i> , <i>Rim</i> , <i>Nhp</i> are defined by the user; example values: <i>Nds</i> =1, <i>Rim</i> =20, <i>Nhp</i> =80]	44
Table 7 Model scoring system: definition of scores for each attribute. [<i>ATT</i> , <i>OBS1</i> , <i>OBS2</i> , <i>OBS3</i> , <i>bins1</i> , <i>bins2</i> , <i>obs1</i> are defined by the user; example values: <i>ATT</i> =4, <i>OBS1</i> =20, <i>OBS2</i> =200, <i>OBS3</i> =20, <i>bins1</i> =5, <i>bins2</i> =10, <i>obs1</i> =20]	47
Table 10 Ringsend Building inventory statistics.....	55
Table 11 Materials by building type in Ringsend (based on IWU, 2011).....	56
Table 12 Single-family building types used in this study for Ringsend.....	57
Table 13 Multi-family building types used in this study for Ringsend.....	61
Table 14 GED4ALL Taxonomy for buildings in Ringsend	62
Table 15 Candidate vulnerability model (based on Huizinga et al., 2011)	64
Table 16 Average replacement cost (based on Yepes-Estrada et al., 2023)	65
Table 17 GED4ALL Building Taxonomy for Archetype A	67
Table 18 GED4ALL Building Taxonomy for Archetype B.....	68
Table 19 GED4ALL Building Taxonomy for Archetype C.....	69
Table 20 GED4ALL Building Taxonomy for Archetype D	70
Table 21 GED4ALL Building Taxonomy for Archetype E.....	72
Table 22 GED4ALL Building Taxonomy for Archetype F.....	73
Table 23 GED4ALL Building Taxonomy for Archetype G	74
Table 24 Selected Fragility/Vulnerability Models for the Patras Pilot Site Archetypes.....	76

Table 25. Approximate asset counts within Wellington study region.....	79
Table 26. List of vulnerability curves used for each asset and their sources.	80
Table 27 Parameter values defining the assumed load model as per ASCE (2022)	85
Table 28 Parameter values defining component capacities for the Baseline case.	87
Table 29 Typology matrix	89
Table 30 Variable groups for the information fidelity sensitivity analysis	90
Table 31 Representative flood scenarios used in the sensitivity analysis.	91
Table 32 Six-point scale used to rate direct dependencies.....	106
Table 33 Results of the survey.....	106
Table 34. Input data and data source for the Wellington case study flood simulation.....	116
Table 35 Example parameters for defining RoS (Pearce 2005).....	120
Table 36 Example parameters for defining FL (Pearce 2005)	120

List of Acronyms and Abbreviations

Term	Description
AHP	Analytic Hierarchy Process
ASCE	American Society of Civil Engineers
ATC	Applied Technology Council
BUI	Build Up Index
CAPRA	Comprehensive Approach to Probabilistic Risk Assessment (CAPRA) platform
CDF	Cumulative Distribution Function
CI	Critical Infrastructure
CO	Continued Occupancy
CP	Collapse Prevention
CSA	Critical Street Arteries
DF	Debris Flow
DS	Damage State
DS1	Damage State 1 – slight damage
DS2	Damage State 2 – moderate damage
DS3	Damage State 3 – extensive damage
DS4	Damage State 4 – complete damage
EDP	Engineering Demand Parameter
EN	Electricity Network
EQ	Earthquake
ESRM20	European Seismic Risk Model 2020
FEMA	Federal Emergency Management Agency
FI	Fire
FL	Fuel Load
FL	Flood
GCRF	Global Challenges Research Fund
GED4ALL	Global Exposure Database for All (multi-hazard exposure taxonomy)

GEM	Global Earthquake Model
GIS	Geographic Information System
HAZUS	HAZUS Multi-Hazard loss-estimation methodology (FEMA)
HFI	Head Fire Intensity
ICT	Information and Communication Technologies
IM	Intensity Measure
INSYDE	IN-depth SYnthetic model for flood Damage Estimation
ISI	Initial Spread Index
JRC	Joint Research Centre (of the European Commission)
LA	Landslide
LC	Low-Code seismic design level
LLRS	Lateral Load-Resisting System
MC	Moderate-Code seismic design level
NRML	Natural Hazard Risk Markup Language
OSM	OpenStreetMap
PAGER-STR	Prompt Assessment of Global Earthquakes for Response – Structural module
RC	Reinforced Concrete
RoS	Rate of Spread
SD	System Dynamics
SIRS	Susceptible–Infectious–Recovered–Susceptible
SYNER-G	European SYNER-G project on systemic seismic vulnerability and risk
TOPSIS	Technique for Order Preference by Similarity to Ideal Solution
TS	Tsunami
UKRI	UK Research and Innovation
UNDRR	United Nations Office for Disaster Risk Reduction
VA	Volcanic Ash
WI	Wind
WSN	Water Supply Network

1 Introduction

1.1 Background

This deliverable presents the methodologies and approaches developed under Working Package (WP) 2 to assess, quantify, and mitigate multi-hazard risks. While it incorporates the physical dimension of vulnerability, it also establishes a general taxonomy that integrates both physical and social dimensions. This comprehensive approach ensures alignment with the project's overarching goal of strengthening disaster and climate resilience for communities.

1.2 Scope and objectives of the deliverable

Task (T) 2.1 will provide models for assessing hazard-induced physical (structural and non-structural) damage arising from climate change and the occurrence of natural disasters in evolving built environments. It will be executed in two related tasks: the first will focus on the vulnerabilities of buildings, and the second on the networks and infrastructure that allow urban environments to function.

T2.1.1: Characterising the Fragility & Vulnerability of Buildings

This sub-task will focus on the development of a robust methodology to allow stakeholders to quantify the fragility and vulnerability of their buildings, allowing them to identify the most significant hazard, be it through climate change and adaptation to the occurrence of hazardous events. The procedure that will be used to develop this methodology will involve:

- Grouping buildings into classes according to specific pertinent characteristics (e.g., geometric parameters, occupancy), including any potential dynamic alterations (e.g., due to corrosion, structural retrofitting, etc).
- Extracting relevant candidate models from interactive databases, model compendia, and literature reviews.
- Scoring the candidates according to a set of criteria (that account for relevance, statistical refinement, and model quality, for instance) to determine the most appropriate ones, identifying key KPIs to be monitored, but kept as geographically agnostic as possible to maximise potential implementation.

T2.1.2: Characterising the Fragility & Vulnerability of Urban Infrastructure

This sub-task will build upon the work of T2.1.1 by extending the analysis of fragility and vulnerability to the meso-scale. The focus will expand from individual buildings to urban infrastructure systems, assessing and quantifying the impacts of climate change and natural disasters on key networks, including Information and Communication Technologies, the Electricity Grid, the Water Supply Network, and Critical Street Arteries. The analysis will also account for the interactions among these systems, to fully capture the indirect consequences of failures within a single network. To achieve this, a series of modular models will be developed to replicate the dynamics of disruptive events such as earthquakes, floods, heatwaves, and fires. Each model will represent a critical infrastructure system, characterized by operational states under shock: functioning operations (running), failed operations (down), and recovered operations (restored over time). Interdependencies between infrastructures will be modelled as a function of the services they are able or unable to provide to one another. These modular building blocks will be iteratively combined and extended to construct a comprehensive System Dynamics (SD) model capable of simulating disruption scenarios in interdependent infrastructures. Based on this modelling framework, multiple damage scenarios will be simulated. The

integrated infrastructure model will capture both proactive absorptive capacity and reactive restorative capacity, while explicitly considering detailed interdependencies among diverse infrastructure components. The outcome of T2.1 will be a formal methodology enabling users to determine the risk profile of their buildings, not only based on their physical characteristics and location but also in relation to the resilience of surrounding urban infrastructure, networks, and systems. This methodology will account for the occurrence of various climate and natural hazard events, as well as the compounding effects of multi-hazard events and the indirect, cascading, and cumulative risks that may arise during disaster response and recovery.

1.3 Structure of the deliverable

- Brief introduction of the topic including background and scope and objectives as set by the proposal.
- Physical dimensions of risk management:
 - Social-Physical Multi-Hazard Vulnerability Taxonomy
 - Scoring, selecting, and developing physical impact models for multi-hazard risk assessment.
 - Methodologies of impact and risk models employed in this work and applications in pilot sites.
 - Physical vulnerability modelling.

2 Dynamic Multi-Hazard Physical Vulnerability

2.1 Social-Physical Multi-Hazard Vulnerability Taxonomy

2.1.1 Introduction

Disaster risk is accelerating worldwide as cities grow, infrastructure becomes more interconnected, climate change shifts hazard patterns, and the built environment ages. Natural hazards rarely act alone; they often coincide or occur in close sequence, creating multi-hazard conditions that strain conventional single hazard assessment approaches (Drakes and Tate, 2022; Lee et al., 2024; Trogrlić et al., 2024). Yet many current assessments still focus on individual hazards or on physical damage and asset loss, offering limited guidance on which methods, spatial resolutions, or decision thresholds are appropriate at each stage of analysis. In response to this gap and the rising complexity of risk, international frameworks including Agenda 21 (UNCED, 1992), the Hyogo Framework for Action (UNISDR, 2005), and the Sendai Framework for Disaster Risk Reduction (UNDRR, 2015) call for integrated multi-hazard risk management as a cornerstone of resilient and sustainable communities.

Multi-hazard interactions can be grouped into two types. Level I interactions are occurrence based and arise from intrinsic relationships between hazards—where one event triggers, modifies, or coincides with another, such as heavy rainfall producing landslides or an earthquake generating a tsunami (Iannacone et al., 2024). Level II interactions are consequence based and emerge through cascading effects on exposed assets and communities. Even independent hazards such as an earthquake and a flood can yield compounded consequences when occurring sequentially, for instance when post-earthquake flooding accelerates structural degradation, impedes recovery, and amplifies economic loss (Zaghi et al., 2016; Nofal et al., 2021b; de Ruiter et al., 2021; Gentile et al., 2022; Ward et al., 2022; Iannacone et al., 2024; Trogrlić et al., 2024).

Traditional probabilistic risk assessment frameworks quantify risk as the convolution of hazard, exposure, and vulnerability (e.g., Krawinkler and Miranda, 2004; Moehle and Deierlein, 2004; Custer and Nishijima, 2015; Englhardt et al., 2019; Cremen et al., 2022; Hogan et al., 2023; Mesta et al., 2023). However, they often treat hazards as independent, overlooking how interactions modify physical and social vulnerability (Gentile et al., 2022; Ward et al., 2022; Trogrlić et al., 2024). As noted by Zaghi et al. (2016), multi-hazard risk cannot be represented by simple aggregation of single hazard results, since interaction effects may disrupt expected repair trajectories, extend recovery timelines, and increase both human and economic losses (Görüm et al., 2025). These challenges highlight the urgent need for a harmonized framework capable of capturing the cumulative and sequential impacts of multiple hazards, including the evolving performance and recovery of the built environment under climate and demographic change.

To address these limitations, we introduce a decision aligned socio-physical taxonomy for multi-hazard, multi resolution community risk assessment. The taxonomy provides a scalable structure that directly maps analytical classes to the risk- and resilience-informed decision questions they support and to the computational tools required to answer them.

2.1.2 Taxonomy description

We build on the Universal Taxonomy for Natural Hazard and Climate Risk and Resilience Assessments (ARUP, 2024) to develop a socio-physical taxonomy for multi-hazard risk modelling. The taxonomy follows a structured, multi-step approach: (1) defines model categories (social people centred, physical-building, and physical-infrastructure); (2) four levels of resolution (Class 0 to 3); (3) specifies a concise template of taxonomy characteristics (question, modelling technique, vulnerability/fragility model selection, data types, resolution or typical scale, model purpose, measures, and example of risk

metrics); and, (4) delineates model categories with specific taxonomy attributes (see example in Table 2 for buildings).

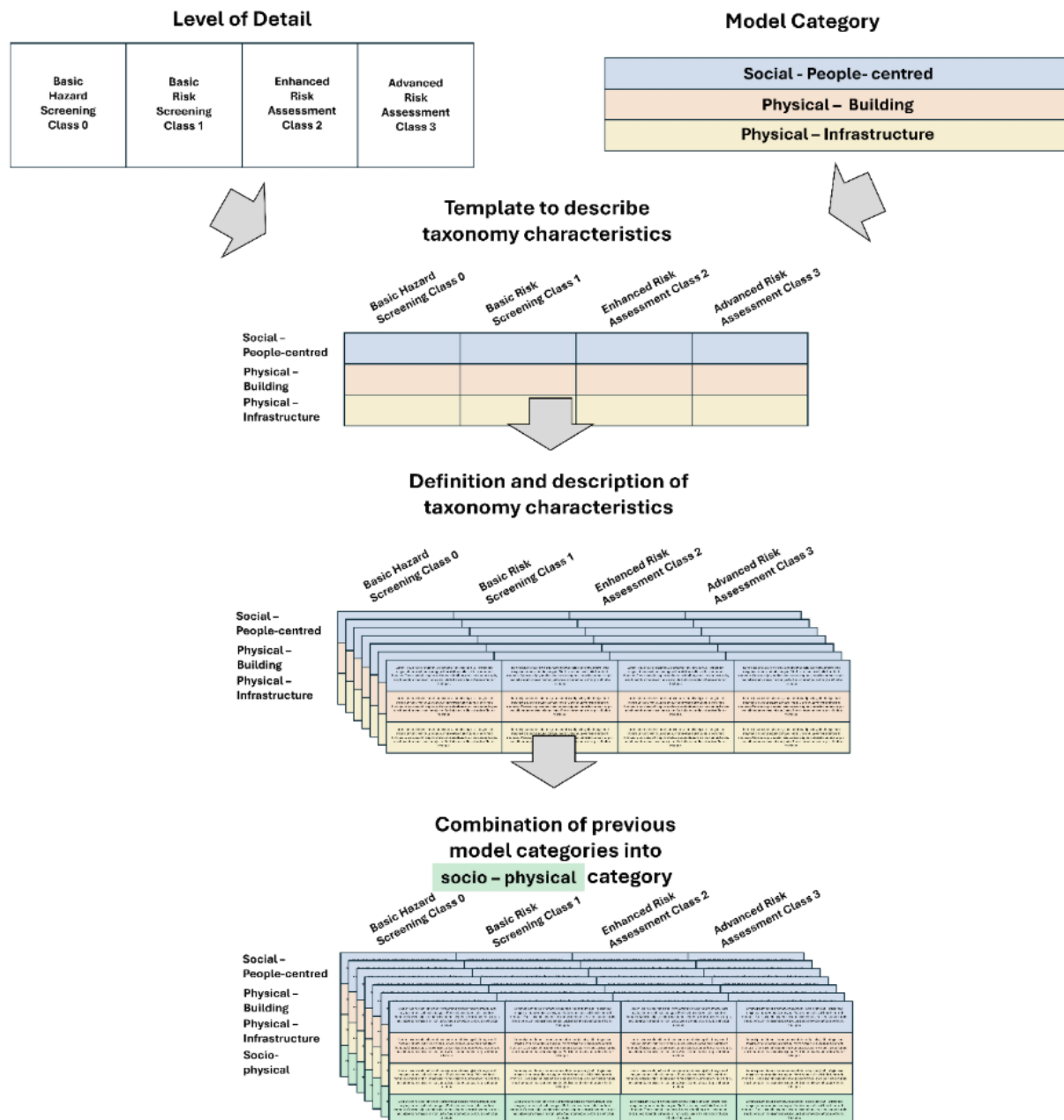


Figure 1 Proposed Taxonomy for Multi-Hazard, Multi-Resolution Risk Analysis of Communities.

Model Categories

The socio physical taxonomy organizes community risk assessment into three interrelated model categories that together represent the full spectrum of factors influencing disaster risk and resilience. Each category captures a distinct dimension of the system (social people centred, physical buildings, and physical infrastructure) while maintaining strong interconnections among them.

Social, people-centred: Represents the human and social dimensions of risk and resilience, focusing on how individuals, households, and communities are exposed to, affected by, and recover from hazards. It includes demographic, socioeconomic, and behavioural attributes that shape vulnerability, adaptive capacity, and functional recovery, such as population distribution, age, income, health,

mobility, access to critical services, and social networks. Further description of the taxonomy for social people centred is available in D2.2.

Physical buildings. Refers to the structural, non-structural, and contents components of the built environment that accommodate people, activities, and assets. This category characterizes buildings by their geometry, materials, load-resisting systems, construction quality, retrofit history, and functional performance under hazard loading. It represents physical vulnerability, fragility, and recovery functions that define potential damage, downtime, and repair trajectories.

Physical infrastructure. Encompasses interconnected lifeline and utility systems, such as transportation, energy, water, communication, and waste networks, that sustain community functioning. It represents the spatial configuration, capacity, redundancy, and interdependencies of these systems, assessing how hazards and cascading failures disrupt essential services and how restoration strategies influence overall community resilience.

Socio-physical. Represents the integrated dimension of people, buildings, and infrastructure within a unified taxonomy. This category links the social aspects of exposure, vulnerability, and adaptive capacity with the physical performance of structures and systems under multiple hazards. It captures how social factors such as population distribution, socioeconomic conditions, and access to services interact with physical characteristics like structural integrity, functionality, and interdependencies of assets. The socio-physical domain supports assessment of cascading impacts, functional recovery, and equity outcomes, providing a holistic basis for resilience informed, community centred decision making. Further description of the taxonomy for the socio physical component will be available in D2.3.

Levels of resolution for physical vulnerability

Class 0 (Risk Pre-screening) Defines where to begin the inquiry by overlaying rapid deterministic or event-based hazard layers with exposure at regional scale.

Class 1 (Basic Risk Screening) identifies which land-use areas warrant deeper analysis through simplified loss estimates at neighbourhood resolution.

Class 2 (Enhanced Risk Assessment) guides preliminary allocation of resilience resources by coupling moderate fidelity building and network loss models with demographic and socioeconomic data at district scales.

Class 3 (Advanced Risk Assessment) informs design or policy interventions that achieve equity and recovery goals by integrating high-resolution physical simulations with fine-scale data at parcel resolution.

Bidirectional information flow ensures high-fidelity insights (i.e., from Class 3) refine initial screening (i.e., Class 0) while coarse methods highlight critical assets (i.e., from Class 0) for detailed modelling (i.e., Class 3). Outputs—functional-recovery targets, outage person-hours, distributional loss metrics, and endangered-population estimates—support transparent evaluation of resilience strategies. This practical, scalable foundation clarifies what is appropriate when and empowers stakeholders to implement cross-scale, equitable, risk-informed resilience enhancements under uncertainty.

Taxonomy characteristics

The socio-physical taxonomy is structured around a set of taxonomy characteristics that define how multi-hazard risk modelling is applied consistently across scales and decision contexts. These characteristics establish a common analytical language, linking each assessment class (from Class 0 to Class 3) with its corresponding purpose, modelling technique, data requirements, and expected outputs. Here we define the taxonomy characteristics:

Question. Refers to the central decision or problem the analysis seeks to answer at each class of resolution. From a socio physical perspective, questions guide the transition from awareness (who and what is exposed) to action (how and where to intervene).

Modelling techniques. Describes the analytical approach and computational methods applied to represent hazard, exposure, vulnerability, and consequence relationships. In a socio physical context, modelling techniques integrate physical processes (e.g., structural response, cascading hazards) with social processes (e.g., mobility, accessibility, recovery behaviour).

Vulnerability and fragility model selection. Defines the procedure for choosing or developing the mathematical relationships that describe how physical systems and social groups respond to hazard intensity. From a socio physical standpoint, this involves not only structural fragility but also social sensitivity and adaptive capacity. We are ensuring that physical damage, service disruption, and human impact are evaluated consistently through a transparent, criteria-based selection process. See section 2.2 Scoring, selecting, and developing physical impact models for multi-hazard risk assessment.

Data types. Specifies the kind, detail, and source of information required to characterize hazards, exposure, vulnerability, and consequences. See Table 3 for physical-building example.

Resolution or typical scale. Defines the spatial and analytical granularity of the assessment. The socio physical taxonomy links scale to decision relevance: from regional or national screening (Class 0) to parcel or household-level modelling (Class 3). The definition of the resolution is provided in Table 1.

Table 1 Definition of the resolution and typical scale

Macro level	Country level; Tag: national	The highest administrative level, representing an entire sovereign state or nation. (millions and more)
	Sub-national level; Tag: state/ province/ region	High administrative divisions within a country, such as states, provinces, or regions. (millions)
Meso level	Large area level; Tag: county / district / municipality	Administrative areas responsible for local governance. (hundreds of thousands)
	Medium area level; Tag: census tract / ward / sub district	Smaller statistical or administrative units used for detailed demographic and socio-economic analysis. (tens of thousands)
	Small area level; Tag: census block / census sector / group level / neighbourhood level	The smallest standard geographic units for census or administrative purposes (hundreds to thousands)
Micro level	Property level; Tag: household / building level	The level of individual households or buildings (~1 to hundreds)
	Person level; Tag: individual	The most granular level, referring to data or analysis focused on individuals. (1 person)

Model purpose. Describes the intended use of results for risk and resilience management. For socio physical analysis, model purpose spans from creating early awareness to supporting investment, design, or policy decisions that balance physical performance, social equity, and recovery efficiency.

Measures. Refers to the tangible outcomes or actions supported by the analysis. In socio physical terms, measures combine structural adaptation options (e.g., retrofitting, reinforcement) with social measures (e.g., evacuation planning, access to services, communication strategies) that collectively reduce risk and improve recovery.

Example of risk metrics. Represents the indicators used to quantify and communicate risk in physical, social, and economic dimensions.

Physical buildings

Table 2 presents the physical building component of the socio physical taxonomy, which defines how buildings are characterized for multi hazard risk modelling across the four classes. The taxonomy specifies the essential attributes, data types, and analytical classes needed to describe structural, non-structural, and contents performance under hazard loading. Building on the GED4ALL taxonomy (Silva et al., 2022), we define specific data requirements to characterize the built environment from a physical building perspective, summarized in Table 3. This structured organization of building data ensures consistency, enables comparison across scales, and supports integration with social and infrastructure models within the broader socio physical taxonomy.

An example of typical outputs for physical buildings is shown in Figure 2. In Class 0 we report only counts of buildings with potential damage within each land use area. In Class 1 we map risk by land use and find that residential areas show higher risk. In Class 2 we move to the building scale inside the Class 1 priority zones and identify which specific buildings are at high risk based on initial models. In Class 3 we use detailed information for those buildings to update the risk estimates and refine priorities for action.

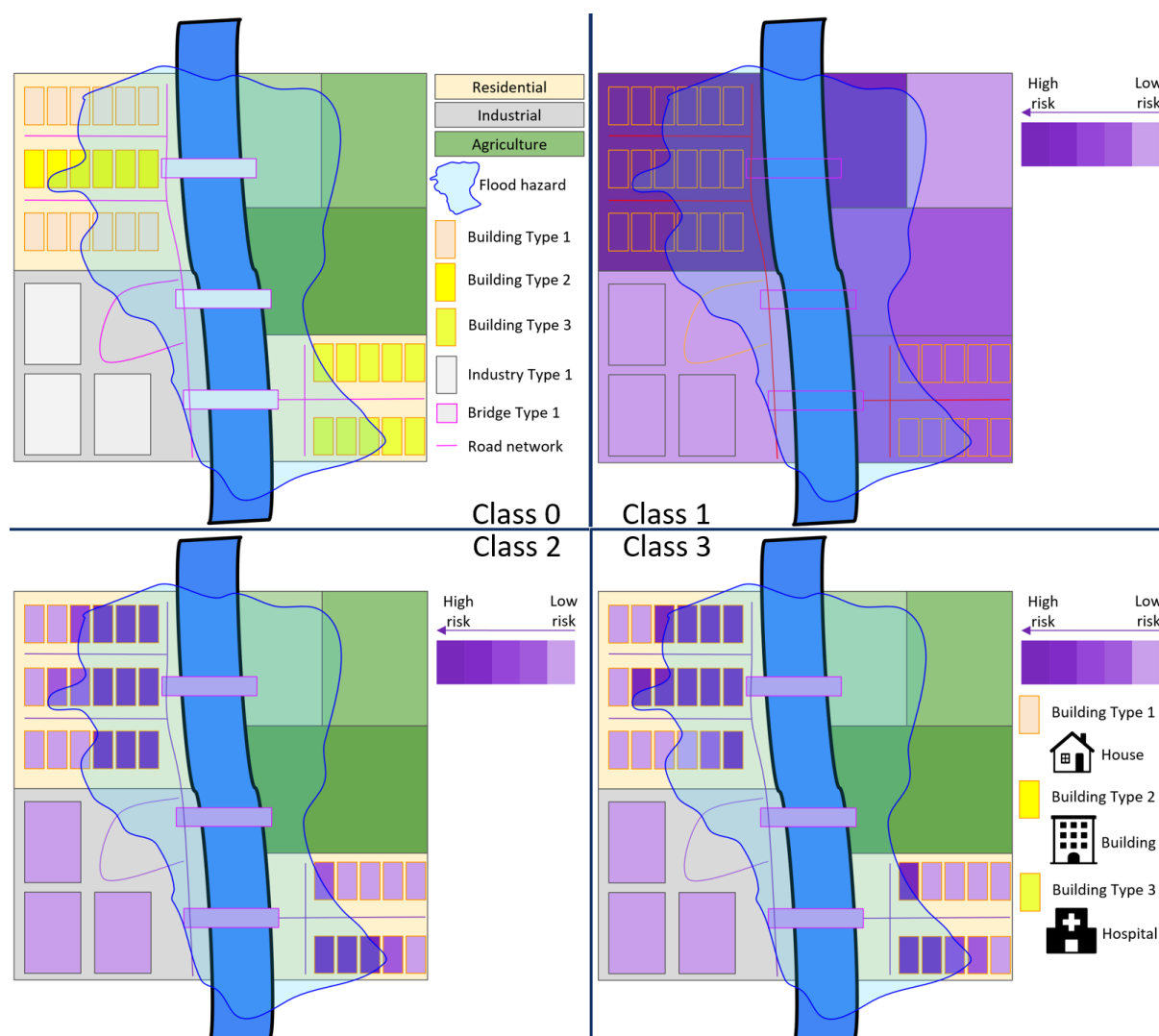


Figure 2 Example of result by class

Physical infrastructure

This part of the taxonomy is currently under development.

Table 2 Physical Vulnerability Taxonomy

Taxonomy characteristics	Taxonomy of risk modelling assessments			
	Risk Pre-Screening Class 0	Basic Risk Screening Class 1	Enhanced Risk Assessment Class 2	Advanced Risk Assessment Class 3
Questions	Are buildings/infrastructures and people exposed to hazards?	Should we take action based on the current risk?	Where do we need to take action?	How could actions be implemented?
Modelling techniques	Deterministic overlays that combine hazard layers with land-use exposure in GIS to flag areas needing further analysis and to run “what-if” scenarios (e.g., changes in exposure and hazard over time).	<p>Probabilistic risk or scenario-based evaluation at the land-level.</p> <p>To compute land-level vulnerability or fragility, start with a building inventory, classify assets into representative building typologies, and then aggregate results to the relevant land-use unit (parcel, block, etc.) according to the zone’s predominant use.</p> <p>Building-typology losses or damage probabilities can come from global functions (e.g., flood depth–damage curves, Huizinga et al., 2017; the Global Seismic Vulnerability Model, Martins & Silva, 2023; ERMESS models by Pandolfi et al., 2023). Aggregate to land units using (a) simple (i.e., unweighted) averages; (b) exposure-weighted averages (recommended), weighting by what matters such as replacement value, floor area, or occupants; (c) indicator-based rules, where you set binary flags for each building type and mark a land</p>	<p>Probabilistic risk or scenario-based evaluation at the building level, where building types (average archetypes or indexed building types) are linked to engineer-validated vulnerability or fragility models. This approach combines enhanced desktop studies with targeted engineering calculations to strengthen hazard–vulnerability–consequence correlations.</p>	<p>Probabilistic risk or scenario-based evaluation at the building level, where vulnerability functions are developed for representative building typologies using high-fidelity numerical models. Monte Carlo methods are applied to propagate uncertainties, and the modelling framework may explicitly account for multi-hazard interactions and cascading effects at the consequences.</p> <p>Multiple return periods can be considered for hazard (i.e., hazard curve)</p>

		unit as “damaged” once a threshold is exceeded (for example, higher than 50% of buildings in the area exceed a selected damage state); or other aggregation forms, depending on the analysis scope.		
Vulnerability/fragility models selections (see Section 2.2 for more details)		<p>Selecting the best candidate function begins with:</p> <p>Screening Step 1 by specifying the asset location, asset taxonomy string, and the hazard of interest.</p> <p>Step 2 performs an automatic search in interactive databases of physical impact models.</p> <p>Step 3 conducts a manual search across non-interactive model compendia, literature reviews, and regional/global models.</p> <p>Step 4 carries out a focused literature review to obtain the most refined definitions of the three fundamental parameters while accounting for user requirements.</p> <p>Step 5 pre-screens the candidate models to select a subset for evaluation and ranking, refining them with engineering principles to match the target building’s characteristics.</p>	<p>Selecting the best candidate function begins with:</p> <p>Screening Step 1: specify the asset location, asset taxonomy string, and the hazard of interest.</p> <p>Step 2 runs an automatic search across available interactive databases of physical impact models.</p> <p>Step 3 performs a manual search of noninteractive model compendia, literature reviews, and regional/global models.</p> <p>Step 4 conducts a focused literature review to obtain the most refined definitions of the three fundamental parameters while capturing specific user requirements; and</p>	<p>The process starts by selecting the best candidate function:</p> <p>first specify the asset location, the asset taxonomy string, and the hazard of interest; then run an automatic search in interactive databases of physical impact models; follow with a manual search of model compendia, literature reviews, and regional or global models; conduct a focused review to refine the three fundamental parameters while accounting for user requirements; and pre-screen the models to choose a subset for evaluation and ranking, refining them with engineering principles to match the target building. Scoring then defines criteria of relevance, statistical refinement, model quality, and user defined requirements; assigns weights using the Analytic Hierarchy Process with suggested values of 25 percent, 15 percent, 40 percent, and 20 percent</p>

		<p>The process then moves to scoring: Scoring Step 1 defines criteria: (i) relevance, (ii) statistical refinement, (iii) model quality, and (iv) user-defined requirements.</p> <p>Scoring Step 2 assigns weights via the Analytic Hierarchy Process (AHP), with suggested weights of 25% for relevance, 15% for statistical refinement, 40% for model quality, and 20% for user-defined requirements.</p> <p>Scoring Step 3 ranks candidates using TOPSIS (Technique for Order Preference by Similarity to an Ideal Solution). The selected model(s) then proceed to Engineering Calculation.</p>	<p>Step 5 pre-screens the resulting models to select a subset for evaluation and ranking, refining them where appropriate with engineering principles to match the target building's characteristics.</p> <p>The process then moves to scoring: Scoring Step 1 defines criteria: (i) relevance, (ii) statistical refinement, (iii) model quality, and (iv) user-defined requirements.</p> <p>Scoring Step 2 assigns weights via the Analytic Hierarchy Process (AHP): suggested weights are 25% relevance, 15% statistical refinement, 40% model quality, and 20% user-defined requirements.</p> <p>Scoring Step 3 ranks candidate models using TOPSIS (Technique for Order Preference by Similarity to an Ideal Solution). The selected</p>	<p>respectively; and ranks candidates using the Technique for Order Preference by Similarity to an Ideal Solution. In parallel, numerical models are developed based on archetypes, empirical observations, synthetic data generated from analytical or numerical models, or expert judgment. For the component based numerical model, define structural and non-structural components, establish building limit states for the hazard, provide component capacities and quantify related uncertainties, and implement a MATLAB based component model with Monte Carlo simulations for uncertainty propagation, leading to Step 5, the fragility functions. For vulnerability functions, define structural, non-structural, and contents components, develop a separate vulnerability function for each component, and implement a MATLAB based component model with Monte Carlo simulations for uncertainty propagation, leading to Step 5, the vulnerability functions.</p>
--	--	--	--	---

			model(s) proceed to Engineering Calculation.	
Data types	Land-use categories, site coordinates, and broad hazard layers (maps, census, satellite) under deterministic or single-return-period analysis; generic building typologies may be used as proxies for exposure.	Building typologies within each land-use zone, combined with hazard-specific exposure assumptions that require only minimal adjustments to global models. Use probabilistic hazard scenarios with intensity measures (e.g., flood depth, spectral acceleration, gust wind speed) for at least one return period. Assume building characteristics from known occupancy type and height category, using data provided by stakeholders or publicly available sources.	Building-level attributes (structural type, condition, retrofit, hazard-specific details) validated with due diligence reports or surveys. Probabilistic hazard scenarios.	Detailed construction documents and component inventories (structural, non-structural, systems), retrofit history, digital twins, high-resolution hazard datasets. Probabilistic hazard scenarios. and Hazard curves.
Resolution, typical scale	Macro-level: Coarse spatial scale; national, regional, or zoning overlays.	Macro to meso-level: Moderate spatial scale; large portfolios or macrozone analysis.	Meso-level: Higher spatial resolution; medium-sized portfolios, campuses, or urban districts.	Micro-level: highest resolution; individual buildings and components, up to 10% of a portfolio for detailed modelling.
Model purpose	Early awareness and land-use pre-screening to identify potential hotspots.	Preliminary risk assessment to judge whether further action is warranted within a land-use area, inform site selection, and support regulatory disclosures.	Hotspot identification across medium-size portfolios and campuses; exploration of adaptation pathways; evidence-based identification of vulnerable components and prioritization of interventions via cost–benefit analysis.	High-stakes investment and design decisions, plus insurance and capital planning at the portfolio level; resilience-based design, evaluation, and optimization of retrofit/adaptation strategies at the building level.
Measures	Rank land-use areas by risk to pre-screen candidates for higher-class assessments.	Rank zones or portfolios for targeted action and regulatory disclosures; develop preliminary building-level risk assessments from de-aggregated information.	Identify priority buildings and areas; evaluate the most vulnerable assets within the study zone; compare ‘what-if’	Develop shovel-ready, component-level adaptation measures based on identified vulnerabilities; optimize resilience strategies at building and portfolio scales; integrate life-cycle

			investment scenarios; and propose retrofit options selected via preliminary cost-benefit analysis.	costing (LCC) and embodied carbon; design new resilient buildings for projected hazard scenarios; and deliver final cost estimates, cost-benefit analyses, capital plans, and insurance optimization.
Example of risk metrics	<p>Number of potentially affected buildings</p> <p>Number of potentially affected infrastructure</p> <p>Qualitative risk rating</p>	<p>Risk as potential damage for land use categories in EUR/ year</p> <p>Risk prioritization: Identification of land-use areas needing further analysis.</p>	<p>Risk as potential damage derived from buildings in EUR/ year.</p> <p>Risk as the potential loss of functionality or delay in functional recovery.</p> <p>Risk prioritization: Identification of assets needing further analysis based on exposure severity, stakeholder value, or cost-benefit thresholds.</p> <p>Initial feature-Level Vulnerability Mapping: Identification of critical features at risk based on probabilistic hazard-vulnerability correlations.</p>	<p>Risk for economic damages per building archetype [€/ year]</p> <p>Propose candidate components that contribute the most to reduce risk at the building archetype level.</p> <p>Component-Specific Risk Mitigation Plans: Technically validated, shovel-ready adaptation strategies tailored to critical building elements, with quantified risk reduction and performance.</p> <p>Resilience-Based Cost-Benefit Assessment: High-resolution estimates of adaptation costs and associated benefits.</p>

Table 3 Data needs per risk

Features	Risk Pre-Screening Class 0	Basic Risk Screening Class 1	Enhanced Risk Assessment Class 2	Advanced Risk Assessment Class 3
Location	Geographic coordinates			Direction (e.g., parallel to street, perpendicular to street)
Material LLRS		Material technology of Primary LLRS based on stakeholder and publicly available information	Material technology of Primary LLRS	Material properties of both primary and additional LLRS
LLRS		Primary LLRS + seismic code level and ductility level from year of construction or retrofit	formal or informal + columns/wall density + additional LLRS	lateral force coefficient + story stiffness + Dynamic properties of the building + seismic code level and ductility level
Height		Height of structure + presence of basement	Number of stories above/below ground + Height of ground floor above grade	Slope of the ground
Data of Construction or Retrofit		To infer compliance with building codes and ductility	physical condition/maintenance (e.g., good, average, poor, unknown)	physical condition/maintenance/retrofit of specific components of the building
Surroundings		type (e.g., attached, detached, semi-detached)	Burnt vegetation close to the asset. Debris potential to be accumulated in the roof. Missile environment	Presence of overhanging trees
Occupancy Type and components		Residential (single-family, apartment); Commercial (shops, offices, warehouses); Industrial; Institutional (schools, hospitals) + Number of people the building can support	Location of equipment and critical components of the building	Number of occupants during typical hours and peak times + Digital twin with a full inventory of components (structural, non-structural and finishes layers) and equipment with location and elevation
Shape of the Building Plans		Shape type (e.g., square, rectangular, I shape, curved, triangular, etc)	Building position within a block	
Structural Integrity		plan irregularity + horizontal irregularity (e.g., regular, irregular, unknown)	primary plan irregularity + primary horizontal irregularity	secondary plan irregularity + secondary horizontal irregularity

Ground Floor Hydrodynamics		presence of openings (yes, no, unknown)	Envelope opening area	openings characteristics (e.g., windows/doors flood characteristics), type of protections (e.g., collapsible walls)
Exterior Walls		material type and resisting system + presence of openings (yes, no, unknown) - Enclosure classification	Envelope opening area + Enclosure classification and criteria	openings characteristics (e.g., windows/doors wind and fire characteristics, type of protections, type of shutter), envelope finishing layers

2.2 Scoring, selecting, and developing physical impact models for multi-hazard risk assessment.

This section builds on the vulnerability/fragility model selection taxonomy described in Section 2.1, providing a clear methodology for identifying the best candidate models during the risk assessment. It also outlines the methodology needed to select the most suitable models for section 2.3.

2.2.1 Introduction and motivation

Natural-hazard-induced disaster risk results from complex interactions between exposure, hazard, and vulnerability. According to widely accepted definitions (e.g., United Nations Office for Disaster Risk Reduction [UNDRR], 2016), a hazard is “a process, phenomenon or human activity that may cause loss of life, injury or other health impacts, property damage, social and economic disruption or environmental degradation”; exposure is “the situation of people, infrastructure, housing, production capacities and other tangible human assets located in hazard-prone areas”; and vulnerability is referred to as “the conditions determined by physical, social, economic and environmental factors or processes which increase the susceptibility of an individual, a community, asset or system to the impacts of hazards”. This section specifically focuses on the physical vulnerability component of (multiple) natural-hazard disaster risk. The section discusses the appraisal, scoring, selection, and development of models - collectively referred to as “physical impact models” (see Overview of physical impact models for natural hazards for more details) - that broadly quantify the consequences of a set of hazard intensity measures (IMs) on physical assets (e.g., buildings, infrastructure). Systemic vulnerability (e.g., Limongi & Galderisi, 2021), originating from the mutual linkages/interactions among physical, economic, and social systems, is outside the scope of this section. Furthermore, specific emphasis is placed on buildings, which act as critical nodes in modelling interacting physical infrastructure systems and social networks (e.g., Cremen et al., 2022a, 2022b).

Detailed information on individual physical assets within a given region of interest may not always be available due to a lack of specific data (particularly in Global South contexts) required to infer (select) or derive appropriate asset-specific exposure models. In addition, for forward-looking risk analyses that focus on possible future configurations of an urban system (e.g., Mesta et al., 2022; Calderón & Silva, 2021), asset-by-asset information is not necessarily considered within the underlying procedures (e.g., urban planning) or modelling (e.g., spontaneous urban growth prediction). Therefore, for vulnerability characterisation purposes, assets are generally grouped into classes based on a set of common attributes that define their exposure. These attributes uniquely describe an asset class (e.g., buildings, bridges, lifeline equipment), detailing the common features directly associated with the physical impacts of multiple natural hazards. Then, each class is assigned relevant fragility (i.e., the probability of reaching or exceeding a certain DS, given a prescribed magnitude of a hazard IM) or vulnerability (i.e., the probability of impact given a prescribed magnitude of a hazard IM) models, which may account for single or multiple hazards. Vulnerability models may be linked to fragility models using appropriate damage-to-impact (i.e., the probability of impact given a certain DS) models.

Each component of disaster risk may involve temporal dependence. Time-dependent fragility/vulnerability is herein defined as a variation over time of the parameters of the physical impact model for a given asset class definition (e.g., ageing of the asset materials increases fragility over time but does not change the considered asset class). Moreover, fragility/vulnerability may change due to environmental asset deterioration (e.g., corrosion of structural components), the effects of sequential hazard events (e.g., damage accumulation due to multiple earthquake aftershock occurrences), or structural strengthening efforts (e.g., structural retrofit, climate adaptation engineering; Bastidas-

Arteaga & Stewart, 2019). For accurate risk estimations, capturing the above dynamic effects is crucial (e.g., Riddell et al., 2020).

Many fragility/vulnerability models are available for different combinations of asset types and hazards (single or multiple) within various sources, including literature review studies, compendia, and interactive online databases. However, selecting the most suitable models for a given asset class within a specific geographical context is a significant challenge for risk modellers or other end-users, particularly in forward-looking contexts such as risk-informed urban planning and future urban development. Different choices of physical impact models may lead to remarkably different risk estimates, which can affect decision making based on these estimates. This section provides a structured methodology for scoring, selecting, and developing multi-hazard physical fragility/vulnerability models of asset classes (with greater emphasis on buildings) within any selected case-study region in support of multi-hazard risk modelling and quantification. The process consists of three main steps: 1) mapping the relevant asset classes in a considered area to a set of existing candidate physical impact models, also accounting for specific modelling requirements (e.g., time dependency, multi-hazard interaction); 2) scoring the candidate models according to relevant criteria, to select the most suitable models for a given application; or 3) using state-of-the-art empirical or synthetic (analytical or numerical) methods to develop fragility/vulnerability models not already available.

2.2.2 Overview of physical impact models for natural hazards

This Section introduces the types of physical impact models (i.e., fragility relationships, vulnerability relationships, damage-to-impact models) that form the basis of the scoring/selection/development methodology proposed in “Proposed characterization procedure for physical impact models”. These models may be empirical, synthetic, or expert elicitation based. Empirical physical impact models require collecting data related to previous observations of natural-hazard (post-event) physical impacts (damage and/or consequences). Synthetic physical impact models are derived from analytical or numerical modelling of an asset’s “response” (e.g., structural and/or non-structural) to one or more hazards of interest, which is linked to physical damage and consequence metrics of interest. Expert-elicitation models involve several experts providing educated guesses of the damage (or consequence) that would occur to a specific asset class when subjected to a prescribed magnitude of a hazard IM. Each model type may be derived based on asset-level damage and/or impact data (i.e., global-level analysis) or damage and/or impact data for each component of the considered asset (i.e., component-by-component analysis) aggregated to obtain asset-level results. Empirical and expert-elicitation physical impact models are usually derived from a global-level analysis, while synthetic models can be based on either global or component-by-component analyses.

This Section begins with the mathematical definitions of these models and then provides a brief overview of their implementation for selected natural-hazard contexts, including the relevant damage causes or mechanisms, adopted IMs, and other pertinent information on how the different physical impact model types are structured.

Mathematical definitions

Fragility relationships

Asset-level fragility relationships define the probability of some discrete limit (or damage) state (DS_i) being reached or exceeded for an asset of interest, as a function of hazard intensity, i.e., $P(DS \geq ds_i | IM = im)$. (Note that lower-case symbols refer to a particular value of the random variables denoted in upper case). The response of an asset to a hazard-induced loading (e.g., earthquake-induced ground-motion time history, flood-induced hydrostatic/hydrodynamic forces, etc.) described by a certain IM is quantified using an engineering demand parameter (EDP, e.g., building horizontal roof displacement, floor accelerations, the stress level in a given structural component). The selected

IM for the analysis should be both efficient and sufficient (e.g., Ebrahimian & Jalayer, 2021). An efficient IM leads to a relatively small variability in estimating the selected EDP given a prescribed value of IM. A sufficient IM renders the estimation of the EDP for all IM levels independent of all other hazard causal parameters (e.g., earthquake magnitude and location). Fragility relationships can also be represented using vector-valued IMs (as described in Section 2.1.4).

Fragility functions typically take the form of lognormal cumulative distribution functions (CDFs; e.g., Tarbotton et al., 2015; Cremen & Baker, 2019):

$$P(DS \geq ds_i | IM = im) = \Phi\left(\frac{\ln\left(\frac{im}{\theta}\right)}{\beta}\right), \quad \text{Eq.1}$$

where $\Phi(\cdot)$ is the standard normal CDF, θ is the median (i.e., the value of IM that results in a 50% probability of reaching or exceeding ds_i), and β is the standard deviation of $\ln(IM)$ for ds_i . This mathematical form has several features that are particularly convenient in the context of fragility modelling, including the exclusion of non-plausible negative IM values and the fact that the θ and β parameters are enough to define the function completely. An extensive description of other potential mathematical forms that can describe fragility is provided in Rossetto et al. (2014) and Lallemand et al. (2015), among many others. Both Lallemand et al. (2015) and Jalayer et al. (2015) also discuss the possibility of updating fragility functions (if more information – from experimental results or post-event fieldwork, for instance – subsequently becomes known) using Bayesian methods. A more advanced fragility function model, which explicitly accounts for the ordinality of damage (i.e., the fact that DSs are both ordered and related in a physical sense) through simultaneous calibration of functions for multiple DSs, was recently presented in Nguyen and Lallemand (2021).

Vulnerability relationships

Vulnerability relationships are used to estimate the probability of continuous outcomes (O) – typically in the form of an impact (or consequence) metric (e.g., economic losses, downtime, casualties) – associated with a given IM, i.e., $P(O > o | IM = im)$. Vulnerability functions that produce absolute values of outcomes are generally expressed in the form:

$$P(O > o | IM = im) = 1 - F(o|im), \quad \text{Eq.2}$$

where $F(\cdot)$ is some type of CDF. Vulnerability functions that output relative values of outcome (e.g., economic loss normalised with respect to the asset value) can take the form of a Beta distribution, given its ability to flexibly model values between 0 and 1 (Silva et al., 2015; Lallemand & Kiremidjian, 2015). In this case,

$$f(o|IM = im) = \frac{o^{q-1}(1-o)^{r-1}}{B(q,r)} \quad \text{Eq.3}$$

where r and q specify the shape of the distribution, and $B(\cdot)$ denotes the beta function.

Vulnerability models often neglect uncertainty in the outcome, simply estimating the mean (absolute or relative) value of an outcome conditional on IM, i.e., $E(O|IM = im)$. These functions are typically derived using some form of regression curve/surface (Carisi et al., 2018; Martínez-Gomariz et al., 2020; Figueiredo et al., 2021; Lagomarsino & Giovinazzi, 2006).

Damage-to-impact models

Damage-to-impact models – often referred to as consequence or damage-to-loss models – bridge the gap between fragility and vulnerability analysis in the absence of appropriate parametric vulnerability relationships, by mapping discrete DSs to continuous impact metrics (Martins et al., 2016a). Probabilistic versions of these models take the form $P(O > o | DS = ds_i)$, and can be used to derive a vulnerability function through:

$$P(O > o | IM = im) = \sum_{i=1}^n P(O > o | DS = ds_i) P(DS = ds_i | IM = im) \quad \text{Eq.4}$$

where $P(DS = ds_i | IM = im) = P(DS \geq ds_{i-1} | IM = im) - P(DS \geq ds_i | IM = im)$, n denotes the number of DSs, and all other variables and expressions are as previously defined. Given the similar mathematical forms of vulnerability and damage-to-impact models, the Beta distribution can also be used to model $f(o | ds_i)$, e.g., Martins et al., (2016b). Deterministic damage-to-impact models - expressed as $E(O | DS = ds_i)$ - translate $P(DS = ds_i | IM = im)$ into $E(O | IM = im)$ through an analogue form of Eq. 4. (e.g., FEMA, 2021).

Extensions to multi-hazard, multi-IM, or time-dependent contexts

Multi-hazard physical impact models can be formulated in a vector-valued (e.g., Reed et al., 2016) or a state-dependent format (e.g., Li et al., 2014). Physical impact models for multi-hazard and time-dependent contexts describes the possible scope of both formats for different hazards. Figure 3a shows examples of vector-valued and state-dependent fragility relationships for dual-hazard interactions. Vector-valued fragility models (surfaces) can be used to model impacts due to concurrent compound hazard intensities (e.g., storm surge and high wind speed in a hurricane; Li et al., 2014). They are expressed in the form $P(DS \geq ds_i | IM)$, where IM is a vector of IMs. $P(DS \geq ds_i | IM)$ can be defined using a multi-variate cumulative lognormal distribution function (e.g., Gehl et al., 2013), which is a multi-variate generalisation of Eq. 1. A general mathematical formulation for single- or multi-hazard fragility relationships based on various multivariate distributions is provided by Zentner, (2017a), who suggests using the Bayesian information criterion to select the most appropriate one. Note that vector-valued fragility models can also be used to characterise single-hazard conditions (e.g., flood models depending on both water depth and flood duration).

State-dependent fragility models define the fragility of an asset for a given secondary hazard of interest, conditional on its (damage) state after a primary hazard of interest. These models are expressed in the form $P(DS(H_k) \geq ds_i | IM(H_k), S(H_j))$ and represent the probability of exceeding the DS threshold (ds_i) for the k -th hazard (H_k), given an IM for hazard k , $IM(H_k)$, and the pre-existing state of the asset after a previous hazard $S(H_j)$, which may refer to damage (e.g., Aljawhari et al., 2021) or an alteration of its structural loading (e.g., Lee & Rosowsky, 2006), for instance. $P(DS(H_k) \geq ds_i | IM(H_k), S(H_j))$ can be determined using Eq. 1, based on data that accounts for $S(H_j)$. State-dependent fragility models for which S coincides with a pre-existing DS implicitly assume that an asset's DS transitions caused by different events are independent, such that the values of DS evolve according to a Markov process, i.e., the present value of DS for the asset only depends on its previous value of DS, rather than its entire history of damage. Note that the state of an asset may also evolve with time, $S(H_j, t)$, and may even be independent of hazard, $S(t)$. $S(t)$ may represent the effect of a physical process (e.g., deterioration due to corrosion) on an asset's ability to resist a hazard loading with a given IM, for instance. Some models (Otarola et al., 2022; Ghosh & Padgett, 2010) use a quadratic model for $S(t)$, and consequently for $\theta(S)$ and $\beta(S)$, to capture the corrosion-induced evolution of earthquake fragility for bridge systems, for instance.

Multi-hazard, multi-IM, and/or time-dependent vulnerability relationships are usually defined analogously to Eq. 2, adopting similar statistical techniques and assumptions. They can be expressed in a vector-valued (e.g., Ming et al., 2015) or a state-dependent format (e.g., Ghosh & Padgett, 2010), as appropriate. Multi-hazard and/or time-dependent vulnerability models can be derived directly (such as in Ming et al., 2015) or by combining a set of state-dependent fragility relationships with a damage-to-impact model (such as in Aljawhary et al., 2021). Damage-to-impact models do not require a multi-hazard or time-dependent formulation (i.e., Eq. 4 can still be used) since they directly depend on damage rather than IMs. Multi-hazard and/or time-dependent fragility and vulnerability models can only be adopted if damage is measured consistently across the entire scope of the analysis (Physical impact models for multi-hazard and time-dependent contexts describes the challenges of achieving this).

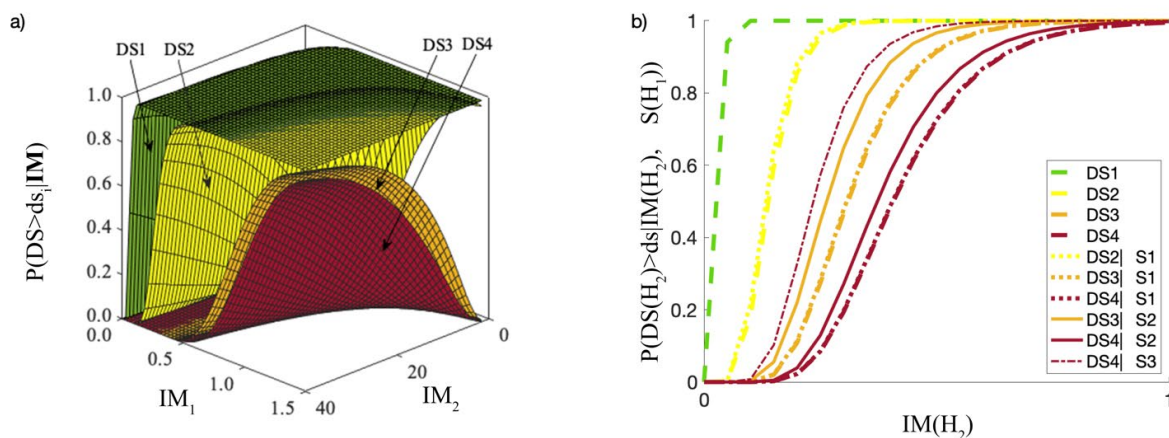


Figure 3: Example a) vector-valued; b) and state-dependent dual-hazard fragility models. IM: intensity measure; DS: damage state; S: state; H: hazard.

Physical impact models for earthquake-induced ground shaking

Earthquakes involve a sudden release of energy from a seismogenic source (e.g., a geological fault). Earthquake-induced ground motions (shaking) represent the surface expression of the resulting propagation of seismic waves (energy) from the source. These motions generate a vibratory response in physical assets. Depending on the dynamic structural characteristics of the asset (e.g., stiffness, strength, ductility capacity, hysteretic behaviour, strength degradation behaviour, plastic mechanism) as well as the nature of the ground shaking experienced at its location, this vibratory response (in the form of displacement/acceleration of its lateral load resisting system) may lead to some level of physical damage in its structural (and non-structural) components. Common damage mechanisms caused by earthquake-induced ground shaking include brittle failure (e.g., in unreinforced masonry and adobe construction), the formation of plastic hinges and shear failures (in reinforced-concrete buildings), anchorage/connection failures (e.g., in timber and steel constructions), and support failures (e.g., in bridges). Typical IMs for earthquake-induced ground-shaking physical impact models typically incorporate some measurement of the amplitude (strength) of the ground motion at the asset's location, such as peak ground acceleration or spectral acceleration at the asset's fundamental period (e.g., Zentner et al., 2017). More comprehensive IMs that also account for the spectral shape of the ground-motion record, such as inelastic spectral displacement (e.g., Luco & Cornell, 2007), as well as its duration (Cornell, n.d.), are becoming increasingly popular because of their superior correlation with the asset's structural response (i.e., their greater efficiency). A more detailed description of the selection of appropriate IMs, as well as a more critical discussion on empirical and synthetic earthquake physical impact models, can be found in Silva et al. (2019). The scientific literature on earthquake physical impact modelling is rich and is likely to be the most extensive across all natural hazards. Discrete DSs considered in asset-level earthquake fragility, and damage-to-impact models

represent a progressive deterioration in the asset's performance. A typical set of earthquake-related DSs for a given asset encompasses "minor", "moderate", "extensive", and "complete" categories (e.g., Federal Emergency Management Agency [FEMA], 2003). The exact damage implications of each state will depend on pertinent characteristics of the asset in question, such as its type (building, bridge, etc.), structural material, geometry and detailing. The most common impact metrics incorporated in seismic vulnerability and damage-to-impact models are economic losses (e.g., Di Pasquale et al., 2005; Martins & Silva, 2021), casualties (e.g., Noh et al., 2017), and repair/recovery time (e.g., Al-Nammari & Lindell, 2009). Recently introduced metrics include debris cover (Grant, 2020) and environmental impact (Caruso et al., 2021).

Physical impact models for flooding and mass-movement hazards

Floods and mass movements (including debris flows, landslides, lahars, etc.) are gravitationally driven flows of water and sediment. Both floods and mass movements are triggered by intense rainfall, which is likely to increase in intensity and frequency due to climate change (e.g., Shrestha et al., 2022). These flows often feature strong morphodynamics that can result in transitional behaviour as erosion and deposition modify the momentum and rheology of the flow (e.g., a dilute flash flood transitioning into a more concentrated debris flow as material is entrained).

Fluvial flooding (herein referred to as flooding) occurs when water levels rise in streams, rivers or lakes and overflow onto adjacent land. In the vicinity of the built environment, this generally results in low-velocity flows dominated by hydrostatic pressure. Flash floods are short-duration, locally isolated events that feature high peak discharge (i.e., high volumetric flow rates) and are triggered by intense rainfall or by the sudden release of large volumes of water, such as from glacial lake outbursts or dam failure (e.g., Ali & Raut, 2017). Flash floods often feature much higher flow velocities in the built environment than fluvial floods, where they can entrain loose and eroded debris (e.g., Douvinet et al., 2013). Because flash floods and debris flows share physical behaviour and potential asset damage mechanisms, and to further differentiate between fluvial and flash floods, flash floods are herein referred to as debris flows, noting that the exact behaviour and damage caused by these flows is a direct function of solids concentration. Landslides are broadly defined to encompass concentrated slips, falls, and flows of debris, rock or sediment down slopes under the influence of gravity. The breadth of this definition includes events with characteristic velocities that span at least ten orders of magnitude (Cruden & Varnes, 1996).

Floods and mass movements cause damage to the built environment via four principal mechanisms: 1) pressure in the bulk flow; 2) collisions from debris transported by the flow; 3) erosion scouring foundations; and 4) sediment deposition partially or fully burying structures and other infrastructure (e.g., roads). The pressure in the bulk flow can be split into hydrostatic and hydrodynamic components. The hydrostatic component depends on the flow thickness (h) and bulk density (ρ) of the flow (ρgh , where g is the acceleration of gravity). As the vertical component of most overland flows can be neglected, the hydrostatic pressure component is a reasonable approximation for bulk pressure. However, during strong impacts with buildings and other structures, vertical accelerations in the flow cause the bulk pressure to increase significantly (e.g., Haugen & Kaynia, 2008; Peregrine, 2003). The maximum (or peak) pressure on a vertical structure depends on the bulk flow velocity squared (ρv^2 ; Haugen & Kaynia, 2008; Hung et al., 1984; Jakob et al., 2012; Luo et al., 2020). Despite their shared physical behaviour and damage mechanisms, physical impacts due to floods, landslides, debris flows, and other mass movements are typically considered separately (excluding some exceptions), and it is challenging to define a unified approach.

The appropriate selection of IMs is crucial to capturing the above mechanisms in related physical impact models. Flood depth is typically employed as an IM for low-velocity flows, such as fluvial flooding (Martínez-Gomariz et al., 2020). Both flood duration (van de Lindt & Taggart, 2009) and flood velocity (Nofal & van de Lindt, 2022) are important to consider as additional IMs in areas with low soil permeability and steep terrain, respectively. The level of contamination in floods (e.g., due to oil) has

additionally been incorporated as a secondary IM for flood damage in some models (Schröter et al., 2014; Elmer et al., 2010). Velocity is used as a single IM for debris flows (Parisi & Sabella, 2017). Momentum-based IMs, which simultaneously account for a combination of velocity, flow depth, and hydrodynamic stresses, are additionally used to quantify damage (impacts) from debris flows (e.g., Jakob et al., 2012; Prieto et al., 2018). Because debris flows propagate as a wave with a leading front comprised of coarse granular material (e.g., Arattano & Marchi, 2008; Iverson, 2003), their impacts on structures can be modelled as impulses, such that earthquake-related IMs like spectral displacement can also be leveraged (e.g., Haugen & Kaynia, 2008). Due to the long timescales involved, defining a single IM for slow-moving landslides is difficult. Physical impact models developed for these hazards have used an IM representing the equivalent cumulative displacement of an area susceptible to landslides (Peduto et al., 2017). The landslide safety factor (Iverson, 2000) has also been used as an IM in slow-moving landslide models since it is related to the mechanical stability of the considered slope. However, there are many challenges in using this measure to quantitatively estimate physical impact, given the large number of parameters required to calculate it and its sensitivity to groundwater infiltration, which is a highly nonlinear and hysteretic physical process.

The physical impact of floods on assets is generally dominated by the contents loss due to inundation (rather than structural or non-structural damage). As such, most physical impact models for flood-related hazards are empirical vulnerability models and account for economic losses as a function of the flood depth (e.g., Gerl et al., 2016; Molinari et al., 2019; Nofal et al., 2020). These models are generally (and rather confusingly) referred to as “depth-damage” vulnerability functions under the implicit assumption that monetary expenses are a reasonable proxy for physical damage. Synthetic models such as INSUDE (IN-depth SYNthetic model for flood Damage Estimation; Dottori et al., 2016) present component-by-component vulnerability functions in terms of monetary losses. Other types of flood impacts captured in developed models include casualties (Deckers et al., 2009) and repair time (Sánchez-Muñoz et al., 2020). Fragility functions are becoming increasingly available for flooding hazards (see Nofal & van de Lindt, 2020, for a review), the most recent being those in Nofal et al. (2020), which describe a series of component-by-component DSs that directly correspond to probabilistic economic loss outcomes for pluvial and fluvial flooding events. However, damage-to-impact models for flooding are rare and may not be hazard-specific (Sánchez-Muñoz et al., 2020). In addition, the development of physical impact models for both debris flows and landslides is limited compared to flooding and earthquake hazards. This can be attributed to the complex dynamics of debris flow and landslide hazards (Papathoma-Köhle et al., 2017), difficulties in estimating the associated dynamic responses of structures (Haugen & Kaynia, 2008), and a lack of significant potential to cause human losses (in the case of slow-moving landslides). Exceptions include: (1) fragility models for debris flows that describe DSs using terminology adopted from earthquake fragility models (see Physical impact models for earthquake-induced ground shaking and Haugen & Kaynia, 2008; Parisi & Sabella, 2017; Prieto et al., 2018); and (2) fragility and vulnerability curves for landslides (Peduto et al., 2017) that use similar DSs to those described for earthquakes (see Physical impact models for earthquake-induced ground shaking) and represent impact in terms of a continuous equivalent damage level.

Physical impact models for multi-hazard and time-dependent contexts

Many regions in the world are prone to more than one natural hazard, such that structures/infrastructure systems can be subjected to more than one hazard during their lifetime (e.g., Asprone, Jalayer, Prota, & Manfredi, 2010). Effective risk-informed decision-making and/or risk management prioritisation is only possible if all relevant threats are considered and analysed (e.g., Kappes, Keiler, von Elverfeldt, & Glade, 2012; de Ruiter et al., 2021; Mignan, Wiemer, & Giardini, 2014; Budimir, Atkinson, & Lewis, 2014; Gill & Malamud, 2014). This requirement is compounded by the fact that two or more hazards affecting the same location in a relatively short period could result in physical

or social impacts greater than the sum of the effects from each individual hazard (Han, Wu, & Wang, 2007; Marzocchi, Garcia-Aristizabal, Gasparini, Mastellone, & Di Ruocco, 2012). A multi-risk approach, accounting for the interaction of risks from multiple hazards, is therefore necessary. This type of approach should incorporate interactions at the level of hazard, exposure, and physical/social impact (Zaghi et al., 2016); therefore, multi-hazard fragility/vulnerability models play a significant role. In addition, a lifecycle risk analysis is likely needed to accurately consider the interaction of single or multiple hazard events of different occurrences and resulting intensities. This involves simulating the time between different events and may require time-dependent (or state-dependent) physical impact models.

Gill and Malamud (2014) define multi-hazard interactions to include situations in which: a hazard triggers one or more other hazards; the probability of a hazard is increased or decreased; or there is a spatiotemporal coincidence of different hazards. As pointed out by de Angeli et al. (2022), these classifications share characteristics with further studies that identify the following three mechanisms of interaction: the trigger or causality, usually referred to as “domino effects” or “triggered hazards”; the influence, indicating increased/decreased probability or magnitude, without acting as a trigger; and the independent coincidence, when the spatial or temporal scale of independent hazards partially intersects. However, the classification proposed by Zaghi et al. (2016), which also considers other risk components apart from hazard, fits best with the scope of this study. This classification considers two levels of interaction: (1) level-one interactions that occur through the source, time and/or frequency of occurrence of two or more hazards and are independent of the presence of physical assets (e.g., earthquake–tsunami sequence); and (2) level-two interactions, which occur through the effects of the hazards on the site of interest, accounting for the presence of physical assets, and capture system-level disruptions as well as social and economic effects (e.g., flood-induced scour may increase a bridge’s earthquake fragility, although the earthquake IM is not affected by the scour). Bruneau et al. (2017) note that the classification in Gill and Malamud is independent of the effects of the hazards, and it therefore only applies to level one interactions. This section only deals with physical impact modelling related to level two interactions (i.e., those that involve a modification of a fragility/vulnerability curve due to cumulative damage to an asset), since level one interactions do not require changes to the underlying impact models. Thus, repeated instances of the same hazard (e.g., earthquake sequences, compound flooding) are considered multiple hazards.

Physical impact models that adequately capture level two interactions must be based on a consistent definition of structural and non-structural damage. These models should adequately capture the damage mechanisms relevant to the considered hazards, also including their cumulative effects (i.e., how damage due to one hazard may reduce safety margins for the considered asset/component, thus increasing damage from other hazards). Most multi-hazard physical impact models are based on uncoupled damage scales for each hazard (e.g., HAZUS; FEMA, 2003), but some attempts to incorporate consistent damage scales have been made in the literature (e.g., Maiwald & Schwarz, 2018; Schwarz & Maiwald, 2012). Describing cumulative damage requires defining an ad hoc scale that depends on the specific asset and hazards (e.g., Korswagen, Jonkman, & Terwel, 2019). Synthetic, physics-based models of an asset that capture damage accumulation under different hazards are possibly the only viable approach to address the above-mentioned challenges. (In fact, it is unlikely that empirical damage data for specific asset/hazard combinations are available.) Furthermore, these synthetic models must use appropriate static or dynamic mechanical characterization of the asset materials and components to capture the interactions of the relevant damage mechanisms. For example, to model the interacting effects of wind and earthquake on a building, it is necessary to characterize the material hysteresis (i.e., the evolution of stiffness under unloading–reloading cycles) and its strength degradation under sustained cyclic deformation (e.g., Fan, Li, & Zhang, 2019).

Quantitative multi-hazard physical impact models are comparatively less common in the literature than single-hazard ones. Rather than providing a thorough literature review, which is outside the scope of this section, this section selects examples of multi-hazard physical impact models for buildings and

bridges to qualitatively assess model availability in terms of the number of considered hazards and their nature (e.g., synthetic, empirical). Most available models involve fragility relationships for two hazards, with some exceptions discussed below. Figure 4 summarizes dual combinations of hazards for which it was possible to find at least one quantitative physical impact model.

Most multi-hazard physical impact models for buildings focus on sequential earthquake events/ground motions (e.g., Li, Song, & van de Lindt, 2014; Aljawhari, Gentile, Freddi, & Galasso, 2021; Jeon, DesRoches, Lowes, & Brilakis, 2015; Raghunandan, Liel, & Luco, 2015; Tesfamariam, Goda, & Mondal, 2015) and take the form of state-dependent fragility models for different types of buildings and DSs of interest. Some such fragility models include time-dependent considerations (measured using a consistent damage scale), such as the effect of structural ageing on concrete buildings during earthquake sequences (e.g., Di Sarno & Pugliese, 2021). Petrone, Rossetto, Baiguera, De la Barra Bustamante, and Ioannou (2020), among others, provide state-dependent fragility models for reinforced concrete buildings exposed to earthquake–tsunami sequences. Earthquake–landslide state-dependent fragility models are provided in Miluccio, Gentile, Galasso, and Parisi (2021), for example. Fragility models combining earthquake and wind actions are available in Li, Liu, Li, and Zheng (2020) and Zheng et al. (2019), for instance. The model in Lee and Rosowsky (2006) describes the state-dependent earthquake fragility of buildings that are preloaded with snow. The proposed model in Asprone et al. (2010) relates to the blast fragility of reinforced concrete structures in the presence of seismic risk. Compound flooding, related to the concurrence of multiple hazard drivers (e.g., heavy rainfall, extreme river flow, and storm surge), can be effectively modelled using standard depth–damage flood vulnerability models based on the maximum-in-time water depth as an IM (e.g., Ming, Liang, Dawson, Xia, & Hou, 2022). Realistic modelling of hurricane impact requires a multi-hazard approach involving wind-induced pressure, surge, and waves. The physical impact model in Nofal et al. (2021) accounts for the probability of structural damage by combining vector-valued flood fragility models, vector-valued surge–wave fragility models, and wind pressure fragility functions. Luo, Zhang, Wang, and He (2020) propose a framework to produce physics-based models for sequentially and concurrently occurring debris-flow impacts. Models in Zuccaro, Cacace, Spence, and Baxter (2008) account for fragility due to earthquakes and pyroclastic flows that follow ash fall events.

Examples of multi-hazard vulnerability modelling involve the flood-induced scour on bridge foundations (e.g., Argyroudis et al., 2019a), the combined effect of flood-induced scour and ground shaking (e.g., Li et al., 2020; Ganesh Prasad & Banerjee, 2013), ground shaking and liquefaction on bridges (e.g., Aygün et al., 2011), liquefaction and lateral ground displacement (e.g., Brandenberg et al., 2011), earthquake sequences (e.g., Ghosh et al., 2015), and earthquake–tsunami sequences (e.g., Xu et al., 2021). A more detailed literature review on multi-hazard infrastructure vulnerability models (including roads, bridges, embankments, tunnels, retaining walls, slopes, etc.) is provided in Argyroudis et al., (2019b), which includes liquefaction, landslides, debris flow, and flood and the combined effects of flood-induced scouring and earthquakes. According to this review, most multi-hazard vulnerability models have been developed for bridges.

	Earthquake	Landslide	Liquefaction	Tsunami	Flood	Strong wind	Snow load	Debris flow	Ash Fall	Pyroclastic flow	Scour	Lateral spreading	Blast
Earthquake	X												
Landslide	X	X											
Liquefaction	X												
Tsunami	X												
Flood					X								
Strong wind	X				X								
Snow load	X												
Debris flow								X					
Ash Fall	X												
Pyroclastic flow									X				
Scour	X				X								
Lateral spreading			X										
Blast	X												

Figure 4 Availability of quantitative multi (dual)-hazard physical impact models. Each mark indicates that the literature includes at least one (building or bridge) physical impact model for the considered dual-hazard combination.

The choice of physical impact models for a given analysis must consider whether the adopted risk model can account for lifecycle considerations. A lifecycle risk analysis should account for the probabilistic distributions of the hazard-event occurrences, use an appropriate multi-hazard model to quantify relevant impact metrics, record the state of the asset after each event, and finally combine the results to calculate the probability distribution of the lifecycle impact (e.g., Gentile et al., 2021a). Choosing an appropriate physical impact model in this context depends on the types of successive events and their inter-event time; the repair (or recovery) strategy in place for the asset (which affects the probability of incomplete repair for a given DS and time); and the considered time horizon for the analysis.

Lifecycle risk analysis models considering only one hazard type (note that multiple events of the same hazard type are regarded as multiple hazards, as discussed above) in the literature often consider an “instantaneous” repair of the considered asset after each event (e.g., Veneziano et al., 2009). These models require a single-hazard physical impact model, which should be time-dependent to capture any asset degradation between two events: in this case, $S = S(t)$ from Mathematical definitions. Lifecycle models considering triggered hazards (e.g., Yeo & Cornell, 2009 for mainshock-aftershock earthquake sequences) require an $S = S(H_j)$ state-dependent physical impact definition. Multi-hazard (dependent or independent) lifecycle risk models that consider the probability of repairs being completed before the next event (e.g., Fereshtehnejad & Shafieezadeh, 2018, for earthquakes and flood-induced scour) require appropriate $S = S(H_j, t)$ state-dependent physical impact models. Lifecycle risk models that relax the Markovian assumption on the DS of the asset require n -variate vector-value physical impact models (as defined in Mathematical definitions), where n is the potential number of hazard events (of the same or different type) that could occur before the asset is repaired. Choosing n , and the considered hazard types, may be determined based on the considered repair strategy for the asset. However, to the best of the authors’ knowledge, no quantitative method is currently available to accomplish this goal.

2.2.3 Proposed characterization procedure for physical impact models

The proposed methodology (Figure 5) for scoring, selecting, and developing physical impact models starts after selecting one or more natural hazards, independent or interacting, which are relevant for

a selected case-study area. Although this is not strictly part of the proposed methodology, a useful tool to assist this choice is Thinkhazard (<https://thinkhazard.org>, last accessed June 2022), which provides a general view of hazard susceptibility on a global scale. Next, assets within the considered area are grouped into classes according to a taxonomy model, which may require different sets of general parameters specific to the identified asset class and hazards (e.g., occupancy, geometric parameters, design level). Preliminary phase: defining the exposure taxonomy string of the asset classes discusses codifying the required asset class characteristics in a multi-hazard taxonomy string and the minimum set of these parameters required for different hazard/asset-class combinations. The taxonomy string is then used to map the hazard/asset-class combination to relevant candidate impact models. As discussed in Screening phase: selecting candidate physical impact models, this process can involve models from interactive databases, model compendia, or literature reviews. It should incorporate general considerations of the trade-off between simplicity, accuracy, and data requirements of the overarching risk model. The considered candidate models are then ranked according to a set of criteria to determine the most appropriate one (Scoring phase: selection of the most suitable model). If the above search does not provide any satisfactory result, the proposed procedure involves developing new physical impact models based on an empirical or synthetic (analytical or numerical) approach, as detailed in Development and statistical fitting of physical impact models. The proposed procedure should be applied for multiple asset classes in parallel to determine whether physical impact models for different classes can be derived using a consistent methodology, which would lead to a desirable consistency in the damage/impact estimations of the considered risk assessment.

The main goal of this procedure is to facilitate the consistent appraisal and selection of a set of candidate physical impact models for use within risk modelling applications. The procedure may also be beneficial for application to new physical assets to be constructed as part of a risk-informed urban development process. Any values provided for relevant input parameters (e.g., specific criteria, threshold values for screening, scoring schemes, and weights; see Screening phase: selecting candidate physical impact models for more details) are only provided as recommendations; users are encouraged to adjust these parameters according to their specific needs. A code repository supporting the application of this procedure is provided at github.com/robgen/rankFragilityVulnerability (last accessed June 2022).

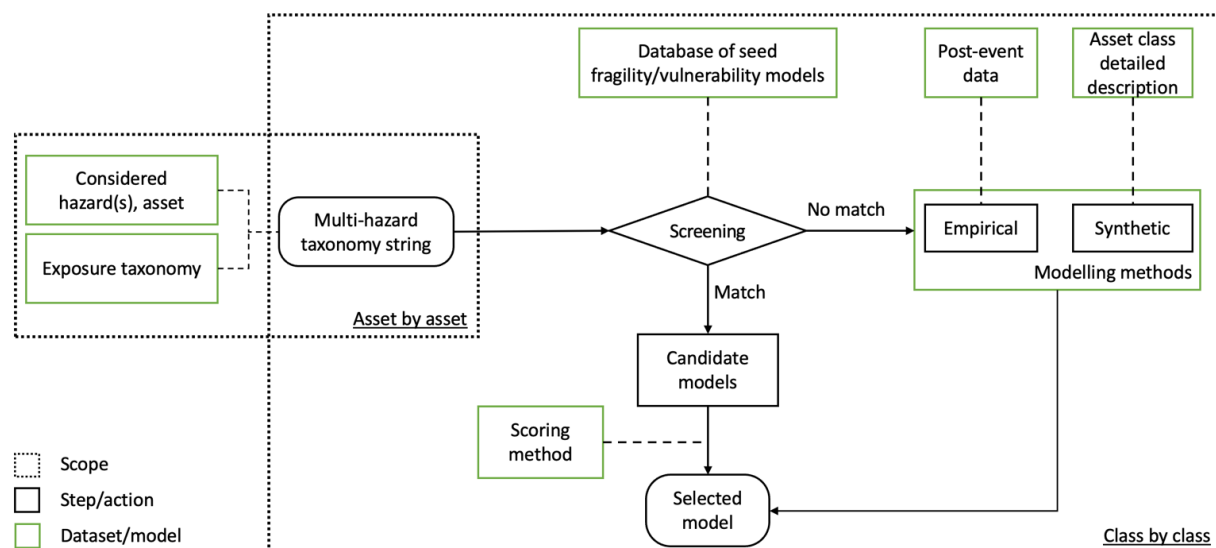


Figure 5 Proposed methodology to score and select physical impact models for a given asset class.

Preliminary phase: defining the exposure taxonomy string of the asset classes

The proposed procedure starts with identifying the physical attributes of the asset classes directly correlated with the physical impacts induced by relevant natural hazards. For example, the lateral load resisting system attribute is used to determine earthquake and wind fragility (among other hazards), the presence of a basement is relevant to flood fragility, and the roof typology (and its features) is a factor that influences hurricane fragility. The building occupancy type affects, for instance, the likely distribution of building occupants during any given day. For example, a school will be (near) fully occupied during certain hours on school days, predominantly by children. Moreover, the occupancy type defines the components likely to be present within a building. For example, industrial buildings contain machinery. These attributes are used to develop a series of exposure taxonomy strings, which consist of a combination of alphanumeric labels that contain asset-class-specific attribute information. These strings are an ideal data format for storage within a database (e.g., Geographic Information Systems, GIS) to facilitate interaction between the exposure and vulnerability modules of a risk model.

A taxonomy string should be general enough to account for multiple hazards, scales, and asset classes. The global exposure database for all (GED4ALL, Silva et al., 2022) best meets the above criteria since it facilitates links to many existing databases of physical impact models and is therefore leveraged in the proposed methodology. It covers buildings, roads, railways, bridges, pipelines, storage tanks, power grids, energy generation facilities, crops, livestock, forestry, and socio-economic data. This taxonomy was developed considering earthquakes, volcanoes, floods, tsunamis, storms, cyclones and drought. GED4ALL, also referred to as global earthquake model (GEM) taxonomy 3.0, is the multi-hazard generalisation of the GEM 2.0 taxonomy (Brzev et al., 2013), which is in turn derived from previous taxonomies such as those of ATC-13 (ATC, 1985), the European macro-seismic scale (EMS-98, Grunthal, 1998), HAZUS (FEMA, 2003b), and PAGER-STR (Jaiswal & Wald, 2008).

The GED4ALL taxonomy strings include different attributes for different asset types and facilitate three different levels of refinement/detail (from Level 1 to Level 3) in the input that accommodate various degrees of available data. This flexibility could be particularly convenient for data-scarce regions, which are especially prevalent in developing countries. Table 4 and Table 5 respectively provide the GED4ALL attributes for buildings and bridges, suggesting those that are strictly required versus optional in relation to the physical impact modelling of different hazards. An example of a Level 1 string is CR/H:2/LWAL/RES, which indicates a two-storey reinforced concrete residential building with a wall lateral load-resisting system. Level 2 information could include data on the material technology, for instance, which may be cast in place (CR+CIP) in the above example. A Level 3 string could include secondary information related to primary (Level 2) structural irregularities, such as the presence of torsion eccentricity and a re-entrant corner for the above example (IRIR+IRPP:TOR+IRPS:REC). Extensive documentation for each asset class is provided at docs.riskdatalibrary.org/ged4all.html (last accessed June 2022). In addition, this webpage indicates that an automatic tool to convert a set of attributes into a single taxonomy string, similar to “TaxtWeb” (platform.openquake.org/taxtweb, related to the GEM2.0 taxonomy, last accessed June 2022), is under preparation.

The GED4ALL attributes are mapped to the keys (or tags) in the OpenStreetMap database, a large open-source mapping repository (openstreetmap.org). Thus, it is possible to derive GED4ALL taxonomy strings for exposure data using the export tool developed by the Humanitarian OpenStreetMap Team (export.hotosm.org, last accessed June 2022). Finally, the GED4ALL repository (github.com/gem/ged4all, last accessed June 2022) includes software for converting taxonomy strings to the natural hazard risk markup language (NRML), enabling compatibility with other exposure taxonomies/models. This can be done using the input preparation tool by GEM (platform.openquake.org/ipt, last accessed June 2022).

Table 4 GED4ALL attributes for buildings exposed to different hazards. OSM: OpenStreetMap; R: required; O: optional; EQ: earthquake; FL: flood; DF: debris flow; TS: tsunami; LA: landslide; FI: Fire; WI: wind; VA: volcanic ash.

Attribute	OSM Key	EQ	FL	DF	TS	LA	FI	WI	VA
-----------	---------	----	----	----	----	----	----	----	----

Direction	building:direction	O	O	O	O	O	-	O	-
Material of LLRS	building:lateral:material	R	R	R	R	R	O	R	R
Lateral Load Resisting System (LLRS)	building:lateral:system	R	R	R	R	R	O	R	R
Height	building:levels	R	R	R	R	R	R	R	R
Date of construction or retrofit	building:age	R	O	O	R	R	O	R	R
Surroundings	building:adjacency	O	O	O	O	-	O	-	-
Occupancy	building	R	R	R	R	R	R	R	R
Shape of building plan	building:shape	O	O	O	O	O	R	R	-
Structural irregularity	building:irregularity	O	O	O	O	O	-	-	O
Ground floor hydrodynamics	ground_floor	-	-	O	O	-	-	-	-
Exterior walls	building:material	O	O	O	O	-	O	O	-
Roof shape	roof:shape	-	-	-	-	-	O	R	R
Floor system material	floor:material	O	O	O	O	O	O	O	O
Foundation	building:foundation	O	O	O	O	O	-	O	-
Fire protection	building:fireproof	-	-	-	-	-	R	-	-

Table 5 GED4ALL attributes for bridges exposed to different hazards. Notation as per Table 4.

Attribute	OSM Key	EQ	FL	DF	TS	LA	FI	WI	VA
General material	bridge:material	R	R	R	R	R	R	R	R
Super structure	bridge:structure	R	R	R	R	R	R	R	R
Deck characteristics	bridge:width;length; height	R	R	R	R	R	R	R	R
Deck structural system	bridge:support	O	O	O	O	O	O	O	O
Pier to deck connection	pier:connection	R	O	O	R	R	O	R	R
Pier to superstructure connection	pier:superstructure	O	O	O	O	O	O	O	O
Number of piers	bridge:total_piers	R	R	R	R	R	R	R	R
Shape of pier section	pier:shape	O	O	O	O	O	-	R	-
Pier height	pier:height	O	O	O	O	O	-	-	O
Spans	pier:span	R	R	R	R	R	R	R	R
Connections to the abutments	Abutment:connection	R	R	R	R	R	O	R	O
Bridge configuration	bridge:configuration	O	O	O	O	O	O	O	O
Level of seismicity	bridge:seismicity	O	-	-	-	-	-	-	-

Screening phase: selecting candidate physical impact models

This step of the procedure involves identifying a list of candidate physical impact models among a given set of seed options. The ideal resource for performing this task would be an extensive database of single-hazard and interacting multi-hazard physical impact models that account for multiple asset typologies consistent with the GED4ALL taxonomy. This type of database should include a search engine actioned by the GED4ALL taxonomy string and should be constantly and systematically updated with relevant advancements in the literature. Although this type of resource is not yet available, related research efforts are ongoing, particularly around storing relevant attributes (e.g., analytical vs numerical vs empirical) of physical impact models (e.g., Rossetto et al., 2015, for earthquake fragility and vulnerability, Galasso et al., 2021 for flood vulnerability), or producing harmonised data schemas that improve data interoperability within the different modules of a risk model (e.g., Murnane et al., 2019).

This screening phase of the procedure involves:

- Defining three fundamental parameters: asset location, asset taxonomy string, and considered hazards. To maximize the model search results, these parameters should be defined with different levels of refinement. For example, “location” may be defined as “Kathmandu”, “Nepal”, or “Asia”; “taxonomy string” may be defined using only level one GED4ALL attributes, or level one and two attributes combined, or also level three attributes; “hazards” may be considered singularly, in relevant pairs or in relevant triplets, etc.
- 1. Performing an automatic search in any available interactive database of physical impact models (with examples discussed below; and the ideal version of this database described above). This should be performed multiple times for any combination of refinement in the above three parameters, starting from their most-refined definitions. Each match encountered during these searches constitutes a candidate model.
- 2. Performing a manual search in any non-interactive available model compendium, literature review study, and regional/global models (with examples discussed below), as per point 1. Any match should be added to the candidate model list.
- 3. Performing a specific literature review for the most-refined definition of the three fundamental parameters that also account for specific user requirements (e.g., time-dependent models accounting for material ageing, specific IMs). This step maximizes the specificity of the matching models, whereas steps (2) and (3) maximize the number of matches;
- 4. Screen the candidate models to determine a subset to be ranked for quality in the subsequent phase. When screening, users should consider the possibility of developing ad-hoc adjustments to improve any given model. An example is to provide a modification coefficient to allow a physical impact model to consider an extra exposure parameter as an input (e.g., a height-dependent modifier to a model not accounting for building height, Selected physical impact models). The screening process is carried out according to three criteria: appropriateness of the damage scale (for fragility models) or the impact metric (for vulnerability and damage-to-impact models) concerning the considered application; the amount of extrapolation required to adopt a given model for the considered application; and the available documentation for a given model. The last criterion directly relates to the model scoring phase in the next step of the proposed procedure, which should avoid excessive guessing. Table 6 provides a set of example qualitative acceptance (i.e., screening) thresholds for the three criteria above, which can be modified appropriately according to user judgement for a considered application.

Table 6 Model screening criteria: minimum thresholds for acceptance [N_{ds} , R_{im} , N_{hp} are defined by the user; example values: $N_{ds}=1$, $R_{im}=20$, $N_{hp}=80$]

Screening criterion	Suggested acceptance threshold
Damage/impact appropriateness	Required DSs are defined (or N_{ds} DSs are missing). Required impact metric is modelled.
Required extrapolation	Required IM range is covered (or R_{im} % extrapolation needed)
Documentation	Documentation justifies N_{hp} % of the model's assumptions (e.g., damage scale, IM selection, fitting methods)

Available interactive databases of candidate models

GEM provides an online tool (platform.openquake.org/vulnerability/list, last accessed June 2022) for mapping a GEM2.0 building taxonomy string to different candidate empirical or synthetic physical impact (or structural capacity curve) models for earthquakes (Yepes-Estrada et al., 2016). Each model in the database is associated with a scientific publication and is classified according to geographical applicability, model typology (synthetic or empirical), adopted IM, etc. The tool also allows users to add more models to the database. A similar tool (vulncurves.eu-risk.eucentre.it, last accessed June 2022) related to physical earthquake vulnerability modelling (empirical or synthetic) of the European Seismic Risk Model, (ESRM20 Crowley et al., 2021, matches GEM3.1 building taxonomy strings to relevant physical impact models (and capacity curves) for European building classes. Stefanoiu et al., (2022) provide an online database (thebridgedatabase.com/existing-fragility-curves/, last accessed June 2022) of earthquake fragility relationships (mainly synthetic) for bridges that can be augmented with user input. Each bridge class is defined using an ad-hoc taxonomy. Each model is classified according to the model type (synthetic or empirical), adopted IM, DS thresholds, etc., and is associated with a scientific publication.

Alam et al. (2020) introduce the Cascadia lifelines program (CLiP) fragility function online database (clip.engr.oregonstate.edu, last accessed June 2022), which involves earthquake and tornado fragility relationships (empirical and synthetic) for a large set of lifeline assets within electric, water, wastewater, and transportation systems. Each model is classified similarly to that for the abovementioned databases, although CLiP adopts ad-hoc taxonomy strings. The fragility function manager (Silva et al., 2014) of the SYNER-G project (Systemic Seismic Vulnerability and Risk Analysis for Buildings, Lifeline Networks and Infrastructures Safety Gain, Pitilakis et al., 2014) is an MS Windows-based application for storing, visualising and managing earthquake fragility relationships (both empirical and synthetic). The database classifies assets based on the SYNER-G taxonomy (largely consistent with that of GED4ALL). It includes models for buildings, bridges, road infrastructure, oil and gas systems, and lifelines, including electric, water, and wastewater. To the best of the authors' knowledge, this is the only interactive database that includes time-dependent models for the corrosion-related ageing of bridges. The vulnerability module of the CAPRA (Central American Probabilistic Risk Assessment platform, CAPRA, 2012) software is an MS Windows-based application to create, visualize and compare new and existing multi-hazard vulnerability functions, expressed in terms of economic or human loss. The software uses a simple analytical methodology to obtain new vulnerability functions based on a few parameters. The software involves vulnerability functions for multiple hazards and assets classified according to an ad-hoc exposure taxonomy model

The flood damage model repository (Bombelli et al., 2021, github.com/mattrighetti/fdm-repository-backend, last accessed June 2022) provides a collection of 42 empirical flood physical impact models related to residential, commercial and industrial buildings, agricultural land, and transport infrastructure. Although the asset classes in the database are not associated with any specific exposure taxonomy strings, the considered models are classified according to different parameters, including their geographical applicability, flood type, model type (e.g., synthetic or empirical), and the adopted IM. The tool by RiskChanges (riskchanges.org/app/#/datamanagement/vulnerability, last accessed June 2022) comprises empirical and synthetic vulnerability relationships for multiple hazards and different asset types. This open database incorporates different single-hazard models (e.g., wind,

drought, fire, technological, earthquake, volcano), allowing users to input new models. To the best of the authors' knowledge, this is the only interactive tool collecting models for different asset typologies and different hazards. This database adopts an ad-hoc exposure taxonomy string and only includes a small number of models. Moreover, this database does not include multi-hazard fragility/vulnerability models.

Available non-interactive databases and model compendia

A short, non-exhaustive collection of physical impact model compendia and global models is herein provided. Rossetto et al. (2015) provide a compendium of empirical earthquake fragility and vulnerability relationships for different building classes worldwide (last updated April 2014; available at ucl.ac.uk/epicentre/resources/gem-vulnerability-databases, last accessed June 2022). Calvi et al. (2006) provides a review of nearly 100 synthetic and empirical earthquake fragility/vulnerability models developed over three decades. The European tsunami risk service provides a compendium of synthetic and empirical fragility curves for buildings subjected to tsunamis (github.com/eurotsunamirisk/etris_data_and_data_products, last accessed June 2022).

Regional- or global-level models provide consistent results across different asset classes, which is particularly desirable within risk models and could be considered within the proposed procedure. Moreover, these models will likely produce matches within the proposed screening procedure. A non-exhaustive list of these models is provided herein. Martins & Silva, (2021b) provide an analytical earthquake fragility and vulnerability model covering the most common building classes at a global scale. Among many others, some studies provide physical earthquake impact models for asset classes in Iran (Motamed et al., 2019), northeast India (Halder et al., 2020), Peru (Tarque et al., 2012), China (Tang et al., 2011), and Pakistan (Ahmad et al., 2018). The Joint Research Centre (JRC) of the European Commission produced a comprehensive global model of empirical flood depth-damage vulnerability functions for a variety of assets (Huizinga et al., 2017). The functions are available in a tabular dataset at publications.jrc.ec.europa.eu/repository/handle/JRC105688. The JRC functions were developed empirically using data from different continents (i.e., Europe, Asia, Africa) and considered residential, commercial and industrial occupancies. These functions can be readily adapted to provide local and regional loss estimations (e.g., Dabbeek et al., 2020). The HAZUS depth-damage regional vulnerability functions are accessible in an online package (CRAN.R-project.org/package=hazus, last accessed June 2022).

Scoring phase: selection of the most suitable model

For a given asset class, selecting the most suitable candidate model is ultimately a subjective decision of the user. Nonetheless, the selection process can be supported by a rational-yet-qualitative model scoring system based on key attributes related to the suitability of a given model.

This step of the proposed procedure enhances and combines different existing model scoring methods for single-hazard conditions and/or a single model typology. These methods provide criteria to evaluate the quality of asset-level physical impact models and are mainly focused on earthquakes. Porter (2011) proposes a scoring system for analytical or empirical earthquake fragility models based on five criteria (data quality, relevance, rationality, documentation, and overall quality) and four scoring levels (superior, average, marginal, or not applicable). Meslem et al. (2014) refined the previous scoring system for analytical earthquake fragility models. Rossetto et al. (2014) further generalised the approach by Meslem et al., (2014) for analytical and empirical earthquake fragility and vulnerability models. The resulting scoring system is based on ten criteria grouped into four categories: data quality, representativeness of a specific class, rationality (e.g., obeying first principles), and documentation quality. Finally, Alam et al., (2020) provide a two-step scoring system for earthquake and tornado fragility models of lifeline infrastructure. Based on a set of 16 criteria (related to regional applicability, IM, structural class, damage characterisation, data quality, analysis model and method,

fragility derivation), the system involves 1) eliciting a group of experts to score each criterion in terms of importance; and 2) aggregating the expert's responses to assign scores to each criterion.

Leveraging the above literature, this study proposes a scoring system for multi-hazard physical impact models related to different asset types and analysis methods. The adopted criteria are based on those in Rossetto et al. (2014) but incorporate the following enhancements: (1) generalisation for a multi-hazard scope; (2) removal of criteria already considered in the screening phase (e.g., documentation); (3) addition of some bespoke criteria (details to follow); and (4) grouping of criteria to facilitate the final scoring part of the proposed procedure. Given a set of candidate physical impact models, the scoring phase of the proposed procedure involves:

1. Scoring each candidate model against four suggested criteria: relevance, statistical refinement, model quality (defined differently for empirical or synthetic models), and user-defined requirements. Each criterion involves one or more attributes, which should be qualitatively scored "high", "medium", or "low" according to the scheme described in Table 7. The "relevance" criterion involves the "geographical area" attribute, which captures the representativeness of a given model for a given area, "asset characteristics", which considers how the parameters of the asset's structural details, materials, and geometry within the model reflect those required for the considered asset class, and "IM", which is related to the sufficiency and efficiency of the adopted IM(s). The "statistical refinement" criterion involves the "uncertainties" attribute, related to the refinement of the treatment of uncertainty for a given model, and "first principles", which accounts for any functional inconsistency in the model (e.g., crossing of fragility functions for different DSs; unreasonably large/small maximum value of the impact metric of a vulnerability function). For empirical models, the "model quality" criterion includes the attributes "impact observations" and "IM observations" that are related to the level of error/bias involved in the fitted data, "constrained asset class" that captures how well the fitted data is suited to a single asset class, and "data quantity", which involves the number of IM vs damage/impact observations used to fit the model. For synthetic models, this criterion involves "fidelity to mechanics", which captures how well an analytical/numerical model reflects the mechanics of an asset subjected to one or multiple hazards, and "aggregation level", which reflects the level of sophistication involved in the model (e.g., asset- vs component-level models). The attribute (and criterion) "user-defined requirements" reflects the level of compliance of the selected model with a set of user-defined features (e.g., time/state dependency, consistency of model assumptions across different asset classes). Note that although the model typology (e.g., synthetic vs empirical) can generally be considered a user-specific requirement, it can also be indirectly related to other requirements (e.g., no time-dependent empirical models are available, and therefore a synthetic model must be selected). Any attribute related to IMs should be disregarded when scoring damage-to-impact models. This set of criteria and attributes are suggested based on the available literature information and engineering judgement of the authors. Consistent with the spirit of this selection procedure, users are encouraged to add or remove specific criteria/attributes according to their specific needs.
- Each criterion has a prescribed weight. The analytic hierarchy process (AHP; Saaty, 1980) is used to produce a mathematically consistent definition of the weights, which has already been successfully applied to engineering decision-making problems (e.g., Gentile & Galasso, 2020). According to this procedure, the user expresses an opinion on every possible pairwise comparison among the criteria. Each opinion quantifies how much criterion *j* is more/less important than criterion *k*. The results of the comparisons constitute a decision matrix. The desired weights are proportional to the first eigenvalue of this matrix. Further details can be found in Saaty (1980). The suggested weights for the criteria are 25% for "relevance", 15% for "statistical refinement", 40% for "model quality", and 20% for "user requirements". However, users are encouraged to apply AHP for their specific circumstances to derive case-specific weights.

- Given the adopted weights, scoring of the available models is carried out according to the technique for order preference by similarity to an ideal solution, or TOPSIS (Hwang & Yoon, 1981). This procedure has been deemed suitable for engineering decision-making problems (e.g., Caterino et al., 2009). First, the user scores each candidate model against the four criteria (using the qualitative scores “low, medium, or high”). The score assigned to a given criterion is the minimum score obtained for all of its attributes (e.g., the minimum score among the attributes “fidelity to mechanics”, and “aggregation level” quantify the score of the “model quality” criterion for synthetic models. For example, this approach penalizes a refined component-by-component numerical model that neglects relevant damage mechanisms and/or impact sources). To be used as an input of TOPSIS, these qualitative scores should be expressed as numerical values. Alternatively, triangular fuzzy numbers may be used in a qualitative TOPSIS approach (Afsordegan et al., 2016). It is herein suggested to use 1, 2, and 3, respectively, for low, medium, and high. However, users are encouraged to test the sensitivity of the final result to these values and alter them if required. The weighted scores for a given criterion are used to define the ideal best and worst models, and the most suitable model maximizes a trade-off between the distances from the ideal worst and best models, Saaty (1980).

Table 7 Model scoring system: definition of scores for each attribute. [ATT, OBS₁, OBS₂, OBS₃, bins₁, bins₂, obs₁ are defined by the user; example values: ATT=4, OBS₁=20, OBS₂=200, OBS₃=20, bins₁=5, bins₂=10, obs₁=20]

Criterion: Attribute	Score	Description
<u>Relevance:</u> Geographical area	High Med Low	Model defined for the required city (e.g., Kathmandu) Model defined for the required country (e.g., Nepal) Model defined for the required region (e.g., South Asia)
<u>Relevance:</u> Asset characteristics	High Med Low	Model matching structural detailing, geometry, and materials parameters appropriate for the asset class Geometry and materials parameters appropriate for the asset class, structural details inappropriate or unavailable Materials params. appropriate for the asset class, geometry and structural details inappropriate or unavailable
<u>Relevance:</u> IM	High Med Low	Adopted IM(s) clearly sufficient/efficient for the required application - Adopted IM(s) clearly not sufficient/efficient for the required application
<u>Statistical refinement:</u> Uncertainties	High Med Low	Appropriate assumptions. Goodness of fit demonstrated. Aleatory (and possibly epistemic) unc. considered Appropriate assumptions. Inappropriate aleatory unc. considered Inappropriate assumptions (e.g., unsound statistical distributions)
<u>Statistical refinement:</u> First principles	High Med Low	Physically sound models (e.g., fragility curves for different DSs not crossing; reasonable maximum) Minor first-principle issues (e.g., fragility curves for different DSs cross outside required IM range) Relationships not physically sound (e.g., fragility curves for different DSs cross)
<u>Model quality (empirical):</u>	High Med	Damage scales/impact measures clearly defined. Negligible non-sampling errors (see Development and statistical fitting of physical impact models)

Impact observations	Low	Damage scales/impact measures clearly defined. Non-sampling errors treated with unchecked assumptions. Damage scales/impact measures ambiguously defined (e.g., two assessors may assign different DSs for the same situation). Non-sampling errors not reduced
<u>Model quality (empirical):</u> IM observations	High Med Low	IM data directly measured or estimated accurately. IM data predicted-vs-true error investigated - IM data directly measured or estimated inaccurately. IM data predicted-vs-true error not investigated
<u>Model quality (empirical):</u> Constrained asset class	High Med Low	Empirical dataset filtered using asset class definition according to GED4ALL, or with similar attributes Asset class defined as per "High", but some aggregated attributes (e.g., different heights considered together) Asset class defined with less than <i>ATT</i> attributes
<u>Model quality (empirical):</u> Data quantity	High Med Low	Continuous functions: more than OBS_2 observations; min $bins_2$ IM bins; min obs_2 observations per IM bin. Discrete functions: more than OBS_2 observations; min obs_2 observations per IM bin Continuous functions: between OBS_1 and OBS_2 observations; between $bins_1$ and $bins_2$ IM bins; min obs_2 observations per IM bin. Discrete functions: min obs_1 observations per IM bin Continuous functions: less than OBS_1 observations; less than $bins_1$ IM bins Discrete functions: less than OBS_3 observations
<u>Model quality (synthetic):</u> Fidelity to mechanics	High Med Low	State-of-the-art. All relevant damage mechanisms/impact sources considered. Sound parameter characterisation Minor simplifications of relevant mechanics (e.g., less-relevant damage mechanisms/impact sources neglected). Sound parameter characterisation Major simplifications of relevant mechanics (e.g., fundamental damage mechanisms/impact sources neglected). Unsound parameter characterisation (e.g., excessive strength assumed for a key structural member)
<u>Model quality (synthetic):</u> Aggregation level	High Med Low	Calibrated using component-by-component analysis. Each component modelled explicitly Calibrated using subcomponent analysis (e.g., aggregating components at the same building storey) Asset-level model. Aggregating all sources of damage or impact
<u>User-specific requirements</u>	High Med Low	Model exactly reflects all the user requirements Model not complying with minor user requirements (e.g., required time dependency not covered) Model not complying with major user requirements (e.g., required state dependency not covered)

Development and statistical fitting of physical impact models

This step of the proposed procedure involves situations in which, because of model availability and the specific minimum requirements set by the user, it is impossible to find a suitable physical impact model

for a particular asset class of interest at the screening phase. In this case, suitable methods can be employed to develop the required model based on existing empirical information (i.e., observed damage and/or impact data from past hazard events), synthetic data derived from analytical or numerical models, or expert judgement. After collecting or synthetically generating the required data, statistical approaches are used to fit relevant mathematical functions (see Mathematical definitions) to the data. The proposed procedure does not involve scoring the developed physical impact models. However, a modelling approach should be selected carefully considering the scoring criteria defined above, emphasising the minimum modelling and user-specific requirements. This Section mainly focuses on empirically- and synthetically derived functions, with no intention of providing a thorough review of modelling approaches for different assets and hazards. Expert-judgement approaches are briefly discussed at the end.

Model development

Empirical physical impact models require collecting data on previous observations of natural-hazard physical impacts. Sources of these data include post-event surveys conducted by reconnaissance teams or through remote sensing techniques, tax assessor or insurance claims data, and experimental testing. Examples of related datasets include: the GEM earthquake consequence database ([GEMECD](#), last accessed June 2022), the emergency events database ([EM-DAT](#), last accessed June 2022), the USA National Oceanic and Atmospheric Administration ([NOAA](#), last accessed June 2022) database, and Earthquake Engineering Research Institute ([EERI](#), last accessed June 2022) reconnaissance data. For each asset in a portfolio, the datasets generally include: 1) the IM level (for fragility and vulnerability); 2) the DS (for fragility and damage-to-impact) and/or the impact (for vulnerability and damage-to-impact); and 3) exposure taxonomy attributes of the assets. Provided enough data is available, empirical models are considered the most credible since they are derived based on actual observations. However, the quality of an empirical database may be jeopardised (e.g., Baker, 2013) by the size and/or statistical representativeness of the sample (i.e., sampling errors). The empirical data need to comprise an unbiased (random) collection of observations in each DS (or across all impact values) of interest that are documented using a consistent reporting protocol. These data can be affected by various non-sampling errors, which may involve: under-coverage errors; inaccurate measurements/estimations of the IM (Lallemant et al., 2015); ambiguous definition of DSs; incomplete definition of the asset classes; and inexperience of the survey teams. Rossetto et al. (2014) describe these error types in the context of earthquake physical impact modelling. However, empirical models are derived similarly (and the same related challenges are encountered) for any hazard.

Synthetic physical impact models are derived from analytical or numerical modelling of the mechanical response of an asset to one or more hazards of interest. The mechanical modelling required depends on the type of mechanical response and, therefore, the specific asset and hazard of interest. The considered asset class is generally represented by one or more archetype (or index) assets (e.g., D'Ayala et al., 2013). These archetypes are characterised in detail by considering the specific geometry (e.g., the height of each pier in a bridge), material properties (e.g., steel yield stress), and relevant structural details (e.g., wall-to-roof connection, relevant for wind fragility). A synthetic model is then generally used to calculate an EDP for a set of hazard loadings with different IM levels. The selected EDP must be representative of the damage levels associated with the considered asset and hazard combination, i.e., it should be possible to associate mechanics-based thresholds of the EDP to different DSs. Different combinations of assets and hazards can produce different damage mechanisms, which are captured to varying degrees by different EDPs. For example, peak EDPs (e.g., maximum displacement, maximum force) tend to be appropriate when the history of the hazard excitation may be disregarded (e.g., single earthquakes, tsunamis, landslides). Cumulative parameters (e.g., number of vibration cycles, hysteretic dissipated energy) are instead more appropriate for capturing progressive damage induced by high-cycle fatigue (e.g., wind-induced vibrations involving a large number of low-amplitude cycles; e.g., Thomas et al., 2022) or cumulative damage (e.g., earthquake sequences, earthquake-tsunami sequences, affecting the asset in a pre-damaged condition; e.g.,

Gentile & Galasso, 2021b). Using these EDPs may be challenging in practice due to the unavailability of corresponding DS scales (e.g., an earthquake damage scale based on deformation is readily available, while obtaining an energy-based one requires further modelling, Gentile & Galasso, 2021b). For each considered level of IM, the user identifies a set of hazard records to which the asset is subjected (e.g., ground-acceleration time series for earthquakes, velocity and depth time series for tsunami or landslides, wind speed time series), calculates the EDP and estimates the associated DS.

Synthetic models can be used to develop impact data for vulnerability fitting by combining asset-level fragility functions fit using synthetic damage data (see below) with empirical damage-to-impact models (Mathematical definitions). More refined approaches (e.g., FEMA P58 for earthquakes; FEMA (2012) combine synthetic analysis response results with pre-determined component-level fragility and vulnerability relationships to produce asset-level vulnerability models. For some hazards, it is not yet possible to model the response and damage physics of each asset component, which means that it is not reasonably simple to estimate EDP values or EDP thresholds that can be linked to different DSs (i.e., EDP-DS relationships). For instance, in the case of floods, different asset components (e.g., a carpet versus industrial machinery) show remarkably different damage mechanisms for a given combination of water depth and flood duration (e.g., carpet damage is related to chemical processes, whereas industrial machinery damage is related to electric/electronic processes), which makes it challenging to define EDP-DS relationships on a component-by-component basis. Nofal and van de Lindt (2020) have recently overcome this challenge using empirical data (water depth, flood duration, economic impact) to define component-level DSs by identifying their depth and duration resistance for different DSs (expressed as ranges of economic loss). They then follow a simulation-based approach to develop component-based fragility and vulnerability curves (surfaces), which are subsequently converted to building fragility and vulnerability curves (surfaces).

Expert-judgement-based functions are used in the absence of observed data from past events and/or a combination of computational resources and modelling skills for conducting relevant numerical analyses. These functions can be derived, for instance, using the Delphi Process (Dalkey, 1969), which requires several experts to provide educated guesses of the damage (or loss) that would occur to a specific asset class when subjected to a prescribed magnitude of a hazard IM. The judgement can then be weighted according to the expert's experience level to produce a physical impact model. This process requires thoughtful vetting of the participants. It will most likely lead to an underestimation of uncertainty, given the well-known tendency of experts to have overconfidence in their opinions (Baker, 2013; Porter, 2021, sloanreview.mit.edu/article/managing-overconfidence). The subjectivity of the weightings can also amplify inaccuracies in the models obtained. Due to the above issues, this approach to fitting physical impact models is not recommended for use within the proposed procedure and is not discussed further.

Model fitting

For fragility function fitting, the underlying empirical or synthetic data can be expressed in two different formats, which are broadly classified as "actual" or "bounded" (Porter et al., 2007). "Actual" data refers to cases in which an asset has actually reached (or exceeded) the DS of interest at a known value of hazard IM and are analogous to the results obtained in an incremental dynamic analysis that is used to determine a structure's earthquake collapse capacity (Baker, 2015). "Bounded" data refers to cases in which only the largest value of hazard intensity reached is known and whether or not the DS of interest was exceeded at (or below) that intensity level and are comparable to the results obtained using a multiple stripes approach for determining earthquake collapse capacity (Baker, 2015). On the other hand, empirical or analytically derived consequence data for vulnerability function and probabilistic damage-to-impact model fitting is continuous (by definition). Across all three data contexts, function fitting can be achieved through a maximum likelihood approach, which -given a prescribed functional form (see Mathematical definitions) that can be multivariate in the case of vector-valued impact models (Dottori et al., 2016)- computes the corresponding parameters of the model with the highest likelihood of producing the data that were observed. Goodness-of-fit measures

(e.g., minimum Akaike information criterion, cross-validation; see Lallemand et al., 2015) can then be employed to distinguish the best model for the underlying data if several functional forms are available for consideration.

For synthetic derivations of fragility functions, it may be important to consider how the structural response analysis is carried out. For instance, it has been demonstrated (Baker, 2015) that analysing the earthquake collapse probabilities of structures using the multiple stripes approach (Jalayer, 2003) produces more efficient (site-agnostic) fragility models than those obtained from incremental dynamic analysis (Vamvatsikos & Cornell, 2002). Furthermore, the choice of IMs used in the fragility function is crucial. For instance, Kohrangi et al. (2017) found that an IM consisting of a geometric mean of multiple spectral accelerations is relatively more sufficient and produces significantly more efficient earthquake fragility functions than a single-period first-mode spectral acceleration value. A more detailed discussion on challenges and issues to consider with synthetic fragility/vulnerability modelling is found in (Silva et al., 2019), which specifically refers to earthquakes but is broadly applicable across any hazard context. Empirical data collection challenges and related errors can negatively affect the derivation of empirical physical impact models, for example leading to biased fits (e.g., Baker, 2013; Lallemand et al., 2015).

2.2.4 Conclusions

This section has described a structured methodology for characterising the multi-hazard physical impact modelling of a portfolio of assets across an urban system. Given a set of relevant hazards for any selected case-study region, the methodology involves 1) mapping the relevant asset classes (i.e. construction types) in a considered area to a set of existing candidate fragility, vulnerability, and/or damage-to-impact models, also accounting for any specific modelling requirements (e.g., models with consistent assumptions valid for multiple classes, time dependency, multi-hazard interaction); 2) scoring the candidate models according to relevant criteria to select the most suitable ones; or 3) using state-of-the-art numerical and/or empirical methods to develop fragility/vulnerability models not already available, supplementing existing models.

The main goal of this procedure is to provide a framework that facilitates the consistent selection of a set of candidate physical impact models to use within risk modelling applications. This selection is based on a rigorous evaluation that considers criteria related to the accuracy, computational complexity, data requirements, and specific user requirements of a risk model. Future repeated applications of the procedure will allow a refinement of the suggested values for all the relevant input parameters (e.g., specific criteria, threshold values for screening, scoring schemes, and weights). The proposed methodology facilitates effective characterisation of the multi-hazard, time-dependent physical impact modelling of a portfolio of assets, which is particularly useful in future-looking (risk-informed urban planning) contexts.

2.3 Methodologies of impact and risk models employed in this work.

This chapter provides the key components for a Class 1 “Basic Risk Screening” assessment of the taxonomy introduced in Section 2.1. Its primary objective is to define and quantify the physical vulnerability of the built environment under multiple hazards (e.g., earthquakes, floods). Specifically, the chapter: (i) establishes an asset taxonomy, (ii) identifies key structural typologies specific to each demo city, and (iii) selects the best candidate models to represent damage mechanisms and performance under diverse hazard scenarios, using the methodology presented in Section 2.2.

Adopted taxonomy of assets

We establish a taxonomy of assets, based on the Multi-Hazard GEM (Global Earthquake Model) taxonomy (Silva et al., 2022), to provide a standardized foundation for describing and classifying assets. For example, in the case of buildings, this taxonomy builds on 14 attributes described below (see Figure 9):

- **Direction.** The orientation of the lateral load resisting system in two principal horizontal directions of the building plan, which are perpendicular to one another.
- **Material of the lateral load resisting system.** The material of the structural members that resist lateral loads or deformations, for example masonry or wood.
- **Lateral load resisting system (LLRS).** The structural system that provides resistance against lateral loads or deformations through vertical and horizontal structural components, for example walls or moment frames.
- **Height.** Building height above ground expressed as the number of stories, for example three stories. This attribute also includes the number of basements, if any, and the ground slope.
- **Date of construction or retrofit.** The year when the building was constructed. If parts of the building differ in age, the earliest date is used. If the structure was retrofitted in a way that improves seismic performance, the retrofit year is reported instead of the construction year.
- **Occupancy.** The building use or activity. A wide range is possible, for example residential uses can include informal housing as well as high rise apartment buildings.
- **Shape of the building plan.** The geometric shape of the building in plan, for example L shape or rectangular shape. The position of a building within a block, for example a detached building is not attached to any other building.
- **Structural irregularity.** A feature of the structural arrangement that produces a known vulnerability during an earthquake, for example a story that is much taller than the others, an irregular plan, or a change of system or material. Because a building can have more than one irregularity, the user can identify a primary and a secondary irregularity.
- **Ground floor hydrodynamics.** Refers to the amount of openings in the ground floor, which are relevant for accessing flood and tsunami risk associated with a building.
- **Exterior walls.** The material of the exterior enclosure, for example masonry or glass.
- **Roof shape.** The roof shape, the material of the roof covering, the structural system that supports the roof covering, and the roof to wall connection. For example, the roof shape may be pitched with gable ends, the covering may be tile, and the system may be a wooden roof structure with light infill or covering.
- **Floor system material.** The floor material, the floor system type, and the floor to wall connection. For example, the floor material may be concrete, and the floor system may be a cast in place beamless reinforced concrete slab.
- **Foundation system.** The part of the construction where the base of the building meets the ground and transmits loads to the soil. For example, a shallow foundation supports walls and columns on hard soils, while a deep foundation is used on soft soils.
- **Fire protection.** Information on a building's fire-resistance rating.

Depending on the available information and the desired level of detail, each attribute may be specified with up to three levels (see Figure 9). Level 1 is shown in blue, Level 2 in purple, and Level 3 in yellow. Some attributes use all three levels. For Structural irregularity, Level 1 indicates the irregularity type (plan or vertical), Level 2 identifies the primary irregularity, and Level 3 identifies the secondary irregularity. The taxonomy is flexible and permits adding new attributes or modifying existing options. Each building or building class is described by a unique taxonomy string, an alphanumeric code that functions as the asset's DNA by collecting the information needed to classify performance under multiple hazards. Each option has a unique identifier. When information for an attribute or a level is not available, use the entry 99. Attributes are listed in the order shown in Figure 9 and are separated by a slash. A plus sign is used to add additional levels of detail for a given attribute. In some cases, a numeric value is appended, for example the number of stories to represent height.

Ged4ALL also has taxonomy description for assets different to buildings, this can be found in Silva et al., (2018).

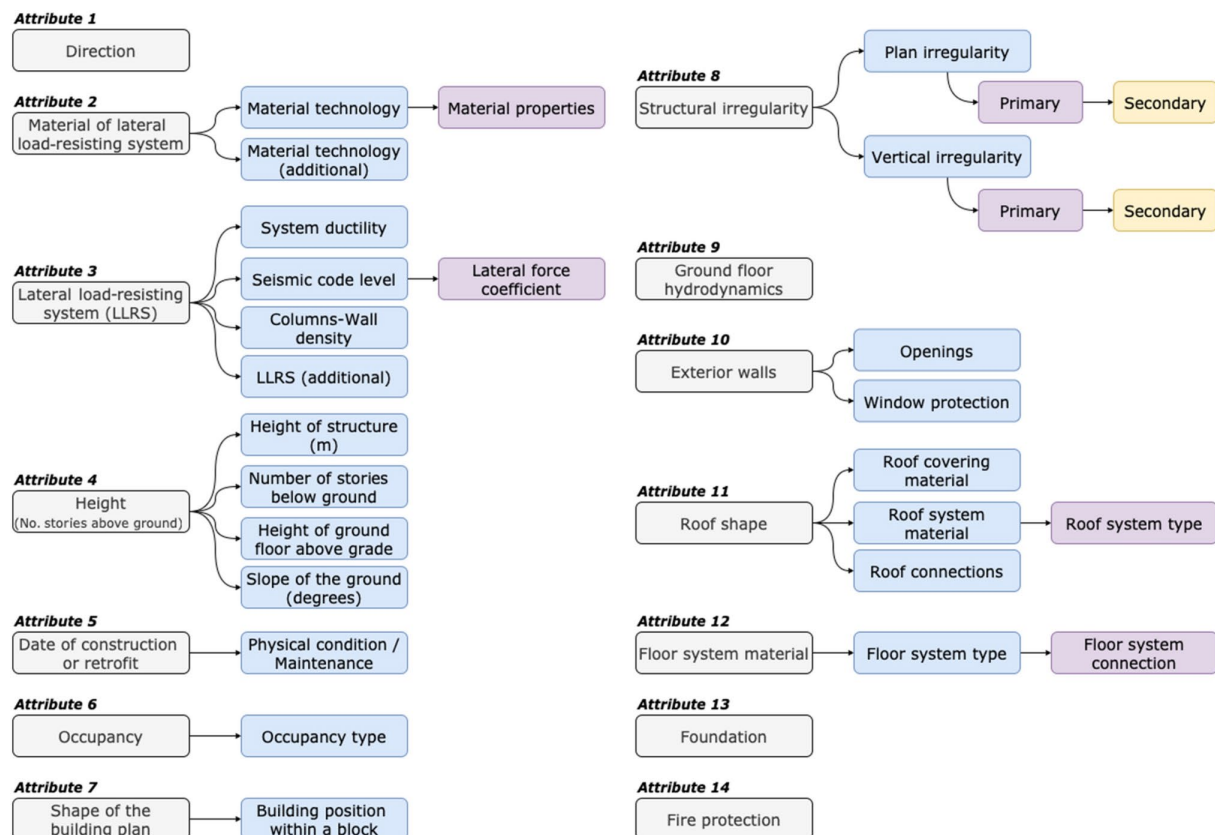


Figure 6 Ged4ALL attributes for describing buildings (taken from Silva et al., 2022).

Assets included

This subtask identifies and classifies the critical assets considered in the assessment, including residential buildings and essential infrastructure. The selection is based on their relevance to community functionality, exposure, and socio-economic importance.

Selection of the best candidate vulnerability and/or fragility model

This step evaluates existing vulnerability and fragility models and selects the most suitable candidates for the demo cities following section 2.2 recommendations. The selection criteria include data availability, hazard compatibility, and scalability.

2.3.1 Dublin, Ireland

Ringsend is an inner suburb in the south of Dublin, Ireland. It lies on the south bank of the River Liffey and to the east of the River Dodder, about two kilometres east of the city centre. It forms the southern end of the East Link Toll Bridge. Ringsend includes the southern area of the Dublin Docklands and, to the west, the South Lotts district and part of Grand Canal Dock. Neighbouring areas include Irishtown, Sandymount, and the Beggars Bush part of Ballsbridge to the south, with the city centre to the west. A community-defined outline of Ringsend, drawn by participants during the Dublin “walk shop,” is shown in Figure 10.



Figure 7 Ringsend suburb, as defined by the community.

Building Inventory

Using data collected by IES Ltd. as part of Work Package (WP) 5, Table 10 summarises building statistics for the area. From a physical and social risk-assessment standpoint, the assets relevant to this analysis are single-family and multi-family residential buildings. Table 10 describes the main characteristics of these types of buildings. Based on the histograms in Figure 11 and the results in Table 10, single-family buildings are predominantly 1–2 storeys with a typical storey height of 3.2 m. In contrast, multi-family buildings are mostly four storeys and show an even distribution from 5 to 8 storeys, with a similar 3.2 m storey height.

Table 8 Ringsend Building inventory statistics.

Building type	Group Count	Median number of storeys (m)	Median storey height (m)	Median building height (m)
dining, cafeteria, fast food	1	2	3	7.6
multi-family	72	4	3.2	12.8
office	912	1	5	5
parking garage	32	1	5	5
performing arts theater	1	1	5	20
religious building	4	1	5	5
retail	40	1	5	5
school or university	24	1	5	5
single-family	2771	2	3.2	6
sports arena	2	4	4	13
town hall	10	1	5.5	11.3
transportation	2	2	3	6

warehouse	302	1	5	5
workshop	122	1	5	5

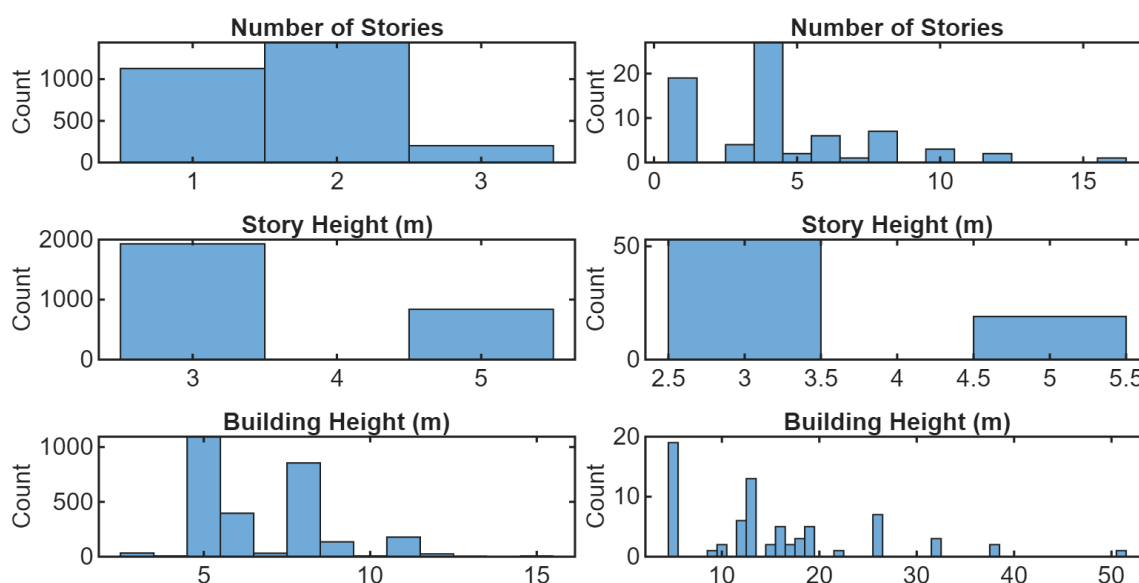


Figure 8 Histograms of attributes for single-family (left) and multi-family (right) residential buildings in Ringsend.

Proposed building types

From an energy perspective, residential buildings were classified by year of construction (see WP5 for details): pre-1900, 1900–1930, 1950–1966, 1978–1982, 1994–2004, and 2004 or later, for a total of 6 categories. We apply these categories to both single-family and multi-family residential buildings. A description of the materials used in single-family and multi-family residential buildings, based on IWU (2011) and complemented with Yepes-Estrada et al., (2023), is provided in Table 11.

Table 9 Materials by building type in Ringsend (based on IWU, 2011)









Building types	Number of stories	Material	
		Walls	Floor/Roof
Pre 1900	1		
	2	Stone, mass concrete / 325mm solid bricks/ concrete hollow blocks	Reinforced concrete / light frame timber
	more than 2		
1900-1930	1	225 mm solid bricks	Reinforced concrete / light frame timber
	2	225 mm solid bricks / 325 mm solid bricks	Reinforced concrete, light frame timber / light frame timber
	more than 2		






1950-1966	1	Concrete hollow blocks	Reinforced concrete, light frame timber / light frame timber
	2	Concrete hollow blocks / 300 mm cavity wall (concrete hollow block + solid bricks)	Reinforced concrete / light frame timber
	more than 2	225 mm solid bricks / 300 mm cavity wall (concrete hollow block + solid bricks)	Reinforced concrete
1978-1982	1		
	2	300 mm cavity wall (concrete hollow block + solid bricks)	Reinforced concrete / light frame timber
	more than 2	225 mm solid bricks / 300 mm cavity wall (concrete hollow block + solid bricks)	Reinforced concrete / light frame timber
1994-2004	1	300 mm cavity wall (concrete hollow block + solid bricks) / light frame timber	Reinforced concrete / light frame timber
	2	300 mm cavity wall (concrete hollow block + solid bricks) / light frame timber	Reinforced concrete / light frame timber
	more than 2	300 mm cavity wall (concrete hollow block + solid bricks)	Reinforced concrete
After 2004	1		
	2	300 mm cavity wall (concrete hollow block + solid bricks) / light frame timber	Reinforced concrete / light frame timber
	more than 2	Reinforced concrete, 300 mm cavity wall (concrete hollow block + solid bricks)	Reinforced concrete/ light frame timber

To define the building types in Ringsend, Ireland, we conducted a Google Street View review and an on-site walk-through. From these observations, we identified 14 building types, categorized by year of construction, residential use (single- or multi-family), and number of storeys. The residential building types are summarised in Table 12 (single-family) and Table 13 (multi-family).

Table 10 Single-family building types used in this study for Ringsend.

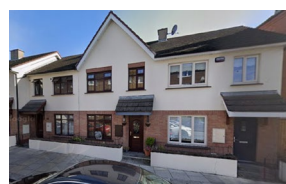
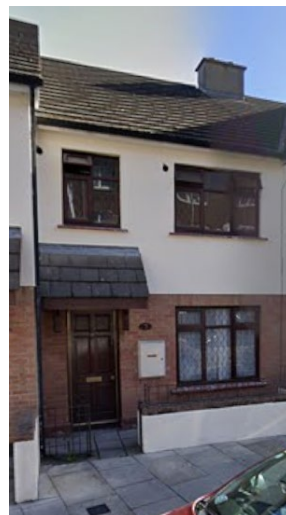
Building types	Single-family 1-story	Single-family 2-story
----------------	-----------------------	-----------------------

Pre 1900	-	
1900-1930	 	  
1950-1966		

		
1978-1982		   

1994-2004

-





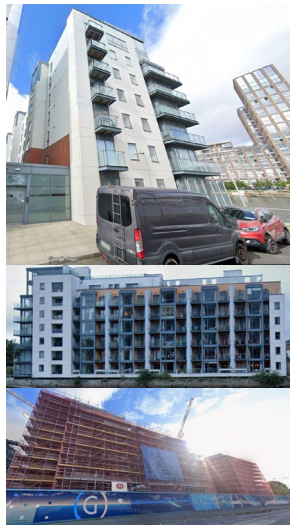
After 2004	-	
------------	---	---

Table 11 Multi-family building types used in this study for Ringsend.

Building types	Multi-family storeys 3–4	Multi-family storeys 5–6	Multi-family +7 storeys
Pre 1900	-	-	-
1900-1930	-	-	-
1950-1966		-	-
1978-1982	-	-	-

1994-2004		-	-
After 2004			

Finally, following the GED4ALL taxonomy for asset characterization (Silva et al., 2022), Table 14 presents the taxonomy strings to identify candidate fragility/vulnerability models.

Table 12 GED4ALL Taxonomy for buildings in Ringsend

Building types	Number of stories	Taxonomy
----------------	-------------------	----------

Pre 1900	1	
	2	MUR+ST/LWAL+CDN/HBET:2/RES MUR+MC/LWAL+CDN/HBET:2/RES MUR+CL/LWAL+CDN/HBET:2/RES MUR+CB/LWAL+CDN/HBET:2/RES
	more than 2	
1900-1930	1	MUR+CL/LWAL+CDN/HBET:1/RES
	2	MUR+CL/LWAL+CDN/HBET:2/RES
	more than 2	
1950-1966	1	MUR+CB/LWAL+CDL/HBET:1/RES
	2	MUR+CB/LWAL+CDM/HBET:2/RES MUR+CL/LWAL+CDM/HBET:2/RES
	more than 2	MUR+CL/LWAL+CDL/HBET:3-4/RES
1978-1982	1	
	2	MUR+CB/LWAL+CDM/HBET:2/RES MUR+CL/LWAL+CDM/HBET:2/RES
	more than 2	
1994-2004	1	MUR+CB/LWAL+CDM/HBET:1/RES MUR+CL/LWAL+CDM/HBET:1/RES W/LWAL+CDL/HBET:1/RES
	2	MUR+CB/LWAL+CDM/HBET:2/RES MUR+CL/LWAL+CDM/HBET:2/RES W/LWAL+CDL/HBET:2/RES
	more than 2	MUR+CB/LWAL+CDM/HBET:3-4/RES MUR+CL/LWAL+CDM/HBET:3-4/RES
After 2004	1	
	2	MUR+CB/LWAL+CDH/HBET:2/RES MUR+CL/LWAL+CDH/HBET:2/RES W/LWAL+CDL/HBET:2/RES
	more than 2	CR/LFINF+CDH/HBET:3-10/RES CR/LWAL+CDH/HBET:3-10/RES

Selection of the best candidate models

Based on the OpenVulnerability web tool (Gentile, 2025) and the selection and method outlined in Scoring, selecting, and developing physical impact models for multi-hazard risk assessment. (Gentile et al., 2022), we assessed candidate models for the Ringsend, Ireland case study, building classes.

Following this review, only one model met the inclusion criteria: the Global Flood Model for Europe by Huizinga et al. (2011). We therefore adopted this model as the basis for our analysis. The corresponding vulnerability function, expressed in terms of economic losses, is provided in Table 15 and Figure 12.

Table 13 Candidate vulnerability model (based on Huizinga et al., 2011)

Water depth (m)	Economic loss
0.0	0.00
0.5	0.25
1.0	0.40
1.5	0.50
2.0	0.60
3.0	0.75
4.0	0.85
5.0	0.95
6.0	1.00

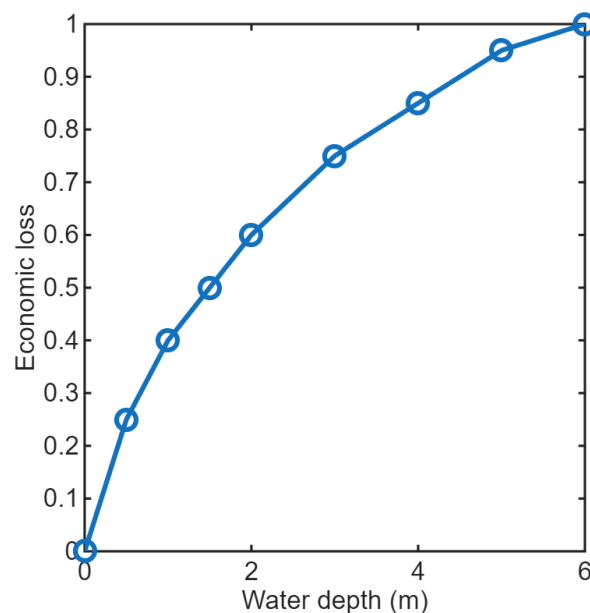


Figure 9 Proposed candidate vulnerability model (based on Huizinga et al., 2011)

According to Yepes-Estrada et al. (2023), Table 16 presents the average replacement cost (USD) for residential buildings in Ireland as a function of building floor area. These costs include contents, non-structural, and structural components.

Table 14 Average replacement cost (based on Yepes-Estrada et al., 2023)

Taxonomy	Replacement Cost USD/m ²
MUR+CL/LWAL+CDN/H BET:1-4/RES	1763.93
MUR+ST/LWAL+CDN/H BET:1-4/RES	1770.98
CR/LFINF+CDN/HBET:4- 10/RES	1970.55
CR/LWAL+CDN/HBET:4 -10/RES	1970.53
W/LWAL+CDL/HBET:1- 2/RES	1746.23

2.3.2 Patras, Greece

Patras is the third largest city in Greece with a population of approximately 250.000 inhabitants. It is a coastal city situated in the western part of the country, in the Region of Western Greece and comprises the southern European case study for the Minority Report project. Patras represents a Mediterranean city characterized by a diverse building stock, complex terrain, and a combination of urban and peri-urban environments that make it an ideal context for assessing multi-hazard physical vulnerability. The area of interest is the greater municipality of Patras and more specifically the surrounding northern suburbs, including Rio, where the University of Patras (UPAT) campus is situated.

More specifically, Patras pilot site, shown in Figure 13 with the highlighted red-shaded border, includes mixed-use infrastructure, combining residential, commercial, educational, and administrative buildings within close proximity. Within the examined area, that covers an approximately 13km long corridor from the urban area to the northern suburbs, are located buildings that share distinct characteristics. The urban area exhibits a high concentration of mid-rise reinforced concrete (RC) frame buildings constructed between the 1960s and the 2000s, complemented by a smaller number of masonry structures and modern energy-efficient buildings from the last two decades. Suburban areas such as Rio and Aktaio are characterized by low-density housing—primarily two- to three-storey detached or semi-detached dwellings—often designed without uniform planning control, leading to variable construction quality and exposure.

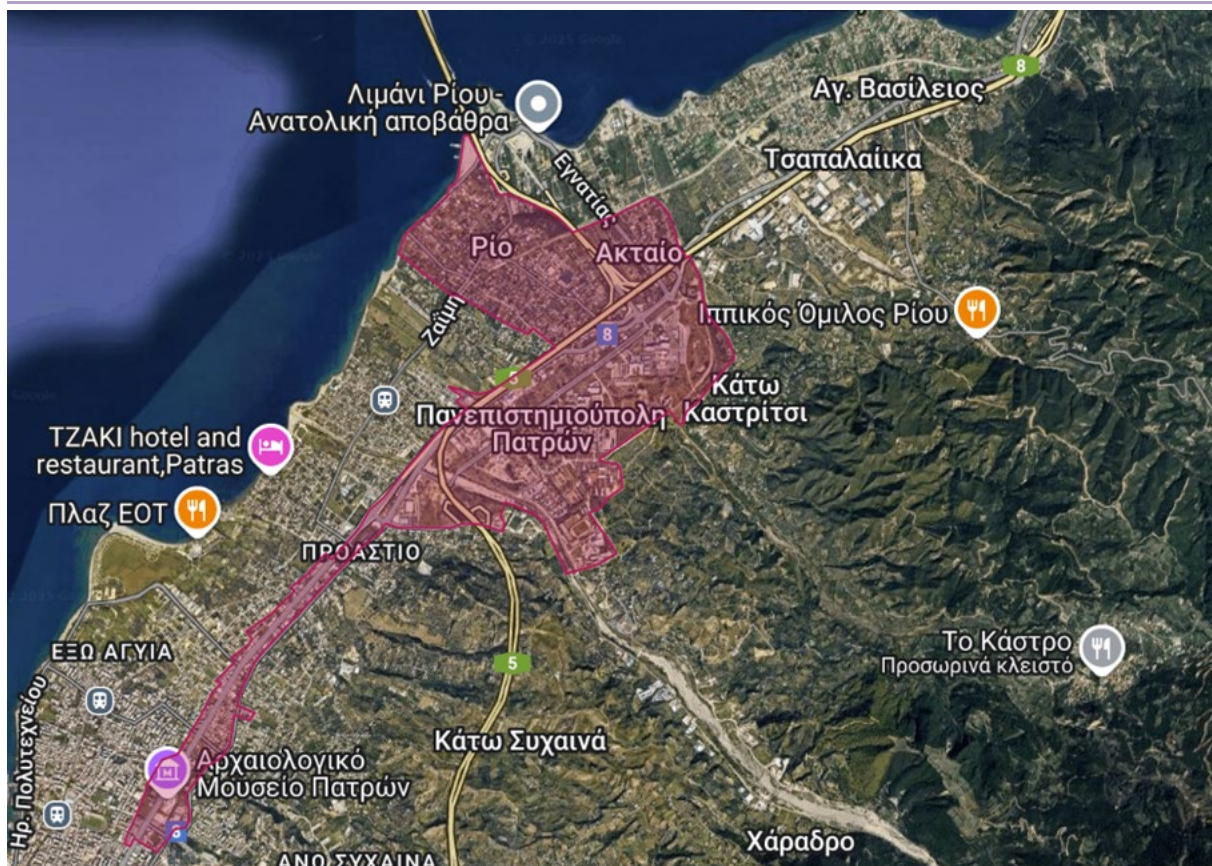


Figure 10 Patras Pilot Site. The red shaded area represents the borders of the examined site.

Moreover, in the northern part of the city are located the University of Patras campus and the adjacent University Hospital of Patras, which form a distinct and strategically important sub-area within the pilot site. The University Campus comprises over 60 buildings while the hospital consists of several interconnected multi-storey buildings accommodating emergency units, operating theatres, and medical laboratories. These institutional facilities are predominantly medium- to large-scale structures (3–6 storeys) constructed between the 1970s and early 2000s, featuring flat roofs, infilled frames, and irregular plan geometries. Their critical societal role and continuous-operation requirements make them priority assets for assessing seismic, flood hazard vulnerabilities.

The built environment of Patras has been shaped by rapid urbanization following the 1965 earthquake sequence and subsequent economic growth. These buildings often exhibit irregular configurations and varying levels of maintenance.

From a hazard perspective, Patras lies in one of the most seismically active regions in Europe. Seismic risk therefore represents the dominant hazard for the area. However, the city is also increasingly exposed to hydrometeorological hazards, including coastal flooding and pluvial flash floods, due to limited drainage capacity and urban expansion along low-lying coastal plains.

The Patras pilot is designed to represent these complex interdependencies by integrating a variety of building types including residential, public, educational, commercial, and healthcare assets. The selected structures capture the typical range of construction practices, code levels, and occupancy profiles found in the region. Together, they form a representative subset of the city's building stock, supporting the development and validation of dynamic multi-hazard fragility and vulnerability models within WP2.

To represent the range of structural and functional typologies within the Patras pilot site, seven characteristic assets were selected. These archetypes include residential, educational, governmental, commercial, and healthcare buildings, capturing the diversity of the local built environment in terms

of construction era, occupancy, and maintenance condition. Each site contributes to defining the local taxonomy and supports calibration of fragility and vulnerability models for multiple hazard scenarios (earthquakes, floods etc).

The classification of the seven representative Patras building archetypes was carried out following the GED4ALL Multi-Hazard Building Taxonomy (Silva et al., 2018). This taxonomy, developed by the Global Earthquake Model (GEM) Foundation, provides a harmonised and extensible framework for describing the physical characteristics of buildings exposed to multiple hazards. It includes 14 attributes capturing material, lateral load-resisting system, height, age, occupancy, structural irregularity, exterior wall characteristics, roof and floor systems, and other multi-hazard parameters such as ground-floor hydrodynamics and fire protection.

Each building type was assigned a unique taxonomy string describing its structural and architectural configuration (e.g., CR+CIP/LFINF+MUR/H:3/CDM/RES1/EWMA/RSH1), allowing direct linkage with the GEM/GED4ALL fragility and vulnerability repository. The classification considered parameters such as number of storeys, code era, ductility, occupancy, and degree of ground-floor openness—ensuring compatibility with both earthquake and flood hazard analyses.

This taxonomy-based approach ensures that every building within the Patras pilot can be consistently mapped to one of the seven archetypes. It also facilitates the integration of local exposure data into the multi-hazard vulnerability modelling framework developed in WP2, supporting the interoperability of datasets across the project's pilot sites.

Archetype A – Detached Residential Building

This building is a two-storey detached residence located in the Rio suburb of Patras (38.30°N, 21.79°E, Table 17). Constructed in 2002, it is representative of modern low-rise single-family dwellings typical of suburban developments after the 1999 Greek Seismic Code revisions. The structure comprises a reinforced concrete (RC) frame with masonry infill walls, designed to moderate ductility standards and moderate code provisions. It features a pitched tile roof, solid rectangular plan, and small façade openings, providing good lateral stiffness. The building is in moderate physical condition and serves as a reference for evaluating seismic and flood vulnerability of private residences built before 2003 in the wider Patras area.

Table 15 GED4ALL Building Taxonomy for Archetype A

Category	Code	Description
Direction	DXP, DYO	Direction X (parallel to street), Direction Y (Perpendicular to street)
Material of the Lateral Load-Resisting System	CR, --, --	Concrete, Reinforced, Unknown concrete technology, Steel connections
Lateral Load-Resisting System	LFINF, DMO, CDM	Infilled frame, Moderate ductility, Moderate code
Height	H:2, --, HB:0, HF:0.7, HD:0	Exact 2 Storeys above ground, Height unknown, no storeys below ground, 0.7m

		above grade the entrance, no slope
Date of Construction	Y:2002, YMM	Year 2002, YMM Moderate physical condition/maintenance
Occupancy	RES1	Single dwelling (residential)
Shape of the Building Plan	BP1, PLFR	Adjoining building on one side, Rectangular, solid
Structural Irregularity	IRRE	Regular structure
Ground floor hydrodynamics	GFN	Not open, few doors and/or windows (i.e. less than 20% of wall surface area).
Exterior Walls	EWWA, WOS, PNO	Masonry exterior walls, Small openings (i.e. less than 20% of the wall surface area is occupied by windows and/or doors), Non protected windows
Roof	RSH2, RMT1, --, --	Pitched with gable ends, Clay or concrete tile
Floor	FC, --, --	Concrete
Foundation System	--	Unknown foundation system
Fire Protection	FIN	Fire protection non presence

Archetype B –Elementary School

Located within the University of Patras campus in Rio (38.28°N, 21.79°E, Table 18), this one-storey school building with a basement was constructed in 1998 and accommodates classrooms and administrative functions. It is composed of a reinforced concrete infilled frame system with flat concrete roofing and masonry external walls containing moderate façade openings. The building is currently in poor maintenance condition, exhibiting signs of ageing in the infill panels and façade finishes. Its regular geometry and low-rise configuration make it a suitable case for studying functional vulnerability in educational facilities, particularly in combined earthquake–flood scenarios due to its low-lying topography and large window openings.

Table 16 GED4ALL Building Taxonomy for Archetype B

Category	Code	Description
Direction	DXP, DYO	Direction X (the road in front of the main entrance)

		Direction Y Perpendicular to street)
Material of the Lateral Load-Resisting System	CR, --, --	Concrete reinforced
Lateral Load-Resisting System	LFINF, --, --	Infilled frame,
Height	H:1, --, HBEX:1, --	1 ground floor and 1 basement
Date of Construction	YEX:1998, YMP	Year 1998, Poor physical condition/maintenance
Occupancy	EDU1	School
Shape of the Building Plan	PLFI	Detached building, Irregular plan shape
Structural Irregularity	IRRE	Regular structure
Ground floor hydrodynamics	GFM	Not open, many doors and/or windows (i.e. more than 20% of wall surface area).
Exterior Walls	EWWA, WOM, PNO	Masonry exterior walls, Moderate openings (i.e. from 20% to 50% of the wall surface area is occupied by windowsand/or doors), Non protected windows
Roof	RSH1, RMN	Flat, Concrete roof without additional covering
Floor	FC	Concrete
Foundation System	--	Unknown foundation system
Fire Protection	FIN	Fire protection, non-presence

Archetype C – Government Office Building

This two-storey public administration building is located within the Patras municipal area (38.26°N, 21.75°E, Table 19) and represents the class of medium-size governmental service buildings. Constructed in 1930 and retrofitted in 2024, it consists of a cast-in-place reinforced concrete moment-resisting frame with deep foundations and flat roof. The structure is in good physical condition and conforms to modern seismic design standards. With its regular plan and minimal openings, it provides an example of totally renovated public buildings designed under improved code requirements.

Table 17 GED4ALL Building Taxonomy for Archetype C

Category	Code	Description
----------	------	-------------

Direction	DXP, DYO	Direction X (the road in front of the main entrance). Direction Y Perpendicular to street)
Material of the Lateral Load-Resisting System	CR, CIP	Concrete reinforced, Cast-in-place concrete
Lateral Load-Resisting System	LFM, DHI	Moment frame, Moderate ductility
Height	H:2, HHT:12.85, HBEX:0	2 floors (inclined ground)
Date of Construction	YEX:2024, YMG	Year 2024 (retrofit), Good physical condition/maintenance
Occupancy	GOV1	Government, general services
Shape of the Building Plan	BPD, PLFR	Detached building, Rectangular solid
Structural Irregularity	--,--,--	
Ground floor hydrodynamics	GFN	Not open, many doors and/or windows (i.e. Less than 20% of wall surface area).
Exterior Walls	EWWA, WOS,--	Masonry exterior walls, Small openings (i.e. less than 20% of the wall surface area is occupied by windows and/or doors)
Roof	RSH1,RMN,--,--	Flat, Concrete roof without additional covering
Floor	FC,--,--	Concrete
Foundation System	FOSDL	Deep foundation, with lateral capacity
Fire Protection	FIP	Fire insulation, presence

Archetype D – Physics Department, University of Patras

This four-storey reinforced concrete educational building, located on the University of Patras campus (38.29°N, 21.78°E, Table 20), was built in 1982. It serves as a teaching and research facility, combining laboratories, offices, and classrooms. The structure consists of a cast-in-place RC frame with shallow foundations and exhibits plan irregularities and non-structural infill panels with moderate openings. The building is in poor physical condition, reflecting deterioration of materials and ageing mechanical systems. Given its height, irregularity, and functional importance, it represents an essential case for analysing seismic performance degradation and progressive fragility of ageing institutional buildings.

Table 18 GED4ALL Building Taxonomy for Archetype D

Category	Code	Description
Direction	DXP, DYO	Direction X (the road in front of the main entrance), Direction Y Perpendicular to street)
Material of the Lateral Load-Resisting System	CR, CIP	Concrete, reinforced, Cast-in-place concrete
Lateral Load-Resisting System	--	
Height	H:4, HHI:3.6, HBEX:0, H --, -	Exact 4 Storeys above ground, average floor height 3.6, no storeys below ground, unknown ground floor height, Slope of the ground unknown
Date of Construction	Y:1982, YMP	Year 1982, Poor physical condition/maintenance
Occupancy	EDU4	College/university, research facilities and/or labs)
Shape of the Building Plan	BP1, PLFR	Adjoining building on one side, Rectangular, solid
Structural Irregularity	--	Irregular structure
Ground floor hydrodynamics	GFM	Not open, many doors and/or windows (i.e. more than 20% of wall surface area).
Exterior Walls	EWWA, WOM, PNO	Masonry exterior walls, Moderate openings (i.e. from 20% to 50% of the wall surface area is occupied by, Non protected windows
Roof	RSH1, RMT3	Flat roof, Clay or concrete til Membrane roofing,
Floor	FC	Concrete
Foundation System	FOSSL	Shallow foundation, with lateral capacity
Fire Protection	--	

Archetype E – Commercial Building

This two-storey retail building is located in Rio (38.29°N, 21.79°E, Table 21) and was constructed in 1998. It represents typical small-scale commercial buildings combining ground-floor retail space and

upper storage or office levels. The structure consists of a reinforced concrete infilled frame with large ground-floor openings and a flat RC roof. It includes a basement and has a total height of approximately 6.5 metres. The building is in good condition, reflecting routine maintenance of commercial assets. Its large façade openings and low ground elevation make it particularly relevant for assessing flood-induced damage mechanisms and hydrodynamic loading effects on RC frame systems.

Table 19 GED4ALL Building Taxonomy for Archetype E

Category	Code	Description
Direction	DXP, DYO	Direction X (the road in front of the main entrance), Direction Y Perpendicular to street)
Material of the Lateral Load-Resisting System	CR	Concrete reinforced
Lateral Load-Resisting System	LFINF, DMO	Infilled frame, Moderate ductility
Height	H:2, HHT:6.45, HBEX:1, HFAPP:0.6,--	Exact 2 Storeys above ground, 6.45 m total height of the structure, measured from the ground floor, 1 storey below ground, 0.6m ground floor height, Slope of the ground unknown
Date of Construction	Y:1998, YMG	Year 1998, Good physical condition/maintenance
Occupancy	COM1	Retail trade
Shape of the Building Plan	BP1, PLFR	Adjoining building on one side, Rectangular, solid
Structural Irregularity	IRRE-	regular structure,
Ground floor hydrodynamics	GFM	Not open, many doors and/or windows (i.e. more than 20% of wall surface area).
Exterior Walls	EWC, WOL,	Concrete, Large openings (i.e. more than 50% of the wall surface area is occupied by windows and/or doors)
Roof	RSH1, RMN	Flat roof, Concrete roof without additional covering

Floor	FC	Concrete
Foundation System	--	Unknown foundation system
Fire Protection	FIP	Fire insulation, presence

Archetype F –Residential Building

This two-storey apartment building, located in the Rio-Aktaio area (38.30°N, 21.79°E, Table 22), was built in 2007 and is a typical modern Greek residential construction. It consists of a reinforced concrete frame with partial open ground floor, reflecting a soft-storey configuration common in newer suburban housing where ground floors are used for parking. The structure features flat roofing, moderate façade openings, and rectangular plan geometry. It is in good physical condition, designed under modern code standards. This archetype is used to explore seismic drift concentration and soft-storey fragility, as well as potential compound flood–seismic vulnerabilities for residential typologies built after 2003.

Table 20 GED4ALL Building Taxonomy for Archetype F

Category	Code	Description
Direction	DXP, DYO	Direction X (the road in front of the main entrance), Direction Y Perpendicular to street)
Material of the Lateral Load-Resisting System	CR, --, --	Concrete reinforced,
Lateral Load-Resisting System	--	
Height	H:2, HHT:7.5, HBEX:1, HFAPP:0.6,--	Exact 2 Storeys above ground, 7.5 m total height of the structure, measured from the ground floor, 1 store below ground,
Date of Construction	Y:2007, YMG	Year 2007, Good physical condition/maintenance
Occupancy	RES1	Single dwelling
Shape of the Building Plan	BP1, PLFR	Adjoining building(s) on one side, Rectangular, solid
Structural Irregularity	IRRE-	regular structure,

Ground floor hydrodynamics	GFH	Ground floor plan partially open (i.e. with at least 50% of walls)
Exterior Walls	EWC, WOM,PNO	Concrete, Moderate openings (i.e. from 20% to 50% of the wall surface area is occupied by, non-protected windows)
Roof	RSH1, --	Flat roof
Floor	FC	Concrete
Foundation System	FOSDL	Unknown foundation system
Fire Protection	FIN	Fire protection, non presence

Archetype G –Hospital Building

The hospital complex at the University of Patras (38.29°N, 21.79°E, Table 23), constructed in phases, is represented in this study by a typical reinforced concrete hospital facility built in 1983. The structure consists of a multi-storey RC frame with large façade openings, flat roof, and regular rectangular plan. The building is in moderate physical condition and houses essential healthcare functions, including treatment rooms, laboratories, and support facilities. As a critical infrastructure asset, it plays a key role in the assessment of functional resilience and downtime modelling under multi-hazard stressors, particularly earthquakes and secondary cascading failures (power, water, or communication disruptions).

Table 21 GED4ALL Building Taxonomy for Archetype G

Category	Code	Description
Direction	DXP, DYO	Direction X (the road in front of the main entrance), Direction Y Perpendicular to street)
Material of the Lateral Load-Resisting System	CR	Concrete Reinforced
Lateral Load-Resisting System	--	Unknown lateral load-resisting system
Height	HHT:3.67	3.67 m
Date of Construction	Y:1983, YMM	1983, moderate physical condition
Occupancy	COM4	Hospital

Shape of the Building Plan	BP1, PLFRO	Adjoining building(s) on one side, Rectangular, with an opening
Structural Irregularity	IRRE	Regular
Ground floor hydrodynamics	GFM	Not open, many doors and/or windows (i.e.more than 20% of wall surface area).
Exterior Walls	EWC, WOL	Concrete, Large openings (i.e. more than 50% of the wall surface area is occupied by windows and/or doors)
Roof	RSH1, RMN	Flat, Concrete roof without additional covering,
Floor	FC	LiNOLEUM
Foundation System	--	Unknown
Fire Protection	FIP	Fire insulation, presence

Selection of the best candidate model

The Patras pilot site is exposed to multiple natural hazards, primarily earthquakes and floods, which constitute the examined physical risks for the local building stock. Consequently, the vulnerability assessment for Patras addresses both hazards in a staged approach. The first phase focuses on seismic vulnerability, while subsequent analyses will integrate flood vulnerability developed in coordination with project partners. The combined outputs will ultimately support the construction of dynamic multi-hazard vulnerability functions within WP2.

Seismic Vulnerability Modelling

For the seismic hazard, the scope was to identify and select the most appropriate fragility and vulnerability models to represent the building stock of the Patras pilot. To structure the analysis, seven representative building types were defined (see Section 2.3.3). These typologies act as archetypes for the Patras building inventory. During the modelling phase, all buildings within the pilot site will be assigned to one of these seven archetypal categories, ensuring consistency between the exposure dataset and the fragility functions. This approach allows the physical vulnerability characterization of multiple buildings through a limited, well-characterised set of reference structures.

The fragility and vulnerability models used for the Patras pilot were retrieved from the interactive model repository available on the OpenVulnerability web tool (Gentile, 2025) and the procedure described in Section 2.2. This online platform provides structured access to the GEM / GED4ALL global database, containing harmonised, peer-reviewed fragility and vulnerability functions for multiple building typologies worldwide. Each model entry includes metadata on the original publication, structural system, occupancy, height class, code era, and regional calibration. This platform consolidates validated fragility models for RC and masonry buildings worldwide, including examples calibrated for numerous structural typologies.

Thus, the candidate models were screened through the associated interactive GEM repository and each of the seven Patras archetypes was then matched to a specific fragility model that best represents its characteristics. The selected models are shown in Table 24.

Table 22 Selected Fragility/Vulnerability Models for the Patras Pilot Site Archetypes

Archetype ID	Building Type / Occupancy	Structural System	Selected Fragility/Vulnerability Model
A	Detached Residential	RC infilled frame (2 storeys)	structural Greece CR-LFM+CDM+DUM-H2-RES
B	Elementary School	RC infilled frame (1 storey + basement)	E21.13b
C	Government Office	RC moment frame	Ahmadetal2010-RC-Regular-Ductile-2storeys
D	University Building	RC cast-in-place frame (4 storeys)	E21.12a
E	Retail/Commercial	RC infilled frame with open ground floor	fatalities Greece CR-LFINF+CDH+DUM-H2-COM
F	Residential	RC frame, soft storey	structural Greece CR-LFINF+CDH+DUL-H2-RES
G	Hospital	RC multi-storey with large openings	E21.21

The seven archetypes thus provide a simplified yet comprehensive representation of the entire Patras building stock. During the forthcoming modelling phase, each building in the exposure dataset will be mapped to its most appropriate archetype, allowing the fragility and vulnerability relationships listed above to be systematically applied across the pilot site.

For each archetype, the corresponding fragility/vulnerability model includes a set of damage-state curves that describe the probability of reaching or exceeding a given damage state as a function of seismic intensity (e.g. spectral acceleration). For completeness and transparency, the selected optimal model for each archetype (A–G) is illustrated in F8.a–g. These plots are directly extracted from the online repository and summarise, for each archetype:

- the intensity measure used,
- the defined damage states (e.g. slight, moderate, extensive, collapse),
- and the associated exceedance probabilities for each state.

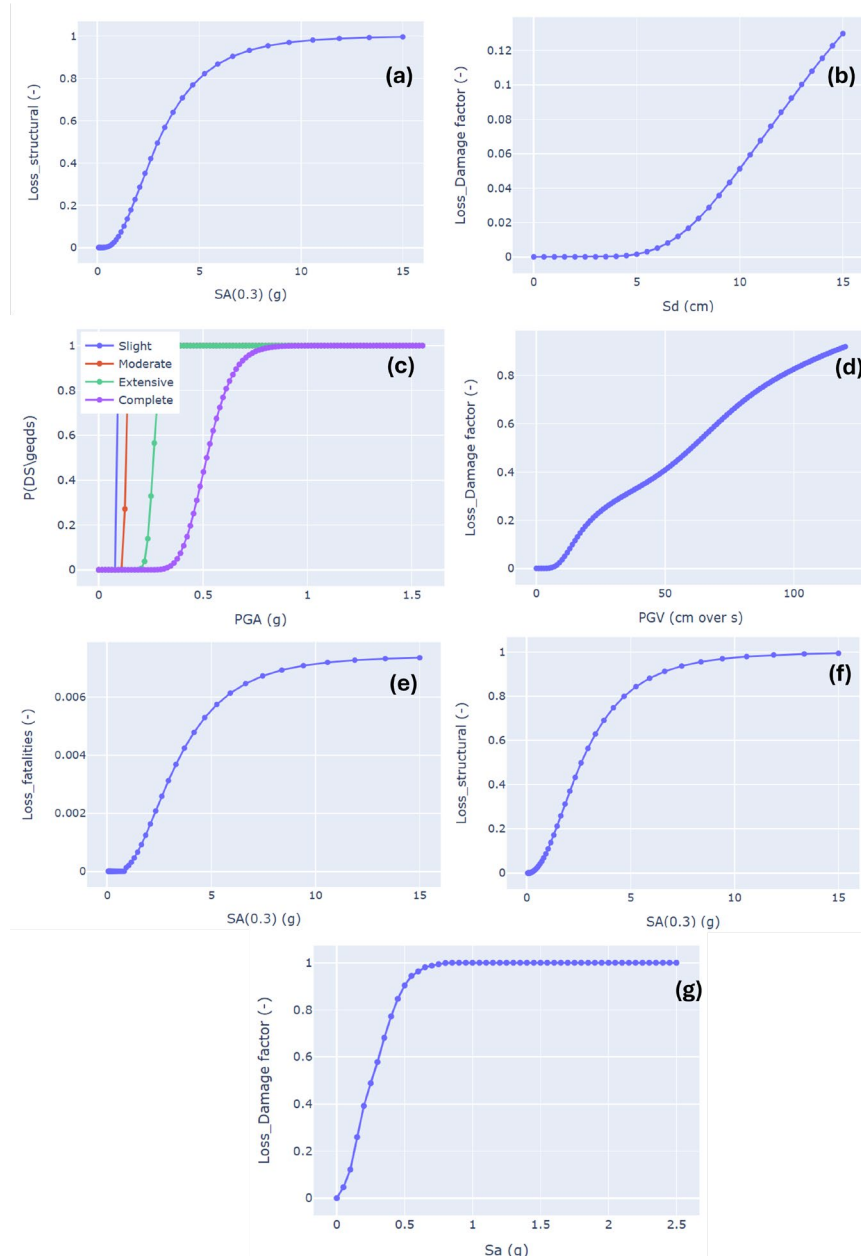


Figure 11 Fragility/vulnerability curves for Archetypes a-g.

Figure 14 will be used in Task 2.1 as the reference seismic fragility input for scenario-based and probabilistic loss modelling in the Patras pilot site.

System dynamic modelling

Urban infrastructures are increasingly exposed to the combined impacts of climate change, natural disasters, and cascading technical failures. Understanding the fragility and vulnerability of interconnected urban systems, such as the Electricity Network (EN), Water Supply Network (WSN), Information and Communication Technologies (ICT), and Critical Street Arteries (CSA), is essential for anticipating disruptions and improving resilience at the city scale. The functionality of each infrastructure depends not only on its internal robustness but also on the interdependencies that couple its performance with that of others. Failures in one sector can quickly propagate across networks, producing complex and non-linear impacts on urban operations and services. This work contributes to Task T2.1.2 “Characterising the Fragility & Vulnerability of Urban Infrastructure”, which aims to extend previous efforts on building-scale fragility analysis (Task 2.1.1) toward a meso-scale,

network-level understanding of urban systems. The objective is to investigate and quantify how climate-induced and natural hazards, such as earthquakes, floods, heatwaves, and wildfires, affect the performance of critical urban infrastructures in the pilot case study of Patras, Greece, considering both direct physical impacts and indirect cascading effects. To achieve this, the study adopts a System Dynamics (SD) modelling framework inspired by the work of Canzani (2016), a “block building” methodology was introduced for modelling disruptions and interdependencies in Critical Infrastructure (CI) networks. The approach decomposes the overall system into three functional components:

- **Disruptive Event Block**, capturing the temporal characteristics of the hazard (onset, duration, magnitude)
- **Single Infrastructure Dynamics Block**, representing the operational states of each CI (running, down, and recovered) over time.
- **Interdependency Block**, modelling the mutual dependencies among infrastructures through a weighted connection matrix that quantifies the services provided and received.

The present work reimplements and extends this framework entirely in Python, enabling open, flexible, and computationally reproducible SD simulations. Using this model, a series of multi-hazard scenarios are generated for the urban system of Patras, covering extreme heat, flooding, wildfire, and seismic events, as well as combined disruptions such as sequential ICT–EN failures. Each scenario explores both the proactive absorptive capacity (the ability to withstand shocks) and the reactive restorative capacity (the ability to recover) of the system. By quantifying the evolution of infrastructure performance and service provision over time, the model provides a platform for impact analysis and dynamic resilience assessment.

2.3.3 Wellington, New Zealand

Within the Wellington case study there are two selected modelling domains that are dependent upon the modelled hazard (Figure 15). For the flood risk assessment, the selected modelled domain is that of the Wellington CBD area whereas for the wildfire model the extent is over the larger vegetative area urban features that lie either within or along the boundaries at the wildland urban interface (WUI).

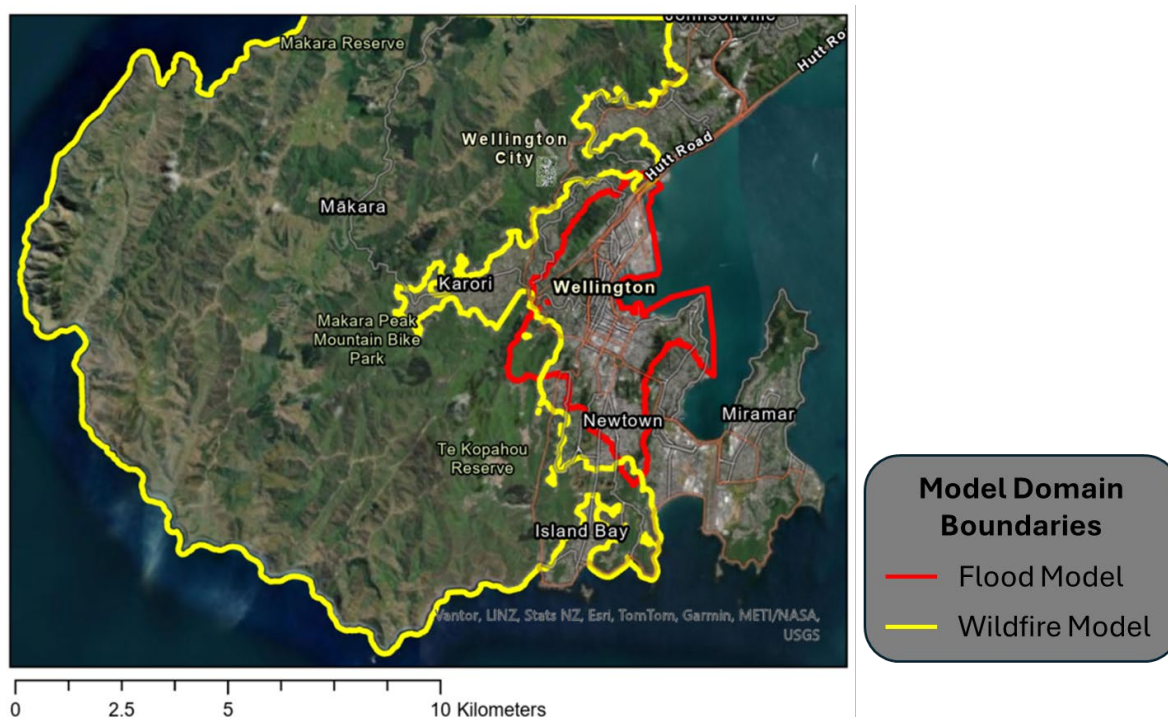


Figure 12. Hazard model domains for Wellington case study

Assets Included

The region is comprised of a large number of assets with an approximate breakdown shown in Table 25.

Table 23. Approximate asset counts within Wellington study region.

Asset Name	Count	Notes
Residential properties	72,232	Where data not available, floor level assumed to be 150mm above ground level (MBIE, 2023)
Commercial properties	5,278	Where data not available, floor level assumed to be 150mm above ground level (MBIE, 2023)
Industrial properties	1,065	Where data not available, floor level assumed to be 150mm above ground level (MBIE, 2023)
Roads	967km	Roads divided into 50m segments to facilitate localised risk assessment
Bridges	317	Locations obtained via WCC Open GIS Portal
Energy transmission lines	119km	Included overhead and underground lines. Split into 50m segments for risk assessment
Energy transmission structures	401	Centre points of structures such as pole, towers (pylons), gantries, and termination points
Energy grid exit points	8	Locations where energy leaves national transmission grid and enters local distribution network. 12,000km transmission lines and 170+ substations
Fire Stations	11	Location of fire stations within the region
Hospitals	5	Locations of hospitals within the region
Police stations	8	Locations of police stations within the region
Schools	84	Locations of schools defined as primary, intermediate, and high schools within the region
Supermarkets	31	Locations of supermarkets within the region

Selection of the best candidate model

A selection of vulnerability curves from literature were used for the Wellington pilot site. Table 26 describes which asset class of vulnerability curve was used. Some assets do not yet have vulnerability curves, so only their exposure is identified in the analysis.

Table 24. List of vulnerability curves used for each asset and their sources.

Vulnerability Curve Type	Assets used for	Literature sources
Residential and commercial buildings properties	<ul style="list-style-type: none"> Residential properties Commercial properties Schools Supermarkets 	<ul style="list-style-type: none"> Huizinga, J., H. de Moel, and W. Szewczyk. 2017. "Global Flood Depth-Damage Functions: Methodology and the Database with Guidelines." Joint Research Centre. https://doi.org/10.2760/16510. Reese, Stefan, and Doug Ramsay. 2010. "RiskScape: Flood Fragility Methodology." NIWA. https://www.wgtn.ac.nz/sgees/research-centres/documents/riskscape-flood-fragility-methodology.pdf.
Industrial buildings	<ul style="list-style-type: none"> Industrial properties Hospitals Police stations Fire stations 	<ul style="list-style-type: none"> Huizinga, J., H. de Moel, and W. Szewczyk. 2017. "Global Flood Depth-Damage Functions: Methodology and the Database with Guidelines." Joint Research Centre. https://doi.org/10.2760/16510. Reese, Stefan, and Doug Ramsay. 2010. "RiskScape: Flood Fragility Methodology." NIWA. https://www.wgtn.ac.nz/sgees/research-centres/documents/riskscape-flood-fragility-methodology.pdf.
Electrical substation	<ul style="list-style-type: none"> Grid exit points 	<ul style="list-style-type: none"> FEMA. 2012. "Multi-Hazard Loss Estimation Methodology: Hazus 2.1 Flood Model Technical Manual." Federal Emergency Management Agency. https://www.fema.gov/sites/default/files/2020-09/fema_hazus_flood-model_technical-manual_2.1.pdf.
Roads	<ul style="list-style-type: none"> Roads 	<ul style="list-style-type: none"> Bruijn, Karin de, Dennis Wagenaar, Kymo Slager, Mark de Bel, and Andreas Burzel. 2015. "Updated and Improved Method for Flood Damage Assessment - SSM2015 (Version 2)." Deltares.

		<p>https://vdocuments.mx/updated-and-improved-method-for-flood-damage-assessment-1220043-003-hye-0012.html?page=1;</p> <p>https://library.wur.nl/WebQuery/hydrotheek/2221326.</p> <ul style="list-style-type: none"> • Ginkel, Kees C. H. van, Francesco Dottori, Lorenzo Alfieri, Luc Feyen, and Elco E. Koks. 2021. "Flood Risk Assessment of the European Road Network." <i>Nat. Hazards Earth Syst. Sci.</i> 21 (3): 1011–27. • Huizinga, J., H. de Moel, and W. Szewczyk. 2017. "Global Flood Depth-Damage Functions: Methodology and the Database with Guidelines." Joint Research Centre. https://doi.org/10.2760/16510. • Kellermann, P., A. Schöbel, G. Kundela, and A. H. Thieken. 2015. "Estimating Flood Damage to Railway Infrastructure – the Case Study of the March River Flood in 2006 at the Austrian Northern Railway." <i>Natural Hazards and Earth System Sciences</i> 15 (11): 2485–96. • Kok, M., H. J. Huizinga, A. C. W. Vrouwenvelder, and A. Barendregt. 2005. "Standard method 2004 damage and casualties caused by flooding." Rijkswaterstaat. https://open.rijkswaterstaat.nl/open-overheid/onderzoeksrapporten/@187575/s-tandard-method-2004-damage-and. • Vanneuville, Wouter, Ruben Maddens, Christophe Collard, Peter Bogaert, Philippe De Maeyer, and Marc Antrop. 2006. "Impact on people and the economy due to flooding viewed in the light of changing hydraulic conditions, environmental factors and climatic conditions." Flanders Environment Agency, MIRA Climate Report. https://archieff.algemeen.omgeving.vlaanderen.be/xmlui/handle/acd/761881.
None	<ul style="list-style-type: none"> • Transmission lines • Transmission structures 	None currently implemented

• Bridges

The curves themselves are shown in Figure 16, with their respective variations.

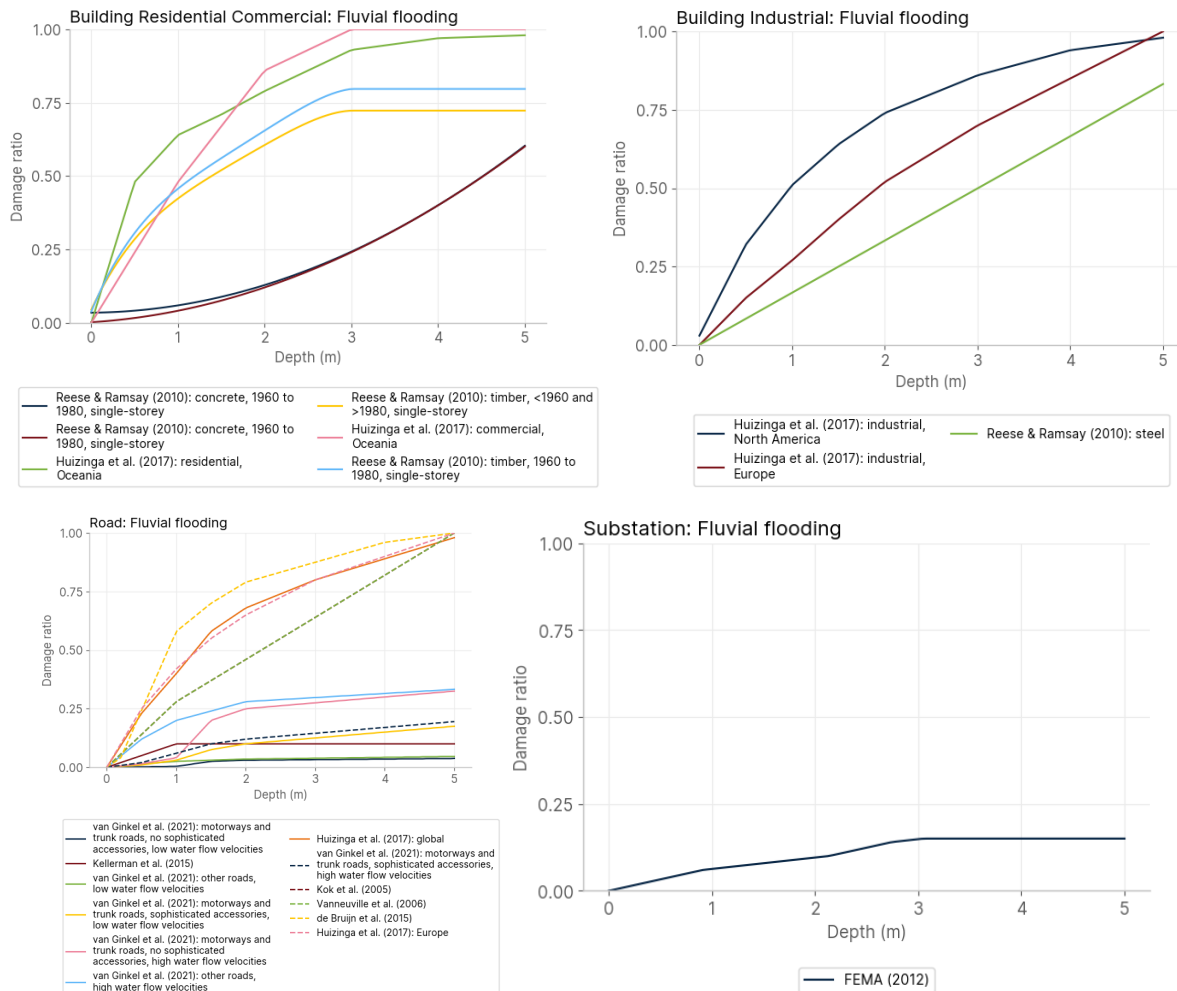


Figure 13. Sample vulnerability curves used in the Wellington pilot.

When using the vulnerability curves to understand the potential damage ratio, the closest curve is matched based on the asset's properties. However, when there is no additional information provided, all curves are taken, giving a range of possible damage, while the highest damage ratio is used to visually show the severity in the output mapping platform Resilience Explorer.

3 Physical vulnerability modelling

This chapter develops and/or adapts numerical and empirical models to characterize structural fragility, damage states, and recovery trajectories of assets under different hazard scenarios. The examples presented illustrate the Advanced Risk Assessment (Class 3) level of detail within the taxonomy introduced in Section 2.1. Although each model is presented for a specific pilot site, the underlying methodologies are applicable to other pilot sites.

3.1 Dublin, Ireland: Performance-based flood engineering for timber buildings: evaluating structural vulnerability and mitigation strategies.

3.1.1 Introduction.

Since the 1990s, hazard-induced disasters have caused tens of billions of U.S. dollars in economic losses worldwide (Botzen et al., 2019). Between 2013 and 2023 alone, insured losses from flood-related disasters totalled \$98.2 billion, underscoring the urgent need to accurately assess the impacts of floods on communities (Munich Re., 2024). Among these impacts, the destruction of residential buildings has had especially severe and lasting consequences for community recovery and long-term resilience (Peacock et al., 2018; Gentile et al., 2022). Flooding, especially fluvial and flash floods triggered by intense rainfall, increasingly affects vulnerable and resource-limited communities, where housing often lacks flood-resistant design features (Noble and Roy, 2010; Ermagun et al., 2024). Given the projected intensification of flood hazards due to climate change and urbanization, addressing the vulnerability of residential buildings in hazard-prone regions has become an urgent priority for sustainable development and the reduction of disaster risk (Nofal and van de Lindt, 2020a; Donatti et al., 2024).

The flood fragility of buildings, defined here as the probability of failure of a building structure or a specific limit state under a given hazard intensity measure (IM), is influenced by hydrostatic and hydrodynamic forces, buoyancy effects, foundation scour, and water infiltration (Custer and Nishikima, 2015). These forces interact in complex ways depending on building materials, structural design, and construction practices (Englhardt et al., 2019). Timber houses (promoted worldwide as sustainable, low-carbon alternatives to conventional construction systems, Tupenaite et al., 2023) exhibit particular vulnerabilities when exposed to flooding (Becker and Lence, 2011). Although timber construction is not yet widespread in Dublin, it is expected to play a growing role in sustainable housing and low-carbon development. Incorporating flood vulnerability analyses for timber buildings therefore provides a forward-looking perspective that anticipates emerging risks, aligns with climate adaptation priorities, supports regulatory compliance, and strengthens long-term resilience by addressing vulnerabilities before they become systemic (Moreno et al., 2022; JCHLGH, 2023; McGetrick, 2024)

Despite the environmental advantages of timber relative to masonry and reinforced concrete, its performance under flood loading remains insufficiently studied. Traditional vulnerability models often rely on empirical depth-damage functions that overlook key failure mechanisms such as envelope breakage, buoyancy-induced flotation, and progressive material degradation from prolonged water exposure (Custer and Nishikima, 2015). Timber structures also face distinct material-level vulnerabilities: unlike masonry or concrete, timber is susceptible to moisture absorption, decay, and mold, which can compromise both structural integrity and indoor environmental quality. Consequently, resilience measures such as protective treatments, elevated floor systems, and rapid post-flood drying protocols are particularly important for timber buildings. Considering these factors ensures that Dublin's sustainability ambitions are supported by robust, practical resilience planning in one of its most flood-exposed urban districts.

Recent advances (e.g., Becker and Lence, 2011; Custer and Nishikima, 2015; Nofal et al., 2020a,b) support component-based, physics-informed modelling approaches that more accurately represent the behaviour of individual building elements, such as windows, doors, shear walls, and diaphragms, under multiparametric flood scenarios, including variations in water depth, flow velocity, and flood duration. These approaches enable more precise and scalable vulnerability assessments by capturing

realistic damage mechanisms, accounting for time-dependent effects, and identifying critical components that should be prioritized for mitigation. This section quantitatively investigates the structural fragility of a representative light-frame timber house archetype under flood conditions, focusing on three critical performance levels: *Breach*, *Collapse*, and *Float*. Using a synthetic modelling framework aligned with ASCE 7-22 guidelines (ASCE, 2022), fragility curves are developed based on flood water depth, flow velocity, and flood duration as intensity measures. The study also assesses the effectiveness of mitigation strategies, such as reinforcing the building envelope and structural system, in reducing structural vulnerability. By detailing damage progression and failure mechanisms, this work seeks to inform the design of flood-resilient timber housing and support community-level adaptation strategies that integrate sustainability, structural performance, and disaster resilience.

3.1.2 Flood performance assessment

Flood performance of the baseline and mitigated timber typologies was assessed using a component-based, performance-based flood engineering framework. In this approach, the building is modelled as an assembly of individual components, each with distinct limit states and capacities.

Flood Demands

The intensity of flooding demands varies with floodwater depth and velocity, highlighting the need to consider multi-parametric hazard inputs. Flood duration also plays a critical role, particularly in determining the extent of water infiltration into the building interior through envelope breaches. Once the interior and exterior water levels equalize, hydrostatic forces are largely compensated, and hydrodynamic forces dominate the structural demands. Following the procedures outlined in Chapter 5 of the ASCE 7-22 Supplement 2 on Flood Loads (ASCE, 2022), these demands are systematically quantified to support the component-based performance assessment.

For calculation purposes, the building footprint is defined as $L \times B$, where L is the dimension aligned with the direction of water flow, and B is the dimension perpendicular to it. The building is also characterized by a height of h_s stories and a total of n_s stories.

Hydrostatic load calculation

Hydrostatic forces result from the pressure exerted by standing water and act perpendicularly on all wetted surfaces. These pressures are calculated using fundamental principles of fluid mechanics, where the pressure at a given point is proportional to the flood water depth. The hydrostatic pressure is calculated as:

$$p_s = \gamma_w \cdot z \text{ (Eq. 1)}$$

where:

- p_s is the hydrostatic pressure at depth z below the flood water depth (N/m^2),
- γ_w is the unit weight of water, taken as $9.807 \times 10^3 \text{ N/m}^3$ for freshwater,
- z is the depth from the water elevation to the point of interest (m).

The total lateral hydrostatic force in N/m on a vertical surface is:

$$F_h = \frac{1}{2} \gamma_w \cdot d_f \text{ (Eq. 2)}$$

where d_f is the flood water depth (m). Then, the vertical buoyancy forces acting on the structure are calculated as:

$$F_B = \gamma_w \cdot V_w \text{ (Eq. 3)}$$

where:

- F_B is the buoyancy (i.e., uplift) force (N),

- V_w is the volume of displaced water (m^3). If the building envelope is sealed (i.e., no water has entered), the displaced volume is simply calculated as $L \cdot B \cdot \min(d_f, h_s \cdot n_s)$. However, if the envelope is breached and water enters the interior, buoyancy is reduced. In this case, the displaced volume is calculated only from the volume of the exterior shear walls, excluding the internal air volume: $2(L + B) \cdot t_{sw} \cdot \min(d_f, h_s \cdot n_s)$, where t_{sw} is the thickness of the envelope shear walls.

Hydrodynamic Load Calculation

Hydrodynamic forces are generated when flowing water impacts submerged structural components or systems during a flood. These pressures are calculated based on fundamental fluid mechanics, where the force exerted is proportional to the square of the floodwater velocity and are given by:

$$p_d = \frac{1}{2} \cdot C_D \cdot \rho_w \cdot V^2 \text{ (Eq. 4)}$$

where:

- p_d is the hydrodynamic pressure at a given velocity of the flood (N/m^2),
- ρ_w is the density of water, taken as $1 \times 10^3 \text{ kg/m}^3$,
- C_D is the drag coefficient based on shape (typically 2.0 for walls),
- V is the flood velocity (m/s).

For individual components (e.g., shear walls), the hydrodynamic force in N/m is calculated using:

$$F_{drag} = \frac{1}{2} \cdot C_D \cdot \rho_w \cdot V^2 \cdot h \cdot b \text{ (Eq. 5)}$$

where:

- h is the submerged height of the element (m),
- b is the width of the element perpendicular to flow (m)

For entire enclosed buildings, the hydrodynamic force is computed as:

$$F_{drag,sys} = \frac{1}{2} \cdot C_D \cdot \rho_w \cdot V^2 \cdot B \cdot d_f \text{ (Eq. 6)}$$

Table 27 presents the distributions of the parameters used to define the flood demand, as per ASCE (2022).

Table 25 Parameter values defining the assumed load model as per ASCE (2022)

Variable	Mean Value	Coefficient of Variation	Distribution Type ^a	Data Source
ρ_w	$1.00 \times 10^3 \text{ kg/m}^3$	0.05	Normal Truncated	ASCE 7-22 Supplement 2 (ASCE, 2022); Nieto et al., (2021)
γ_w	$9.81 \times 10^3 \text{ N/m}^3$	0.05	Normal Truncated	ASCE 7-22 Supplement 2 (ASCE, 2022); Nieto et al., (2021)

C_D	1.6 range (1.2 to 2.0)	0.15	Uniform	Jalayer et al., (2016); AASHTO (2013); FEMA P-55 (FEMA, 2011)
-------	------------------------------	------	---------	---

Notes:

a) Distributions are assumed truncated normal following Valdivieso et al. (2024), unless a specific source for a given variable indicates a different distribution type.

Components and Component Capacities

Flood loads are used to assess the failure of key structural and non-structural components, including windows, doors, wall studs, shear walls, roof and floor diaphragms, and roof-to-wall, floor-to-wall, and shear wall-to-foundation connections, by comparing the applied demand to their respective capacities. These components were selected because of their association with failure modes commonly observed in residential buildings during past flood events. Component capacities (summarized in Table 28) were defined based on data from Valdivieso et al. (2024) and supplemented with values from the existing literature. Since the focus of this study is on evaluating the structural performance of the building system, the interior contents, which are essential to assessing the building's total vulnerability, were not considered. Each component was assigned a limit state based on physical thresholds informed by experimental data and engineering judgement.

3.1.3 Probabilistic Performance Assessment

Performance Levels of Interest

Following Parammal et al. (2022), the performance levels used to evaluate the light-frame timber house case study, serving as a representative application of the proposed performance model, are *Continued Occupancy* (CO) and *Collapse Prevention* (CP). The *Life Safety* level is not considered because, under flood loading, post-elastic progression to failure is typically rapid (Parammal et al., 2022). The two levels of interest are defined in terms of three key limit states, namely *Breach*, *Collapse*, and *Float* (Becker & Lence, 2011). *Breach* refers to the penetration of floodwaters through the building envelope, typically resulting from the failure of windows, doors, or the out-of-plane resistance of exterior walls. *Breach* impedes CO by causing excessive water intrusion (Drdácký, 2010). *Collapse* corresponds to structural failure due to hydrostatic and hydrodynamic forces and accounts for multiple failure mechanisms. These include: out-of-plane bending and shear in the studs located in the perimeter walls perpendicular to the flood flow; shear capacity of shear walls and diaphragms; axial tension/compression in diaphragm chords and collectors; axial tension/compression capacity of end studs in shear walls; in-plane and out-of-plane shear resistance of connections between shear walls and both the roof and foundation; and the tensile strength of hold-downs located at shear wall boundaries. *Float* is governed by the combined effects of buoyancy and drag forces acting on the structure. The self-weight of the superstructure and foundation resists buoyancy. In contrast, drag is opposed by the shear capacity of the shear wall-to-foundation connections and the frictional resistance at the interface between the structure and its supporting base. Both *Collapse* and *Float* are considered failures of CP, as each can result in total structural loss (Drdácký, 2010).

Flood Fragility Curves

Fragility curves were developed for each limit state using a probabilistic framework that characterizes component failure as a function of three intensity measures (IM), namely: flood depth, flow velocity, and flood duration. Monte Carlo simulations with 1000 realizations per hazard level were conducted to account for uncertainties in both flood demands and component capacities (see Table 27 and Table

28). Component-level failures were evaluated for each limit state, and system-level fragility was determined as the union of individual component failures.

3.1.4 Case study

The baseline archetype analysed in this study represents a typical light-frame timber building in flood-prone residential areas across Ireland, where flood risk is generally not addressed in detailing. Its characteristics are based on field observations in Ringsend, Dublin, and on construction information reported in IWU (2011). The baseline case has a 10 m × 10 m plan and a story height of 2.5 m (see Figure 17). Shear walls, floors, and roof are modelled with 2×4 members, assuming Southern Yellow Pine specie. This archetype mirrors standard practice and includes no flood-resistant design features.

Table 29 summarizes the key characteristics of the baseline model and four variants (Cases 2–5) developed to assess the incremental effects of selected mitigation measures. We consider Case 4 as the fully mitigated archetype. Drawing on the flood-mitigation literature (e.g., DCLG, 2007; Drdácý, 2010; Becker & Lence, 2011; Custer & Nishijima, 2015; Nofal et al., 2020a, 2020b; Ullal & Estrella, 2021; ASCE, 2024) and established engineering principles, the measures include: (i) strengthening doors and windows; (ii) increasing structural mass, for example, by adding a concrete topping at each story; (iii) increasing the capacity of shear walls and diaphragms via denser nail patterns and reduced stud spacing in wood-frame systems or by changing the lateral system to cross-laminated timber (CLT) shear walls and diaphragms; (vi) strengthening connections between components: roof-to-wall and shear-wall-to-floor/foundation to resist in-plane shear (lateral) loads, and using hold-downs to resist uplift and overturning from flood-induced lateral forces; and (v) modifying the building envelope to delay or control water intrusion. We assess interventions based on their influence on overall flood performance (i.e., reduction in failure probability) and on each defined performance level. In both the baseline and mitigated sets, the number of stories is varied from 1 to 4 to capture responses from single-family to low-rise multifamily buildings.

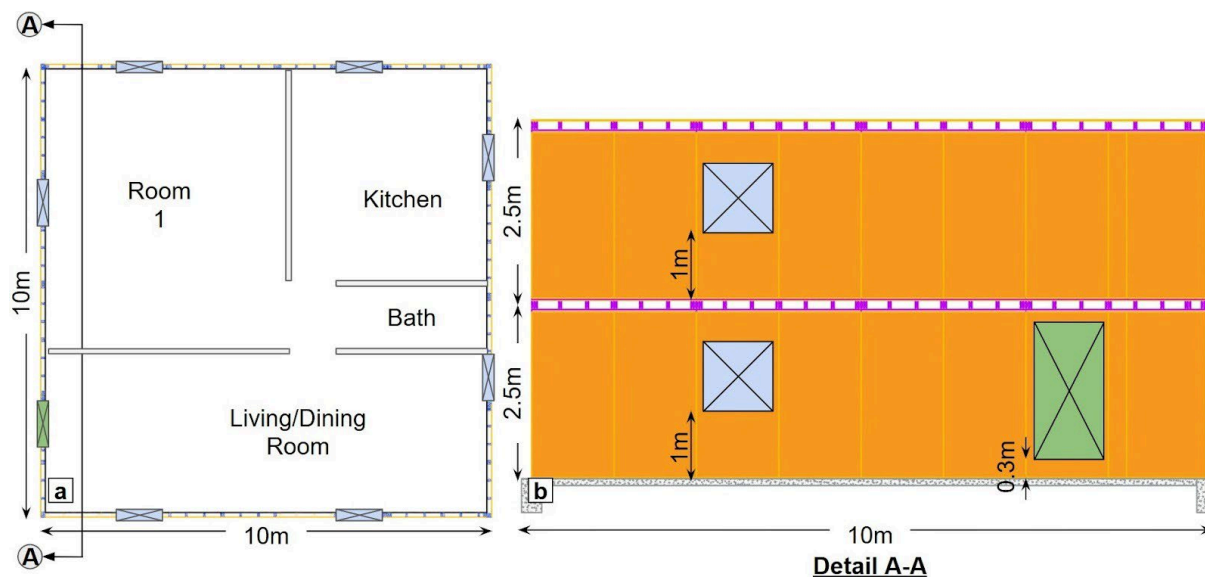


Figure 14 Timber house typology: (a) First story plan layout and (b) Representative elevation view of a two-story house.

Table 26 Parameter values defining component capacities for the Baseline case.

Variable	Mean Value	Coefficient of Variation (CV)	Distribution Type ^d	Data Source
----------	------------	-------------------------------	--------------------------------	-------------

Young's modulus	$7.90 \cdot 10^9$ N/m ²	0.15	Normal Truncated	ASCE D2555 (ASTM, 2006)
Wood bending strength	$4.95 \cdot 10^7$ N/m ²	0.16	Normal Truncated	ASCE D2555 (ASTM, 2006)
Wood tensile strength	$9.03 \cdot 10^6$ N/m ²	0.10	Normal Truncated	NDS 2018 (AWC, 2018)
Wood compressive strength	$1.75 \cdot 10^7$ N/m ²	0.16	Normal Truncated	ASCE D2555 (ASTM, 2006)
Wood shear strength	$5.75 \cdot 10^6$ N/m ²	0.14	Normal Truncated	ASCE D2555 (ASTM, 2006)
Shear wall strength	$9.78 \cdot 10^3$ N/m	0.08	Normal Truncated	SDPWS 2021 (AWC, 2021); Valdivieso et al., (2023)
Diaphragm strength	$1.05 \cdot 10^4$ N/m	0.08	Normal Truncated	SDPWS 2021 (AWC, 2021); Valdivieso et al., (2023)
Shear wall-to-Foundation Shear Connection ^a	$5.56 \cdot 10^3$ N	0.10	Normal Truncated	Simpson Strong-Tie (2024); Valdivieso et al., (2024)
Shear wall-to-Roof/Floor Shear Connection ^b	$3.17 \cdot 10^3$ N	0.10	Normal Truncated	Simpson Strong-Tie (2024); Valdivieso et al., (2024)
Hold-down Connector ^c	$1.87 \cdot 10^4$ N	0.10	Normal Truncated	Simpson Strong-Tie (2024); Valdivieso et al., (2024)
Mass of the house	244 kg/m ² /story	0.05	Normal Truncated	Becker et al. (2011); Yi et al., (2025)
Window strength	$1.00 \cdot 10^3$ N/m ²	0.25	Weibull	Kelman (2003); Becker et al. (2011)
Door strength	$1.00 \cdot 10^3$ N/m ²	0.25	Weibull	Kelman (2003); Becker et al. (2011)

Density of Concrete	$2.50 \cdot 10^3$ kg/m ³	0.05	Normal Truncated	Nowak and Collins (2012).
Coefficient of friction	0.6 range (0.4 - 0.8)	0.2	Uniform	Nieto et al., (2023)

Notes:

- a) One row of 9.5 mm ribbed steel bars at 400 mm spacing in the baseline archetype.
- b) Two rows of 2.9 mm x 64 mm (diameter x length) common nails, per NDS 2018 (AWC, 2018), at 400 mm spacing in the baseline archetype.
- c) DTT1Z hold-down connector from Simpson Strong-Tie (2024).
- d) Component capacity distributions are assumed to be truncated normal, following Valdivieso et al. (2024), unless a specific source for a given variable indicates a different distribution type.

Table 27 Typology matrix

Variable	Baseline	Case 2	Case 3	Case 4	Case 5
Wood member size	2x4 (41mm x 89mm)			-	2x4 (41mm x 89mm)
CLT thickness in mm				120	
Doors and windows strength in N/m ²	see Table 28	$3.0 \cdot 10^3$	$6.0 \cdot 10^3$	$1.1 \cdot 10^4$	$1.1 \cdot 10^4$
Diaphragm nail spacing in mm	150 x 150	100 x 150	63.5 x 100	-	150 x 150
CLT Diaphragm panel-to-panel connector	-	-	-	LSSR strap ^d	-
Shear wall nail spacing	150	150	76.2	-	150
Shear wall stud spacing	600	600	300	-	600
Overstrength factor on shear wall-to- foundation shear connection ^a	1.0	2.0	3.0	8.0	1.0
Overstrength factor on shear wall-to- roof/floor shear connection ^b	1.0	1.2	3.5	2.0	1.0
Overstrength factor on Hold-down connector ^c	1.0	2.0	3.5	6.0	1.0
Roof/Floor-to-wall shear connection spacing in mm	400	200	200	500	400
Wall-to-foundation shear connection spacing in mm	400	300	300	500	400

Notes:

- a) The factor is computed as the ratio of the mitigated connection strength to the baseline connection strength (Table 28). For Cases 2–4, the measures are, respectively, a 13 mm steel rebar, a 9.5 mm Titen HD anchor (Simpson Strong-Tie, 2024), and an AE116 connector (Simpson Strong-Tie, 2024).

- b) The factor is computed as the ratio of the mitigated connection strength to the baseline connection strength (Table 28). For Cases 2–4, the measures are, respectively, an SDWS16300 screw, an SDWS22300 screw, and an AE116 connector (Simpson Strong-Tie, 2024).
- c) The factor is computed as the ratio of the mitigated connection strength to the baseline connection strength (Table 28). For Cases 2–4, the measures are, respectively, DTT2Z, HTT4, and HTT5 hold-down connectors (Simpson Strong-Tie, 2024).
- d) For CLT roof and floor systems, lateral load resistance is controlled by the connection between adjacent CLT panels. We use the LSSR strap with screws at 100 mm on centre (Simpson Strong Tie, 2024).

3.1.5 Assessing the impact of information fidelity on fragility response

This section evaluates how the fidelity of input information affects the computed probability of failure for two performance levels, CO and CP. We consider the baseline archetype and the Case 4 mitigated archetype; each modelled as a single story and a four-story building.

Information fidelity sensitivity analysis

All stochastic variables that govern the flood load model, including hydrostatic and hydrodynamic loads and drag forces, and the component capacities, including envelope breach resistance, lateral system capacities, and connections, are organized into eight groups, G1 to G8, as defined in Table 30. Grouping follows engineering judgement so that variables expected to have similar influence on system response are varied together. For each group, the baseline uncertainty is characterized by a truncated normal distribution with a specified CV, unless a different distribution is indicated in Table 27 and Table 28.

To represent information fidelity, we scale the CV of each variable within a group by a weight W_{CV} from the set {0.25, 0.50, 1.00, 1.25, 1.50}, following Yi et al. 2025. A value of 0.25 represents high-fidelity data, and a value of 1.50 represents low-fidelity data. For each setting, we recompute the failure probabilities for CO and for CP.

Table 28 Variable groups for the information fidelity sensitivity analysis

Group ID	Variables
1	Window and door strength in the building envelope
2	Out-of-plane capacity of exterior walls controlled by stud bending, tension, compression, and shear
3	In-plane strength of shear walls and diaphragms
4	Connections between shear walls and roof or floor, and between shear walls and foundation
5	Uplift connections for shear walls (hold-downs)
6	Mass of the house and foundation
7	Flood load model input parameters, see Table 27

8	Flood water density
---	---------------------

Distribution type sensitivity analysis

To test robustness to distributional assumptions, each variable with a truncated normal distribution is, in turn, replaced by a lognormal, beta, or uniform distribution. We then recompute the failure probabilities for CO and for CP and compare the results across distribution families. In this analysis, the CVs of each variable reported in Table 27 and Table 28 were not weighted by the w_{cv} factor.

Sediment concentration scenarios and representative flood events

Because sediment concentration changes fluid density and, in turn, hydrostatic and hydrodynamic forces, four mixture classes are analysed, with representative flood events listed in Table 31. The selected scenarios build on previous work on flood-related events worldwide reported in Contreras and Escariza (2020). From computing the density of the considered mixture, we build on Luo et al., (2020), Quick et al., (2023), and Vasquez-Tarrio et al., (2024) work, considering the following approximation:

$$\rho = \rho_w(1 - c) + c\rho_s \text{ (Eq. 6)}$$

where:

- ρ is the density of the mixture considered in the analysis (kg/m^3),
- c is the solid volumetric concentration,
- ρ_s is the sediment density (2650 kg/m^3),

In this analysis, the CVs of each variable reported in Table 27 and Table 28 were not weighted by the w_{cv} factor.

Table 29 Representative flood scenarios used in the sensitivity analysis.

Flood type	(kg/m^3)	h (m)	v (m/s)
Clear water	1000	1.5	0.5
Lightly sedimented flows/ hyperconcentrated flows 10%	1165	1.6	0.5
Moderately sedimented / hyperconcentrated flows 20%	1330	1.7	0.4
Moderately sedimented / hyperconcentrated flows 40%	1660	1.8	0.3
Debris-flow-like / very high sediment content 60%	1990	1.9	0.7

Computation and outputs

The sensitivity analysis covers all relevant combinations of intensity measures, namely water depth, flow velocity, and flood duration. For reporting, we present results for representative events within each sediment class as shown in Table 31. Outputs include the probability of failure for CO and CP as a function of W_{cv} , by group and intensity measure, and the change in failure probability due to distribution type and sediment concentration, illustrated with fragility curves.

3.1.6 Results

Flood fragility analysis

Figure 18 to Figure 22 present fragility curves for baseline and fully mitigated light-frame timber house typologies. The curves were obtained from numerical simulations with water depth and flow velocity increments of 0.1 m and 0.1 m/s, respectively, and flood durations of 0, 60, and 120 seconds.

Performance of baseline typologies

In general, baseline configurations exhibit limited performance. At the onset of flooding, the median water depth at which both Continued Occupancy and Collapse Prevention are exceeded is approximately 0.6 m. Continued Occupancy is governed by *Breach*, that is, failure of windows and doors under hydrostatic and early hydrodynamic pressures. Collapse Prevention is governed by *Float* due to uplift-induced failure of the shear wall to the foundation connections. These patterns are consistent with post-event field observations reported in the literature (e.g., Drdácý, 2010). Since *Float* is controlled by buoyancy, an increase in the number of stories and thus in structural mass improves resistance against Collapse Prevention. The median depth at Collapse Prevention increases by up to about 115% (from 0.6m to 1.3m) when the one-story case is compared with the four-story case. After water enters the structure, hydrostatic pressures equalize and buoyant uplift reduces to a minimum, as shown by comparing Figure 18a and Figure 19b with Figure 21a and Figure 21b, respectively.

When flow velocity is introduced as an additional intensity measure at the onset of inundation, before interior flooding occurs, the probability of failure at the Continued Occupancy and Collapse Prevention levels remains essentially unchanged across cases as a function of velocity. This is because Continued Occupancy is mainly governed by hydrostatic actions on openings, and Collapse Prevention is governed by buoyancy acting on the hold-downs at the shear wall-to-foundation connections (i.e., *Float* failure mode). Hence, the response depends primarily on water depth. After about 2 minutes, once the interior and exterior water levels have equalized, the structural response changes (see Figure 21a and Figure 21b). In the baseline case, hydrodynamic actions become dominant and failure probabilities increase with both velocity and depth, producing a bivariate fragility response for Collapse Prevention in the absence of structural mitigation.

Performance of fully mitigated typology

The mitigation measures produce a marked performance improvement. At the onset of flooding, the median water depth increases by up to 320% for Continued Occupancy and up to 115% for Collapse Prevention compared with the baseline typologies.

Reinforcing the building envelope increases resistance to *Breach*, as seen when comparing Figure 18 and Figure 19 panels a to c and b to d. The associated delay in water intrusion, however, increases the volume of trapped air, which amplifies buoyancy and elevates the likelihood of *Collapse* and the *Float* failure mode through hold-down failure. As a result, the probabilities associated with Collapse Prevention may rise in ranges where Continued Occupancy and Collapse Prevention thresholds lie close to one another, particularly up to three stories.

These results point to a clear trade-off in flood mitigation. Strengthening openings, for example by upgrading door and window performance, helps prevent water ingress and delays damage to interior contents, which can shorten recovery. At the same time, delayed ingress may increase buoyancy and the risk of collapse, leading to loss of stability and the total loss of the building and its contents. This point is particularly important because many studies on flood vulnerability prioritize contents over structural performance (e.g., Custer and Nishikima, 2015; Nofal et al., 2020a,b)

When flow velocity is introduced at the onset of inundation, in contrast with the baseline case, the mitigated configurations show a dependence of the failure probabilities for Continued Occupancy and

Collapse Prevention on velocity. After about 2 minutes, once interior and exterior water levels have equalized, the response departs further from the baseline because the strengthened envelope delays *Breach*.

Envelope mitigation alters the Collapse Prevention level behaviour for specific flood conditions. For depths below about 3.0 meters and velocities below about 3.0 m/s, delayed water ingress increases air entrapment and buoyancy. This produces a local peak in the Collapse Prevention probability around 1.4 to 1.5 m at zero velocity for the one-story archetype and around 2.0 m for the four-story archetype. As velocity increases from 0.0 to 3.0 m/s, the Collapse Prevention probability decreases, a counterintuitive effect linked to earlier failure of openings at higher dynamic pressure. Earlier *Breach* equalizes water levels more quickly, reduces uplift and lateral demands, and lowers the risk of collapse. For velocities above about 3.0 m/s and depths above about 1.0 m, the influence of envelope strengthening becomes negligible, hydrodynamic actions govern, and a bivariate response in depth and velocity is observed. In this regime, the probability of failure remains noticeably lower than in the baseline archetype.

Enhancing the capacity of hold-downs and shear keys at the shear wall-to-foundation interface is a more reliable way to reduce Collapse Prevention risk across a wide range of flood conditions.

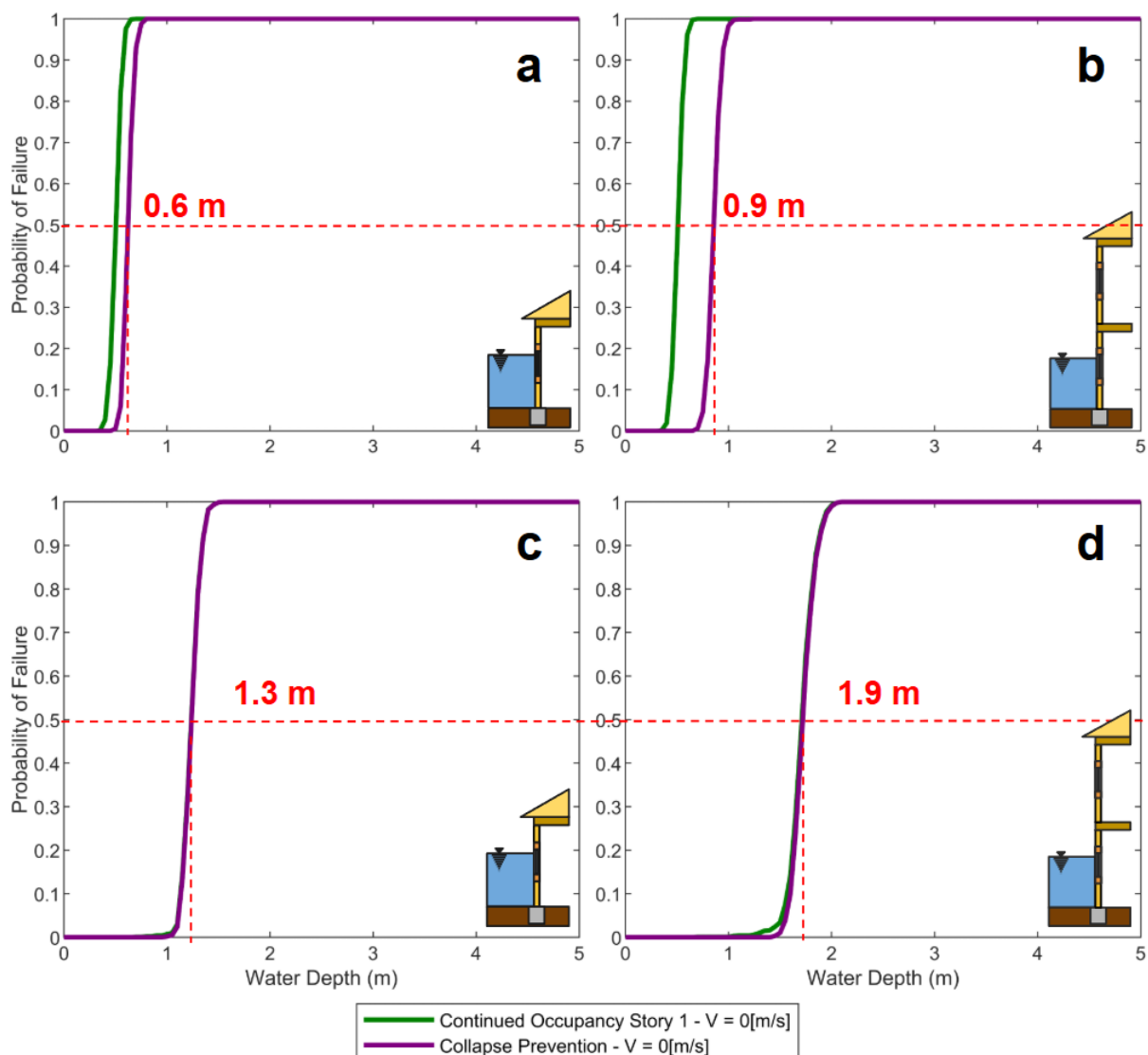


Figure 15 Impact of mitigation measures on the fragility response of archetype light-frame timber houses: (a) one-story baseline, (b) two-story baseline, (c) one-story fully mitigated, and (d) two-story fully mitigated.

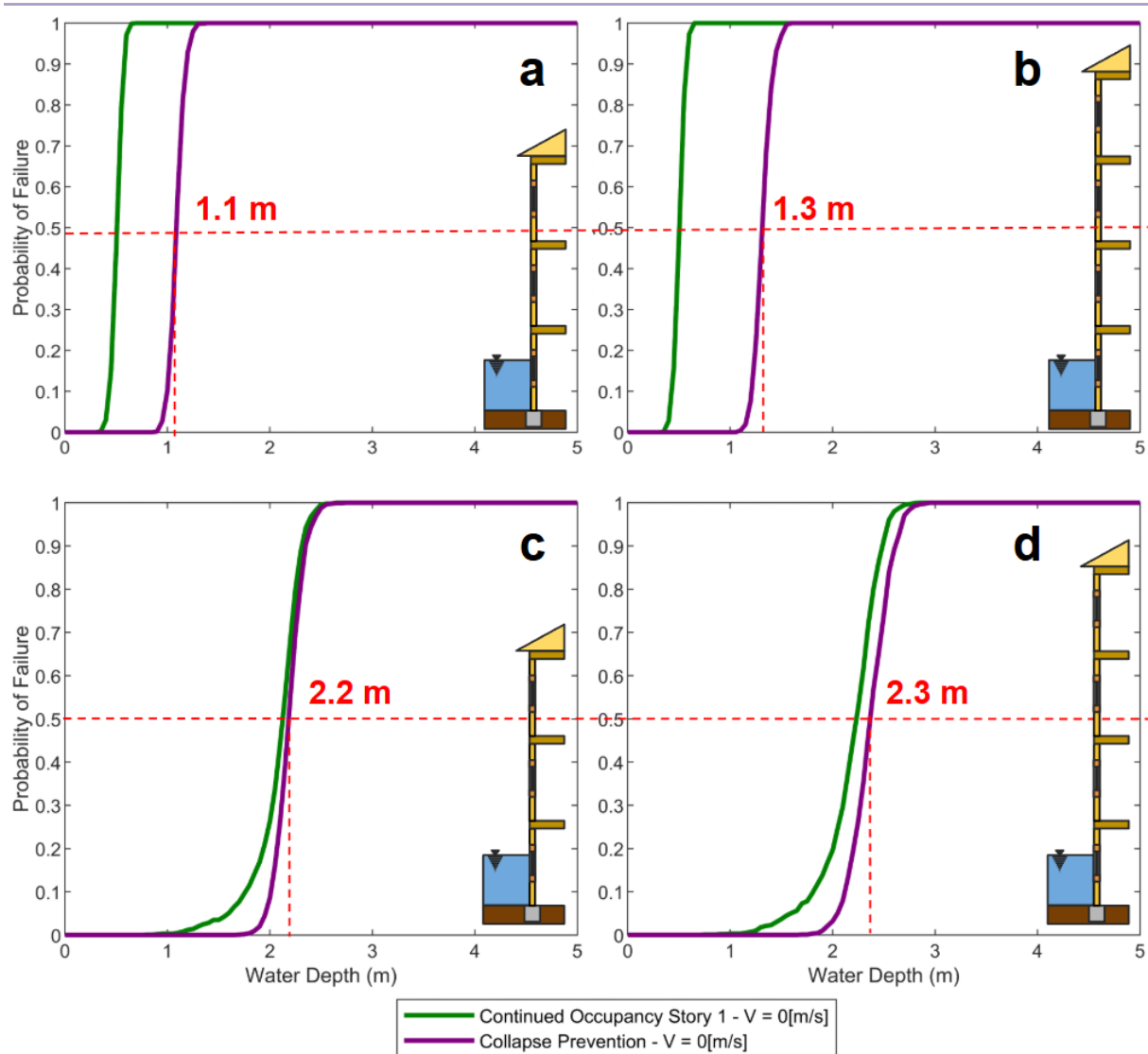


Figure 16 Impact of mitigation measures on the fragility response of archetype light-frame timber houses: (a) three-story baseline, (b) four-story baseline, (c) three-story fully mitigated, and (d) four-story fully mitigated.

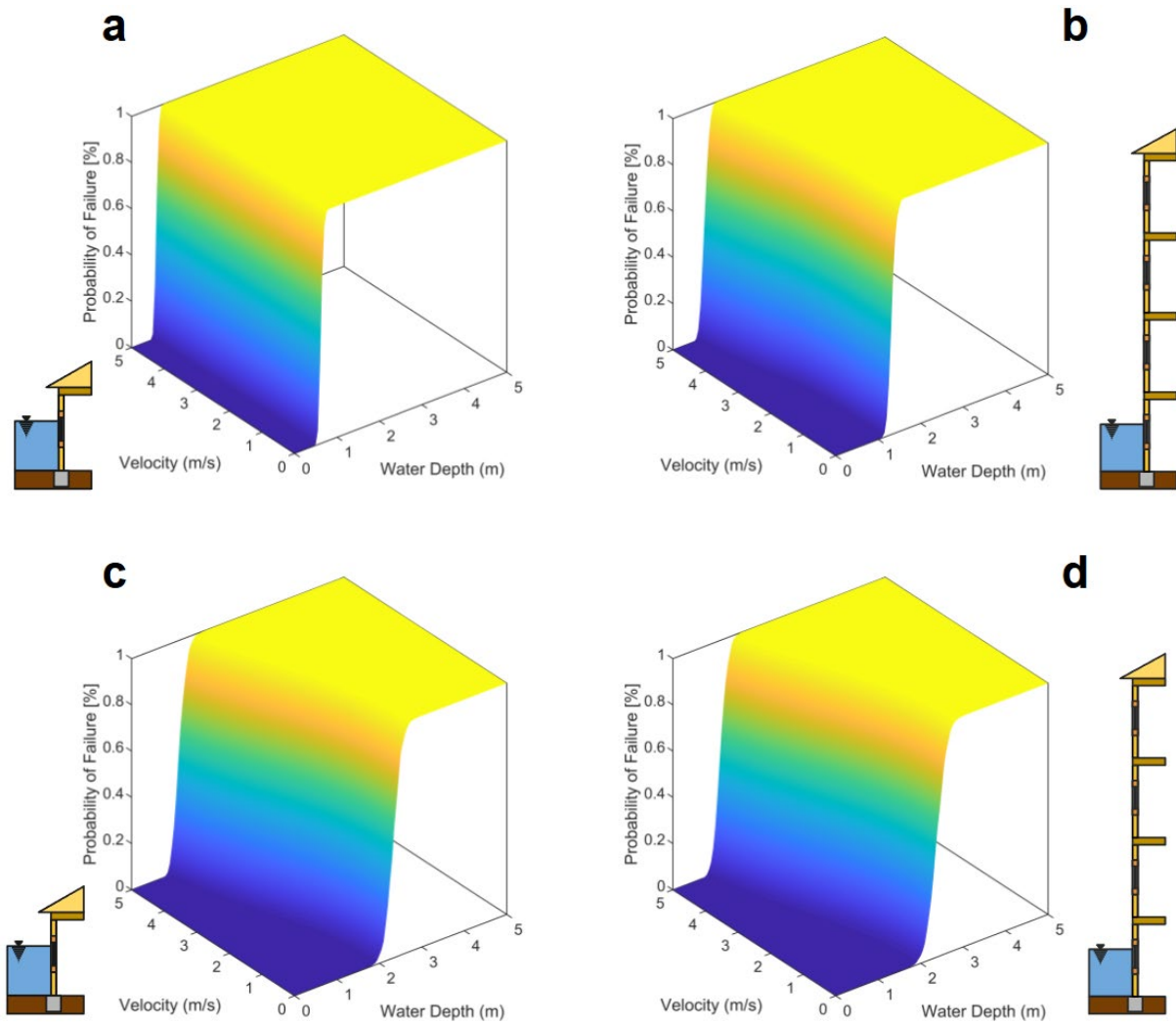


Figure 17 Evaluation of the impact of IMs on the Continued Occupancy performance level response: (a) one-story baseline; (b) four-story baseline; (c) one-story fully mitigated; (d) four-story fully mitigated at the onset of the flood event.

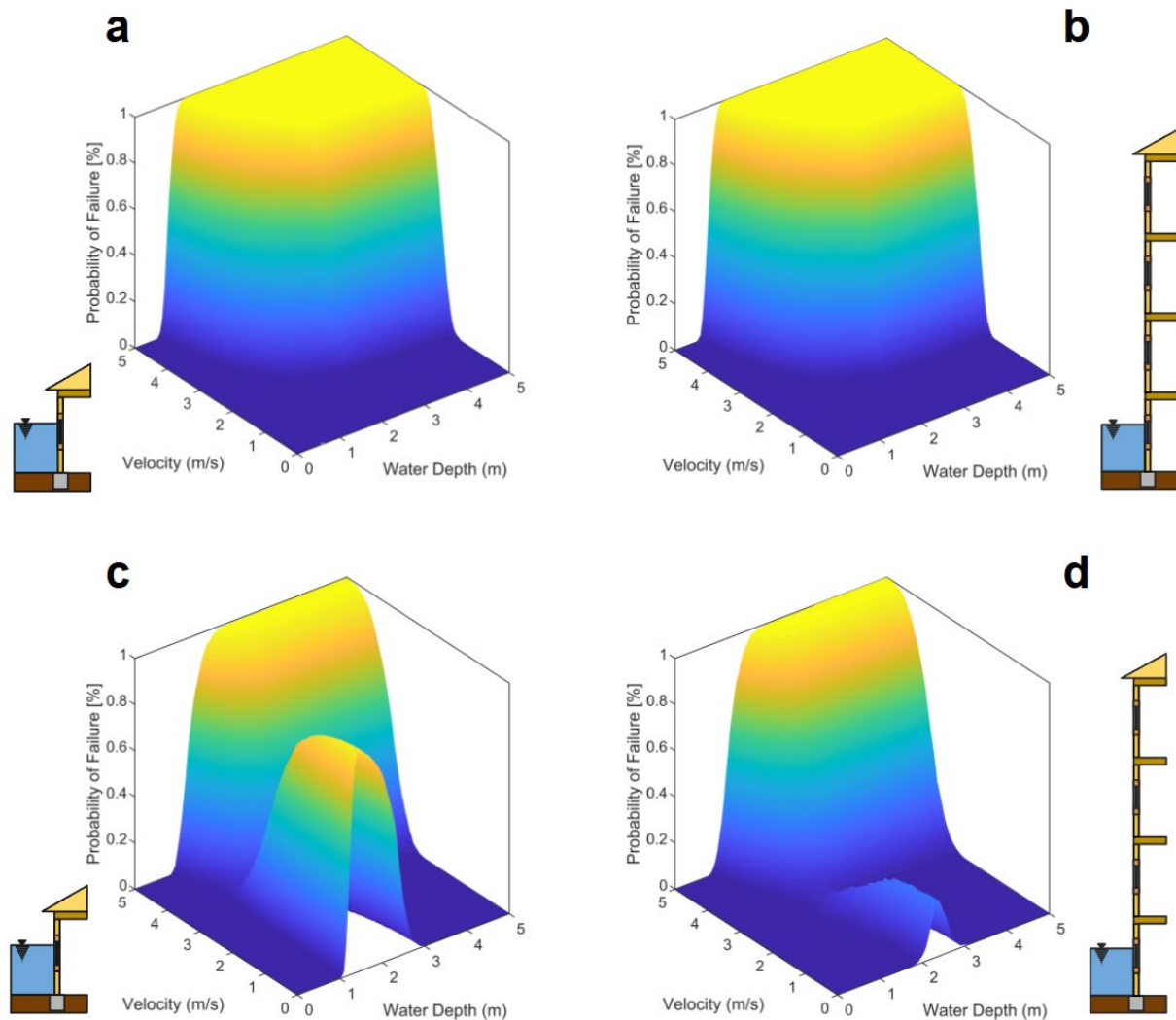


Figure 18 Evaluation of the impact of IMs on the Collapse Prevention performance level response: (a) one-story baseline; (b) four-story baseline; (c) one-story fully mitigated; (d) four-story fully mitigated after water get inside the structure.

Parametric sensitivity analysis

Information fidelity

Figure 22 to Figure 24 show the flood performance model's response to information fidelity for the variable groups in Table 29. Results are reported for the baseline and the fully mitigated cases in one-story and four-story configurations. Information fidelity is represented by the coefficient of variation adjustment factor W_{CV} . Lower values indicate higher fidelity in the data; $W_{CV} = 0.25$ represents high fidelity, and $W_{CV} = 1.5$ represents low fidelity. Comparing Figure 22 with Figure 23 shows that the groups that control failure probability change with the mitigation measures, the number of stories, and the performance level considered.

Continued Occupancy

In the baseline case, envelope strength (group ID 1) is the primary driver of model accuracy. In mitigated cases, envelope capacity remains the primary influence, but water density (group ID 8) becomes essential for one-story houses when data fidelity is low. This occurs because strengthening

windows and doors shifts the Continued Occupancy threshold closer to Collapse Prevention (see Figure 18a, Figure 18b, Figure 19a, and Figure 19b), making buoyancy effects more consequential and the predicted probability of failure more sensitive to the assumed water density.

Collapse Prevention

In the baseline case, the capacity of hold-downs at the shear wall-to-foundation interface (group ID 4) dominates the accuracy of Collapse Prevention predictions. In mitigated cases, at high fidelity, the response shows weak dependence on individual groups; the residual influence is concentrated in the connections at the shear wall-to-roof/floor, and shear wall-to-foundation interfaces. Under low fidelity, the one-story case becomes most sensitive to water density (group ID 8). In contrast, the four-story case is more sensitive to the strength of the non-structural envelope components, especially windows and doors (group ID 2). This pattern is consistent with the mechanics observed in Figure 21c and Figure 21d. For low-rise structures, buoyancy is strongly dependent on water density. In the mid-rise configuration, the capacity of openings influences the timing of Breach, which, in turn, affects hydrostatic force equalization, increasing the failure probability at depths and velocities below about 3.0 m and 3.0 m/s.

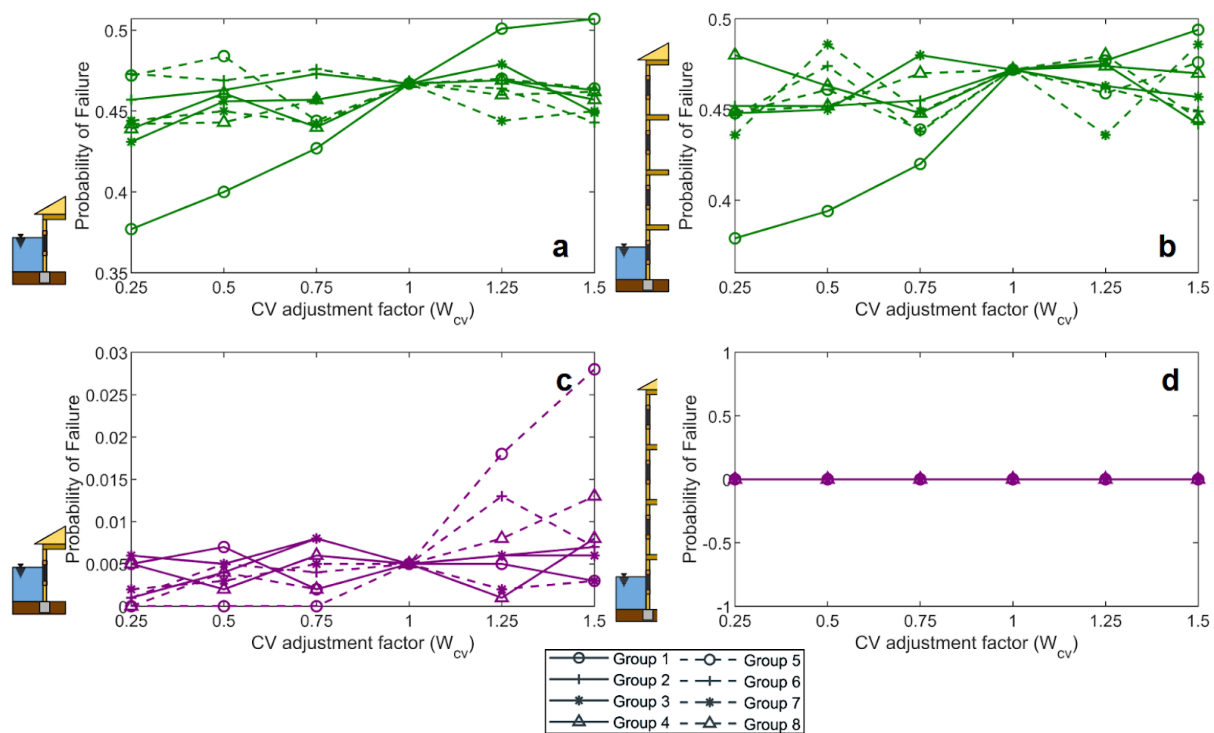


Figure 19 Parametric sensitivity of failure probability for the baseline archetype as a function of information fidelity (grouped as in Table 29) at the onset of a flood event with depth 1.0 m and velocity 0.0 m/s: Continued Occupancy, a) one story and b) four story; Collapse Prevention, c) one story and d) four story.

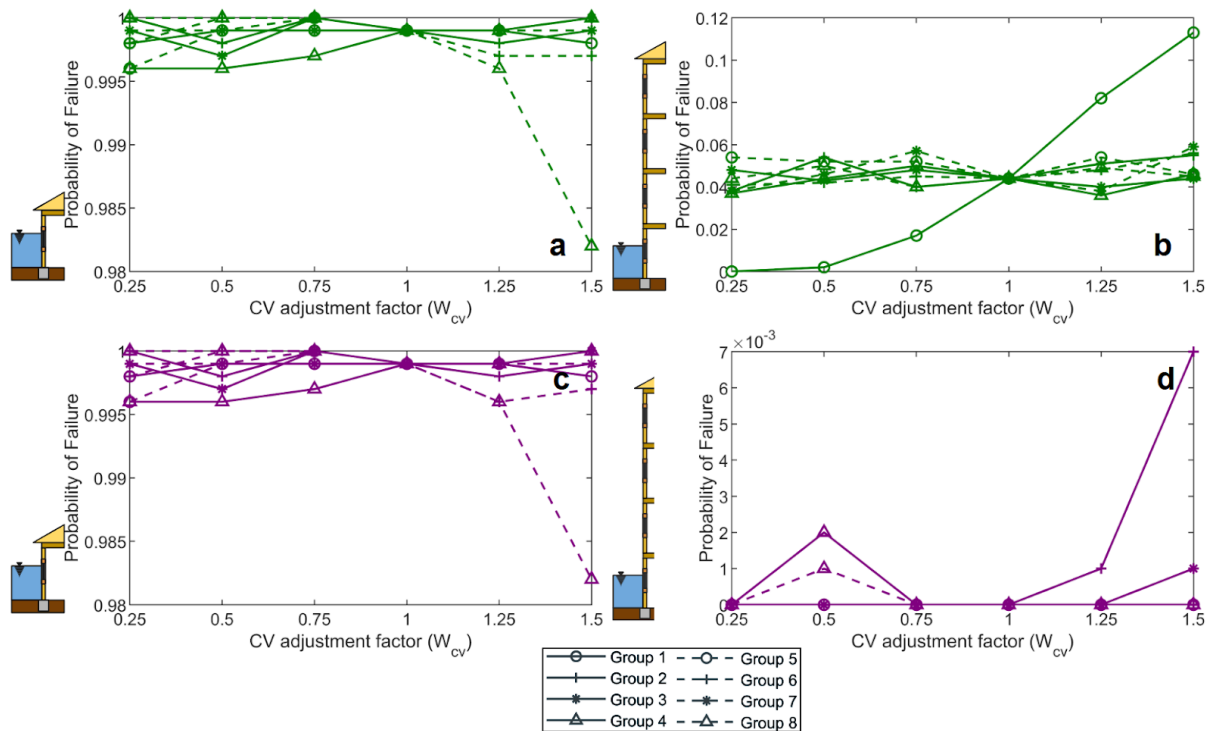


Figure 20 Parametric sensitivity of failure probability for the fully mitigated archetype as a function of information fidelity (grouped as in Table 29) at the onset of a flood event with depth 1.0 m and velocity 0.0 m/s: Continued Occupancy, a) one story and b) four story; Collapse Prevention, c) one story and d) four story.

Post-Breach regime

About two minutes after openings fail and water enters, interior and exterior water levels reach equilibrium. For low rise structures, the dominant influence shifts to the groups associated with flood water mixture density, which govern lateral demands on the structure (compare Figure 23a and Figure 24a). In the four-story case, sensitivity to data fidelity remains comparatively small after equalization relative to the onset condition (compare Figure 23b and Figure 24b).

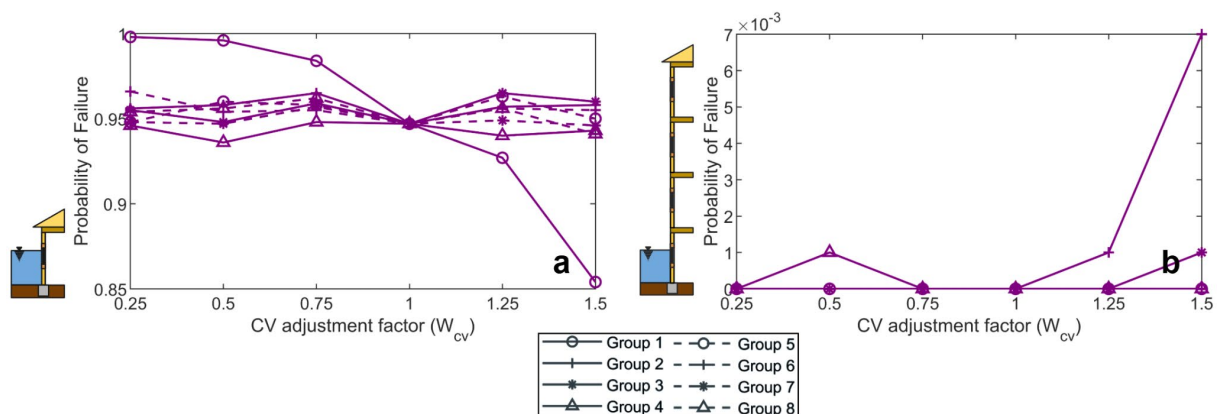


Figure 21 Parametric sensitivity of failure probability for the fully mitigated archetype as a function of information fidelity grouped as in Table 29, evaluated at the Collapse Prevention level for a flood with depth 1.5 m and velocity 0.5 m/s, two minutes after onset: (a) one story, (b) four story.

Distribution assumption

Figure 25 shows the effect of the assumed response distribution on the predicted probability of failure for the one-story baseline case. The choice of distribution has only a minor influence. As a function of water depth with velocity equal to zero, the curves for the truncated normal, beta, and uniform assumptions are nearly indistinguishable (see Figure 25a). The lognormal assumption yields slightly higher failure probabilities, with differences up to about 10% in some ranges for a flood event of water depth of 0.6m (see Figure 25b). Overall, the model is largely insensitive to the distribution choice. However, the justification should focus on whether a truncated normal or a lognormal provides the most appropriate tail behaviour for the variables under consideration.

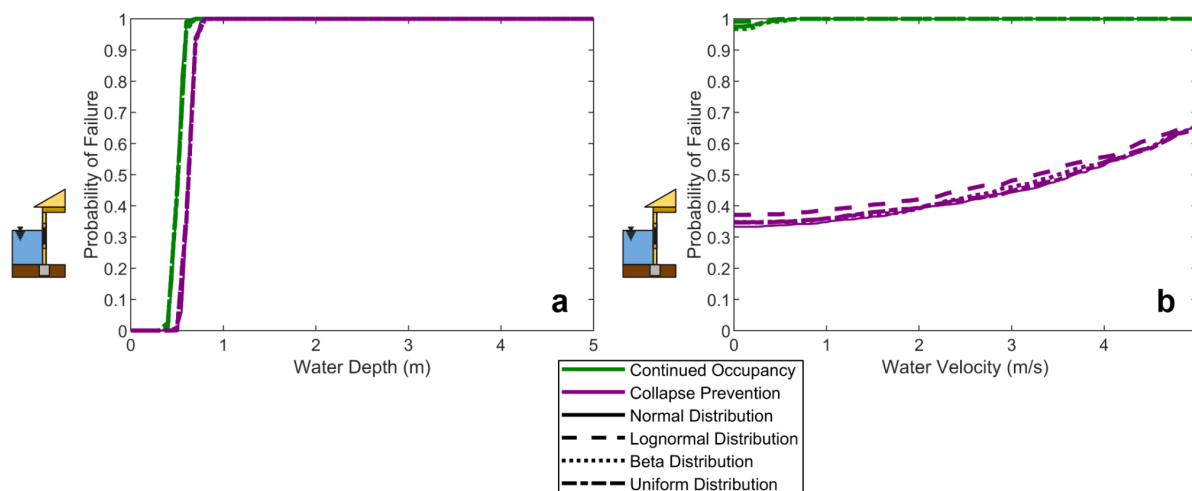


Figure 22 Assessment of the influence of the assumed response distribution on performance levels for the one-story baseline case: (a) as a function of water depth with velocity set to 0.0 m per second, and (b) as a function of flow velocity at a fixed water depth of 0.60 m, both at the onset of the flood event.

Flood water mixture

Since water density plays a vital role in model fidelity for both Continued Occupancy and Collapse Prevention, the composition of the flood water is also consequential. Figure 26 evaluates the effect of sediment concentration on the Collapse Prevention two minutes after the onset, when interior and exterior water levels have equalized. The results show a nearly monotonic increase in failure probability with increasing sediment content, consistent with the higher mixture density and the associated rise in hydrostatic and hydrodynamic demands. Accurate characterization of flood water mixtures is therefore necessary to obtain reliable predictions of structural response.

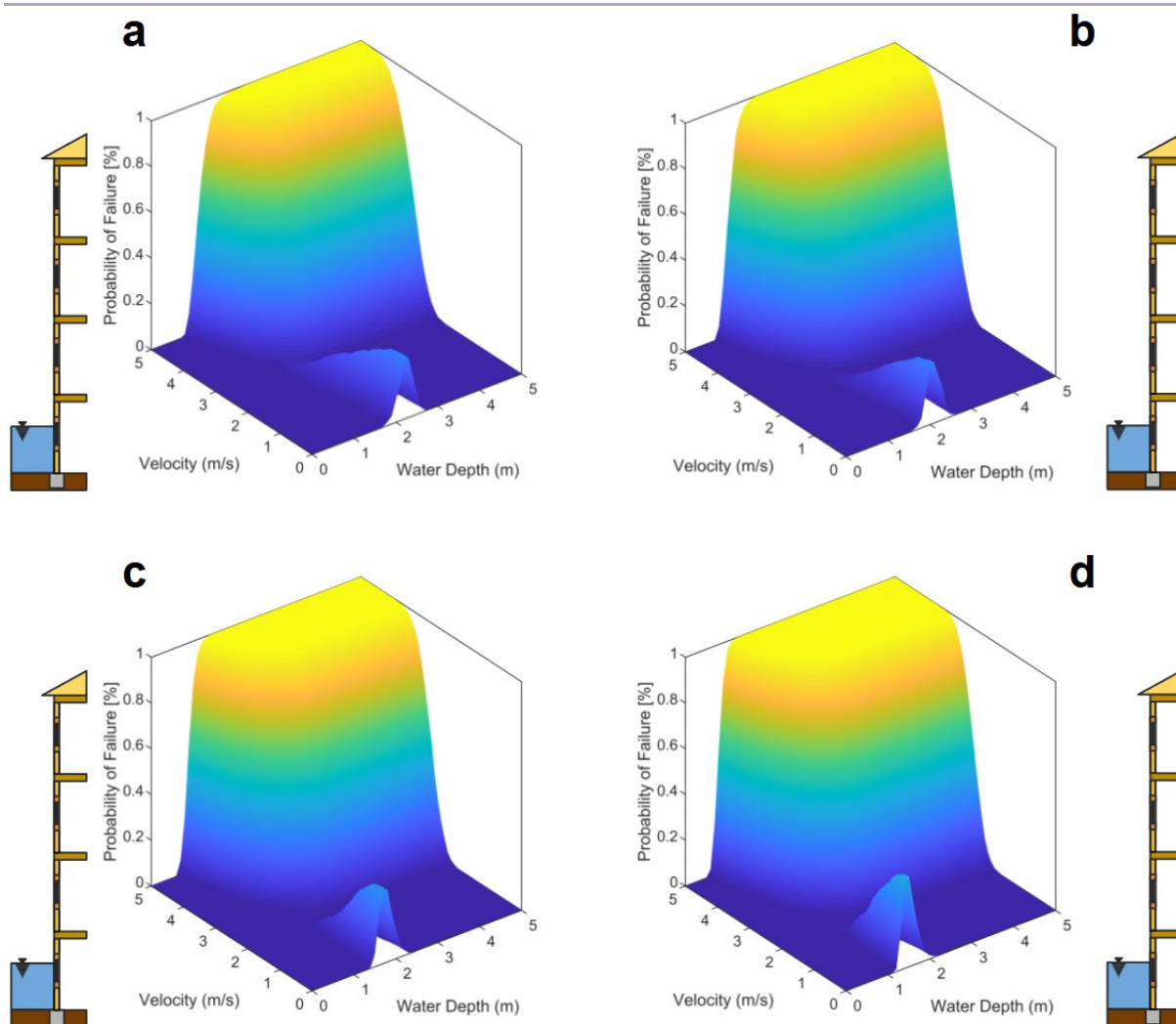


Figure 23 Evaluation of the effect of flood water mixture on the Collapse Prevention performance level two minutes after the start of the event for the four story fully mitigated archetype: (a) lightly sedimented hyper concentrated flows; (b) moderately sedimented hyper concentrated flows; (c) moderately sedimented hyper concentrated flows; (d) debris flow like mixtures with very high sediment content.

3.1.7 Conclusions

This study develops and applies a physics-informed, component-based flood performance framework for light-frame timber housing and demonstrates its value for design and mitigation. Baseline archetypes show low capacity at the onset of inundation, with Continued Occupancy governed by *Breach* of openings and Collapse Prevention by buoyancy-driven *Float* at the shear wall-to-foundation interface. Increasing the number of stories increases mass and improves Collapse Prevention capacity, consistent with reduced susceptibility to uplift.

Mitigation measures deliver significant performance gains. At the onset of flooding, the median depth associated with Continued Occupancy and Collapse Prevention increases by approximately 320% and 115%, respectively. These gains are not unconditional. Delaying water ingress protects contents and reduces the risk of early interruption of function. Still, it can amplify buoyancy and raise the probability of *Float* and *Collapse* if anchorage and lateral connections are not upgraded in parallel. The most robust improvements in Collapse Prevention are achieved by strengthening hold-downs, shear wall-to-roof/floor interfaces, and shear wall-to-foundation interfaces.

Time dependence governs the controlling mechanics. Before water enters the interior, Collapse Prevention is primarily a function of depth because buoyant forces dominate. After interior and exterior levels equalize, uplift decreases, and hydrodynamic actions become more critical, so fragility depends on both depth and velocity. Under moderate conditions, greater velocity can decrease Collapse risk by causing earlier *Breach* and faster equalization of hydrostatic forces; at larger depths and velocities, hydrodynamic actions increase vulnerability regardless of envelope strength.

Parametric sensitivity studies clarify modelling priorities. The choice among common distribution families has a minor effect on predicted fragility, with lognormal assumptions yielding slightly higher probabilities in some ranges. Information fidelity exerts a more substantial influence. Model accuracy for Continued Occupancy is most sensitive to envelope capacity and, for low-rise mitigated cases, to water density. Accuracy for Collapse Prevention is most sensitive to connections capacity (i.e., hold-downs and shear wall-to-roof/floor/foundation) in baseline configurations. It remains governed by connection detailing in mitigated configurations, with water density again critical for low-rise cases. Because mixture density increases both hydrostatic and hydrodynamic demands, characterizing sediment concentration is necessary for reliable assessment.

The results support three design implications. First, combine envelope upgrades with strengthening hold-downs and shear wall connections to the roof, floor, and foundation so that vulnerability is not shifted from contents to the structure. Second, adopt a multivariate and time-dependent assessment that includes depth, velocity, and duration to capture the transition from buoyancy-controlled to hydrodynamic-controlled behaviour. Third, prioritize high-quality data for opening capacity, connection capacity, and flood water density, since these variables govern prediction accuracy and mitigation effectiveness. The framework is adaptable to additional hazards and calibration data sets and to decision models that balance interior protection with structural integrity to improve functional recovery of flood-prone housing.

3.2 Patras, Greece

3.2.1 Theoretical background

Critical infrastructures are the backbone of modern society, encompassing essential systems such as energy, water supply, transportation, and communication networks that sustain economic stability and public safety. These infrastructures are highly interdependent, meaning that disruptions in one system can trigger cascading failures across multiple sectors, leading to severe social and economic consequences (Rinaldi et al., 2001). The increasing complexity of urban environments, combined with the growing threats posed by climate change, natural disasters, cyberattacks, and aging infrastructure, has heightened the urgency of enhancing CI resilience and adaptive capacity (Ouyang et al., 2014). The critical infrastructures considered in this work are taken from the European Commission's "Green Paper" on the European Programme for Critical Infrastructure Protection (Directive 2008/114/EC, 2008) i) ICT, ii) EN, iii) WSN, iv) CSA. The Council Directive 2008/114/EC of the European Union (European Commission, 2005) emphasizes the vital role that critical infrastructures play in modern society. A national (or regional or international) critical infrastructure is a complex system of interconnected and dependent critical infrastructures because individual CIs need products and/or services from other CIs to operate normally (Lauge et al., 2015). CI dependencies are unavoidable, and their presence makes individual critical infrastructures and the critical infrastructure as a whole more vulnerable to failure (Bologna et al., 2006).

As studying one specific infrastructure as an isolated and independent system is a concept now obsolete, we consider the larger system of networked CIs to understand dynamics of a single CI. We assume every infrastructure produces commodities to satisfy the demand while needs products and services from other CIs in order to operate normally (Canzani, 2016). Our model also accounts for the service level of each CI, but differently we distinguish between operational and service levels by

introducing the demand factor. This is to say that even though some CI operations are damaged, the CI may still be able to provide services that meet the demand.

3.2.2 Critical infrastructure modelling

SD is a methodology used to comprehend complex systems, their simulation, and analyses of dynamic behaviours evolving over time. First developed in the 1950s at MIT by Jay W. Forrester, SD employs stocks, flows, feedback loops, and time delays to represent the structural elements of a system (Sterman, 2002). The goal of SD modelling is to uncover the interactions among the components driving the behaviour of the system; it provides users with the opportunity to gain insight into the possible effects different policies, strategies, or exogenous changes might have. SD modelling describes complex systems through two tools, the causal loop diagram and the stock and flow diagram (Gravelsins et al., 2018).

Over the last decade, several studies implement system dynamics approach to understand and analyse specific challenges and problems in urban areas. Mavromati et al. presented a SD model for sustainability of urban coastal systems (Mavrommati et al., 2013). The study introduced the use of an index for estimation of the system's condition for an assessment of specific policy measures. Mylonakou et al. (2023) developed a SD model to assess how changes in urban transport, such as accessibility, safety and sustainability, affect citizen's satisfaction Armenia et al. (2015) and Cavallini et al. (2014) presented an approach for modelling the effects of CI failures due to unexpected events. The CIs of Transport, Energy and Telecommunications were modelled using SD. The model was developed as a component of a European Commission-funded project focused on developing a tool to evaluate the impacts of critical events. Canzani (2016), employed an SD model to investigate the cascading effects of failures in the CIs of Energy, ICT, Water, Financial, and Transport due to a cyber-attack or disruption in ICT. The model is based on the Susceptible -Infectious-Recovered-Susceptible (SIRS) model from epidemiology, where the Susceptible, Infected, and Recovered represent the Running, Down, and Recovered operations in a CI, respectively (Brauer et al., 2008). Canzani extracted a table of constants from Laugé et al. (2015) to prepare a matrix of constants, representing the effect of failure in one CI resulting from a less than two hours failure in another. This matrix was incorporated into Canzani's model to regulate the failing CIs' breakdown rates. Abdelgawad et al. (2019) further extended it to all eleven CIs, introducing a dynamic cube of interdependency matrices to represent time-dependent cascading effects. Collectively, these studies highlight SD as a powerful and adaptable methodology for modelling the complex dynamics, feedback, and fragilities of interconnected urban and infrastructure systems.

3.2.3 Methodology

The modelling framework developed in this study builds upon the SD approach proposed by Canzani (2016). Canzani introduced a "block building" methodology to represent the nonlinear and time-dependent behaviour of interdependent CIs under disruptive events. The approach decomposes the overall complexity into three modular components (blocks), which can be implemented and later integrated to simulate cascading effects and resilience dynamics.

Block 1 – Disruptive Event

This component defines a disruption as a time-dependent function $d(t)$ characterized by its *onset time* t_0 , *duration* ΔT , and *magnitude* (Equation 7). In the present study, parametric event functions were used to represent shocks such as heatwaves, floods, or cyberattacks. Each event temporarily reduces the operational capacity of one or more infrastructures.

Equation 1
$$d_i(t) = m_i \times PULSE(t_{0i}, \Delta T_i)$$

where

- t_{0i} = onset time of disruption for infrastructure
- ΔT_i = duration of the disruption,
- $m_i \in [0,10]$ = magnitude factor describing the intensity of the shock.

In this work, the **PULSE** function is represented in Python as a binary time series or continuous square pulse, applied to modify the breakdown rate of the affected infrastructure during the disruption window.

Block 2 – Single Infrastructure Dynamics

Following the adaptation of the SIRS epidemic model in the work of Canzani (2016), each CI is modelled as a dynamic system whose *running*, *down*, and *recovered* operational states evolve through differential equations. Transitions occur according to a breakdown rate $\alpha(t)$, a repair rate β , and a recovery rate γ . The total number of operations for each CI is defined as $C_{i,max} = 100$, and the system is considered to operate under normal conditions when all operations are running. In this study, the SIRS-based formulation is numerically solved using Python's ODE solvers, enabling flexible simulation of continuous-time recovery dynamics. The model tracks three operational states over time:

- $OP_{run}(t)$: running (active) operations,
- $OP_{down}(t)$: failed operations,
- $OP_{rec}(t)$: recovered operations.

Ideally all CI operations are available and running, but system capabilities may change when a disruption occurs. This means that OP_{run} can break with a certain rate α due to the disruption and become out of service (i.e. OP_{down}). In this case, CI operators must intervene to repair down operations, so that OP_{down} move to OP_{rec} with rate β . Once recovered, OP_{rec} are finally restored back to function (i.e. OP_{run}) with rate γ . In this work, we assume constant average rates for β and γ , as we mainly focus on the breakdown rate $\alpha(t)$. The dynamic transitions among these states are governed by the following system of differential equations:

Equation 2
$$\frac{dOP_{run}(t)}{dt} = -\alpha(t) \frac{OP_{run}(t)}{n_{op}} + \gamma OP_{rec}(t)$$

Equation 3
$$\frac{dOP_{down}(t)}{dt} = \alpha(t) \frac{OP_{run}(t)}{n_{op}} - \beta OP_{down}(t)$$

Equation 4
$$\frac{dOP_{rec}(t)}{dt} = \beta OP_{down}(t) - \gamma OP_{rec}(t)$$

where:

- $\alpha(t)$ = time-dependent breakdown rate,
- β = repair rate,
- γ = recovery rate,
- n_{op} = total number of operations of the infrastructure, i.e. $OP_{run}(t) + OP_{down}(t) + OP_{rec}(t) = n_{op}$

Block 3 – Interdependent Network of Infrastructures

This block serves to replicate dynamics of cascading effects occurring in interdependent C is when one or several of them are disrupted. For simplicity, the variable n_i used to represent epidemic-like CI dynamics is replaced by the maximum capability $C_{i,max}$. This reflects that a system's capacity is defined

by its total number of operations. A CI operates at full capacity—its “normal operational state”—when all operations are active, i.e., $OP_{i,run}(t) = C_{i,max}$. Block 3 represents the overall system as a network of interconnected SIRS-based models, capturing both internal and cross-infrastructure dynamics. It integrates the operational behaviour of each node (from Block 2) and their responses to disruptive events (from Block 1).

Interdependencies among infrastructures are represented through a weighted connection matrix $E = \{e_{ij}\}$, where each coefficient quantifies the dependency of infrastructure i on the services provided by infrastructure j . Note that with the term “service” we mean also products, commodities, and all needs CIs provide one another. As in the original model, cascading failures occur when a disrupted CI reduces its service provision $S_j(t)$, which in turn increases the breakdown rate $\alpha_i(t)$ of dependent infrastructures. This feedback structure captures the propagation of cascading effects across the network. $S_j(t)$ varies over time between 0 (no service provided) and 1 (when the current capability is bigger or equal to the demand).

The service level $S_j(t)$ of infrastructure j at time t is defined as:

Equation 5

$$S_j(t) = \begin{cases} 1, & \text{if } C_j(t) \geq D_{j,avg} \\ \frac{C_j(t)}{D_{j,avg}}, & \text{otherwise} \end{cases}$$

Where $C_j(t) = \frac{OP_{run,j}(t)}{C_{max,j}}$ represents the current capability and $D_{j,avg}$ the average demand for services.

The breakdown rate $\alpha_i(t)$ of each infrastructure i is then adjusted according to the services it receives from other infrastructures $j \in J_i$ (the set of providers on which i depends):

Equation 6

$$\alpha^i(t) := \sum_{j \in J_i} \frac{e_{ij}(1 - S^j(t))}{|J_i|}$$

This formulation allows cascading failures: when a service $S_j(t)$ falls below normal levels, it increases the breakdown rate of dependent infrastructures. The matrix E is typically asymmetric ($e_{ij} \neq e_{ji}$), reflecting directional dependencies between sectors such as energy supply, communication, and transportation. Summarizing, a disruption (Block 1) occurring in a CI is the trigger event that influences the breakdown rate of the target CI (Block 2) and consequently may provoke disruptive dynamics in other CIs due to their interdependencies (Block 3).

Integration of Blocks

The three blocks are combined into a unified dynamic system where: the disruption functions $d_i(t)$ triggers initial performance losses in specific infrastructures, the operational dynamics govern internal degradation and recovery, and the interdependency matrix propagates these effects across the network. Figure 27 illustrates how they have been integrated one another in SD stock and flow model of two generic infrastructures i and j s.t. j is disrupted and i depends on services provided by j (i.e. $j \rightarrow i$).

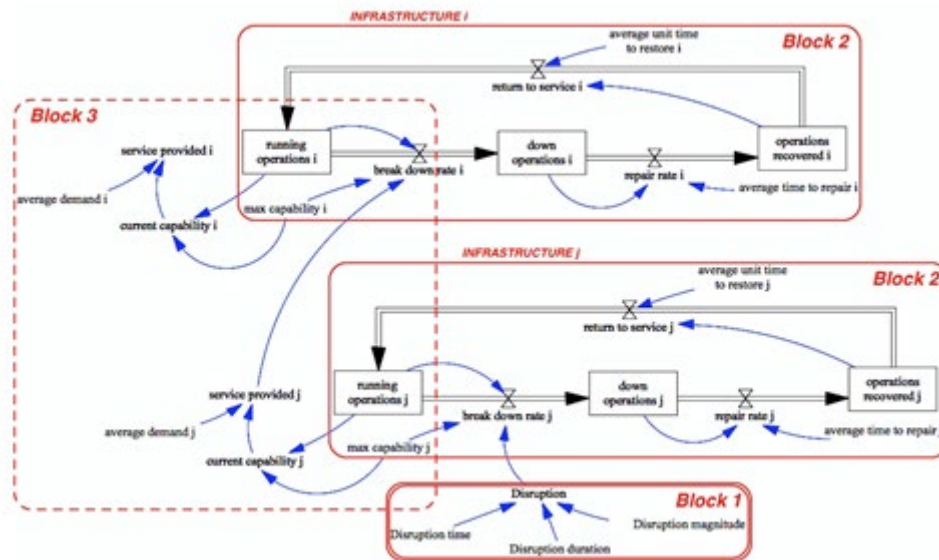


Figure 24 Integrated building blocks, developed by Canzani (2016).

3.2.4 Simulation and impact analysis

In this section we build and simulate different scenarios of disruptions to demonstrate how our model can support risk assessment and management processes. Data were collected from experts through an online questionnaire conducted following a discussion-based workshop. These data served as input parameters for the model and were applied to a hypothetical scenario designed to demonstrate the model's applicability for dynamic impact analysis.

Scenario setting

Causal links across CIs with respect to services they provide to each other are depicted in Figure 28. This qualitative characterization of CIs interdependencies is based on Canzani (2016). Note that this particular setting does not limit further applications of our modelling approach to other scenarios.

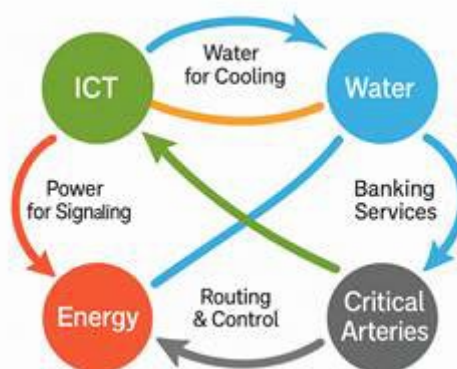


Figure 25 Causal links across CIs.

Survey results

Experts associated with critical infrastructure organizations located in Patras, Greece were invited to a discussion-based workshop with potential end-users of the Minority Report tool, including urban planners, emergency and security organisation representatives, and policymakers working on urban risk resilience in Patras. The quantitative assessment of interdependencies is based on the results of a

survey of CI experts from Patras using an online questionnaire. The questionnaire was designed to discover the magnitudes of the dependencies existing between critical infrastructures due to the inherent complexity of critical infrastructure systems. Specifically, the experts were asked to quantify the magnitudes of the effects on their own critical infrastructures if they did not receive products and services from each of the other critical infrastructures. Thus, each expert essentially rated the dependence of their critical infrastructure on each of the other critical infrastructures. After the workshop, the experts were contacted by email to fill in the survey. Each email message included an explanation of the research, the goals of the questionnaire and a request for survey participation. A total of 33.8% of the recipients returned completed questionnaires.

An important goal was to obtain the magnitude of the effect on each critical infrastructure based on the period that another critical infrastructure was non-operational. For this reason, each expert was asked to provide assessments of the dependence of a critical infrastructure on the ten other critical infrastructures for failure periods ranging from less than two hours. The question posed was “What effect would your critical infrastructure have if a given critical infrastructure was down for: (i) less than two hours?”. The answers to each part of the question were required to be provided on a six-point scale ranging from 0 (no effect) to 5 (very high effect). Table 32 describes the scores in the six-point scale. Note that the scores express the effects suffered by a critical infrastructure due to a direct dependence on another critical infrastructure that fails for a specific period.

Table 30 Six-point scale used to rate direct dependencies.

Scale	Definition
0	No effect: My critical infrastructure can operate as normal
1	Very low effect: My critical infrastructure can operate deploying a few extra resources
2	Low effect: My critical infrastructure can operate deploying a huge number of extra resources
3	Medium effect: My critical infrastructure can deliver critical products and services by deploying a few extra resources
4	High effect: My critical infrastructure can deliver critical products and services by deploying a huge number of extra resources
5	Very high effect: My critical infrastructure can deliver critical products and services by deploying a huge number of extra resources

Table 33 shows the results obtained from the survey. Specifically, the table expresses the CI dependencies when the other critical infrastructures are down for less than two hours. The values listed in the tables were obtained by averaging the individual scores provided by the surveyed critical infrastructure experts Luglio (2016).

Table 31 Results of the survey

		Effect on i			
Failed j	e_{ij}	ENERGY	WATER	TRANSPORT	ICT
	ENERGY	-	1.7	2.7	4.1
	WATER	0.8	-	1.6	0.5
	TRANSPORT	0.8	0.6	-	1.2
	ICT	0.7	0.5	1.2	-

The first row of Table 33 shows the effect that an Energy infrastructure (power) outage of less than two hours would have on each of the other critical infrastructures. On the other hand, the first column of Table 33 shows how failures of less than two hours in the other critical infrastructures would affect the energy infrastructure. Specifically, experts assessed the dependency levels of Energy as 1.7 for Water, 2.7 for Transport, and 4.1 for ICT. Conversely, the first column of the table shows how short-term failures in the other CIs would affect the Energy infrastructure: 0.8 from Water, 0.8 from Transport, and 0.7 from ICT. The results indicate, for example, that the dependency of Energy on ICT was quantified at 0.7. This means that when ICT is down for less than two hours, Energy must deploy additional communication and control resources to maintain critical service delivery. On the other hand, the dependency of ICT on Energy is considerably higher, at 4.1. This implies that ICT operations would be strongly disrupted by even a short-term energy outage, requiring immediate back-up solutions such as emergency generators. This quantitative approach provides valuable insights into the asymmetric and nonlinear nature of interdependencies. For instance, while Water has only a moderate dependence on ICT (0.5), Transport relies on ICT at a higher level (1.2). Similarly, Transport shows a strong dependence on Energy (2.7), highlighting how cascading failures in power supply could rapidly propagate across the network of critical infrastructures.

A deep understanding of the direct dependencies and the higher order dependencies— even for critical infrastructures with low probabilities of disruption— is essential for critical infrastructure operators to be able to prevent, manage and minimize the effects of future crises. The data provided in Table 33 can be used to compare the dependence that one critical infrastructure has on other critical infrastructures versus its influence on other critical infrastructures. The great influence of the energy and ICT infrastructures matches the assessment of van Eeten et al (2011) as the critical infrastructures whose failures are most responsible for initiating cascading effects. This means that critical infrastructure operators should place a priority on analysing the dependencies on energy and ICT and on developing policies and procedures that would reduce or eliminate the consequences of failure in the energy and ICT infrastructures. Upon analysing the dependencies on energy and ICT, critical infrastructure operators should identify the vulnerabilities introduced by the dependencies in order to implement policies and procedures that would reduce the dependencies. For example, the deployment of back-up power generators could minimize the dependence of a critical infrastructure on energy, at least for a few hours. Also, critical infrastructure operators should implement alternative or redundant control and communications systems in the event of an ICT failure.

Scenario results

The present model is implemented in Python, allowing for reproducible computational experiments and easy integration with empirical datasets. The simulation structure preserves the conceptual integrity of the original three-block framework while extending it to incorporate multiple hazard scenarios relevant to the Patras case study context (e.g., heatwave-induced power stress, flooding, wildfire, and earthquake events). The simulation horizon is set to two weeks (336 hours) with an hourly timestep. Each scenario defines one or more disruptions through the parameters (t_0 , ΔT , m) and the resulting coupled dynamics of operational states and service levels are observed for all infrastructures.

The model takes data in Table 33 as input to set values of the connection matrix $E = \{e_{ij}\}$, $0 \leq e_{ij} \leq 5$, that exactly aim to estimate the level of effects of eventual failures in infrastructure j on infrastructure i (Block 3). We remark that E serves only to mutually assess interdependent effects between CIs. This means that input data must fit our simulations' time scale (Hours). In our model, magnitudes of interdependencies will change over time that determine system behaviours accounting for nonlinear dynamics of disruptions (Block 1), CIs operations (Block 2), and services (Block 3).

For convenience, we assume each CI has max capability $C_{i,\max} = 100$ operations. By definition of 'normal operational state' (Block 2), $OP_{i,\text{run}}(t) = C_{i,\max}$ per $0 \leq t < t_d$ (i.e. before the stress of the system with a disruptive event). The average demands for services, Di_{Av} is then assumed being 90% of $C_{i,\max}$ as in

real-world situations infrastructures do not usually work at the maximum of their capabilities for being able to meet the demand. Assumptions only serve to run simulations with the purpose of demonstrating applicability of our original modelling approach; therefore, they do not limit further model application to different scenarios.

Starting from this model setting, we carry out a simulation-based impact analysis by comparing different scenarios of disruptions. The model computes the evolution of two key variables for each infrastructure:

- Running operations $0 \leq OP_{i,run}(t) \leq 100$, which indicates the operational state of single CIs; representing the proportion of operational capacity at time t ; and
- Service provided $S_i(t)$, $0 \leq S_i(t) \leq 100$, which determines if disruption impacts make a CI unable to provide adequate services to other CIs and so damage effects are cascading among them.

Single scenario results

Scenario 1 – Summer Heatwave and Power Stress

A severe heatwave triggers an overload in the EN at $t_0 = 72h$, lasting for 48 h with magnitude $m=7$. The model shows a rapid decline in EN operational capacity, leading to partial degradation of ICT services due to reduced power availability. WSN pumping efficiency decreases because of electricity-driven operations, while CSA experience increased congestion as traffic signals fail intermittently. The system gradually recovers after approximately 4 days, demonstrating moderate resilience. This scenario validates the model's ability to capture cascading effects, where a single-sector failure (energy) propagates through dependent infrastructures.

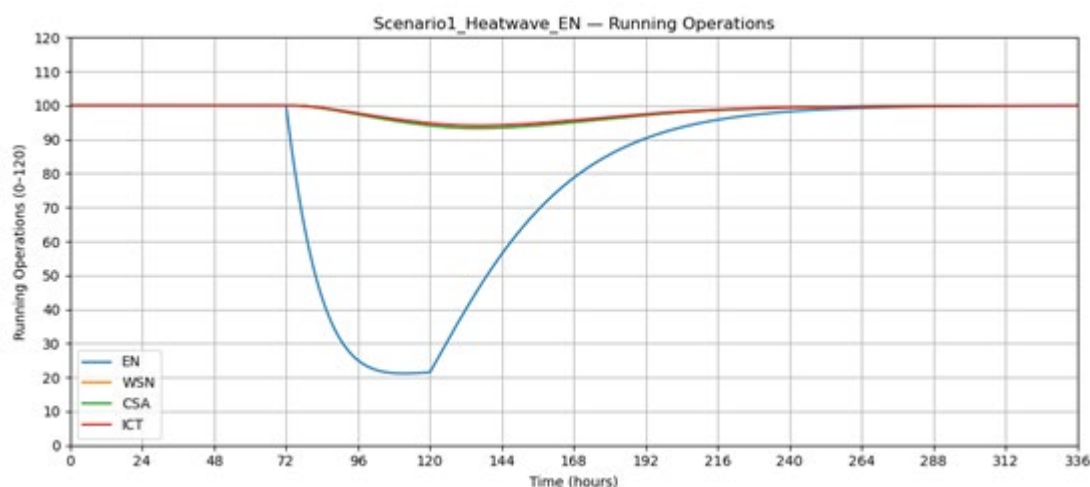


Figure 26 Scenario 1 - running operations.

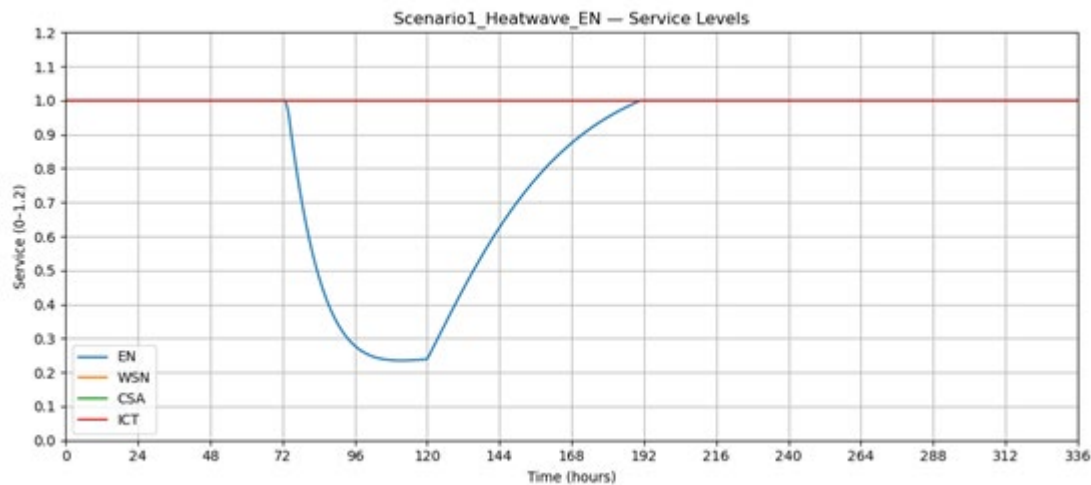


Figure 27 Scenario 1 - service levels

Scenario 2 – Flooding of Street Arteries

A flood event at $t_0 = 120\text{h}$ disrupts CSA for 24 h with magnitude $m = 6$. The direct operational impact on CSA is limited in duration, yet the indirect effects are more persistent: ICT technicians and repair crews face delayed access to network facilities, extending recovery times for both ICT and EN systems. WSN operations also experience temporary pressure drops due to blocked road access to pumping stations. The model reproduces the logistical coupling between transport and repair operations, illustrating how physical accessibility constraints can indirectly reduce resilience

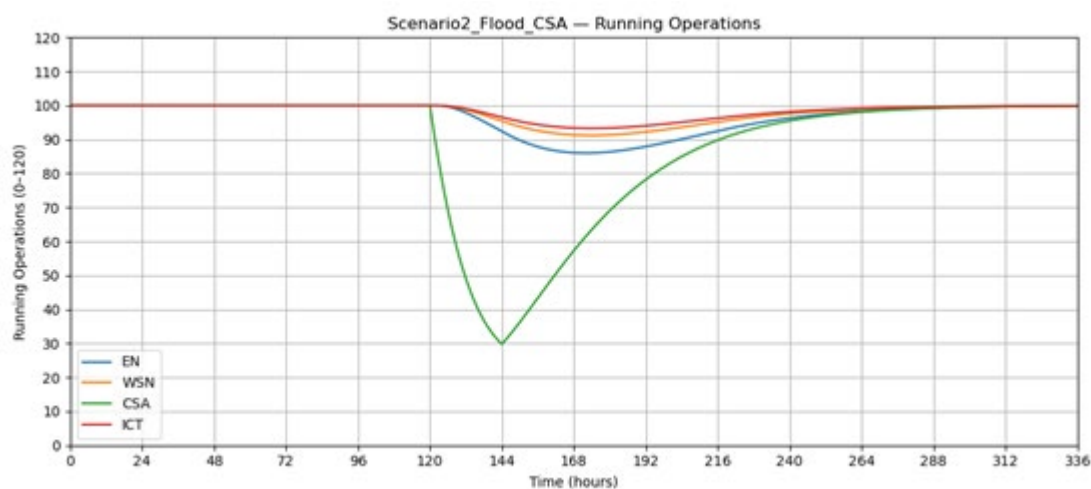


Figure 28 Scenario 2 - running operations.

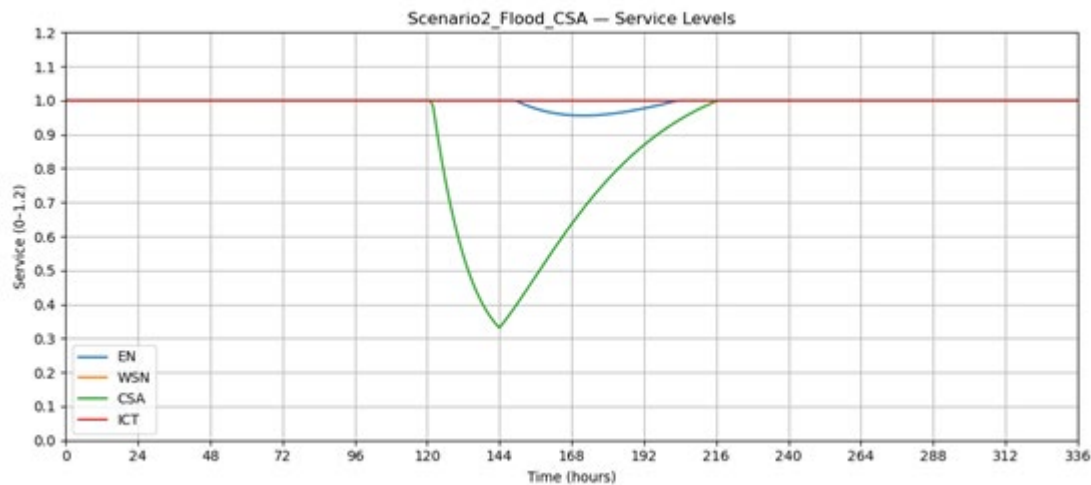


Figure 29 Scenario 2 - service levels.

Scenario 3 – Wildfire in Suburbs

Simultaneous disruption of EN and ICT infrastructures occurs at $t_0=48h$ for 36 h, with magnitudes $m_{EN} = 8$ and $m_{ICT} = 5$. The model demonstrates strong cross-sectoral dependency: as ICT functionality degrades, control and coordination of the electricity grid slow down, amplifying recovery delays. The cascading failure extends to CSA and WSN, whose performance drops by over 30% during the event window. This combined hazard scenario reveals synergistic effects, where concurrent moderate disruptions can jointly produce severe system-wide impacts.

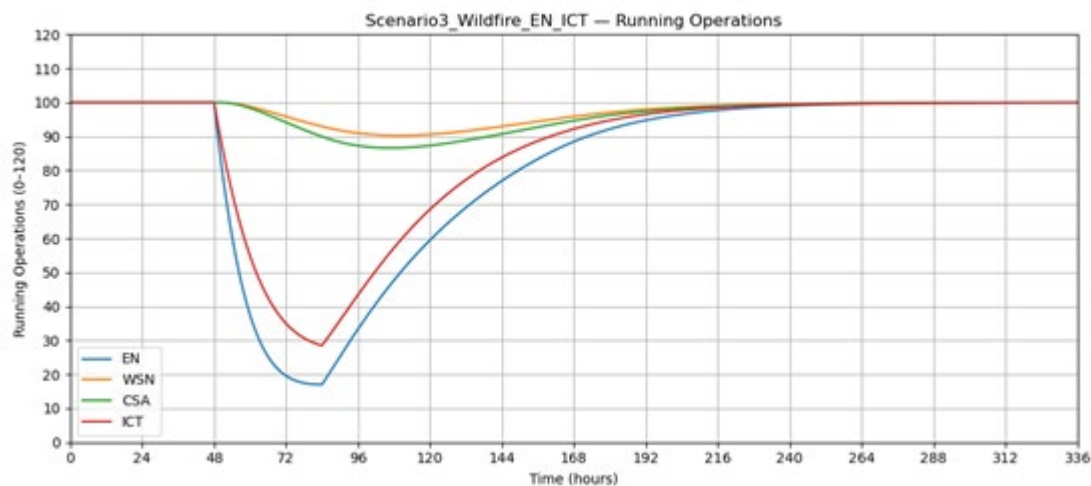


Figure 30 Scenario 3 - running operations.

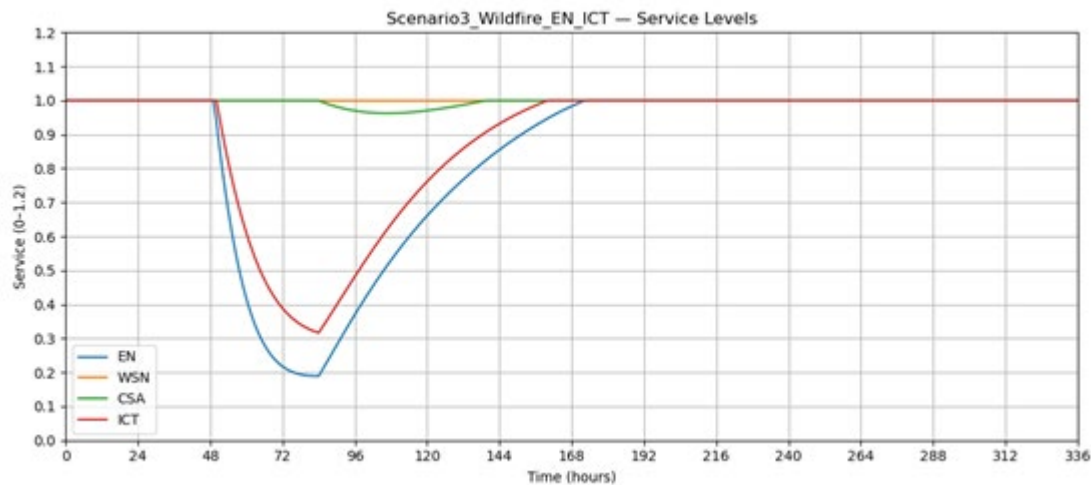


Figure 31 Scenario 3 - service levels.

Scenario 4 – Earthquake Shock

An instantaneous multi-sector disruption is introduced at $t_0 = 0$, affecting EN, ICT, and CSA with magnitudes $m_{EN} = 9$, $m_{ICT} = 7$ and $m_{CSA} = 5$. The model shows an immediate collapse in operational capacity across all three sectors, consistent with a high-intensity event. The WSN experiences secondary degradation due to water main breaks and energy shortages. Recovery is non-uniform: EN and ICT regain near-normal service levels after ~ 120 h, while CSA requires ~ 200 h to restore full functionality. The asynchronous recovery patterns align with the nonlinear resilience dynamics emphasized by Canzani (2016).

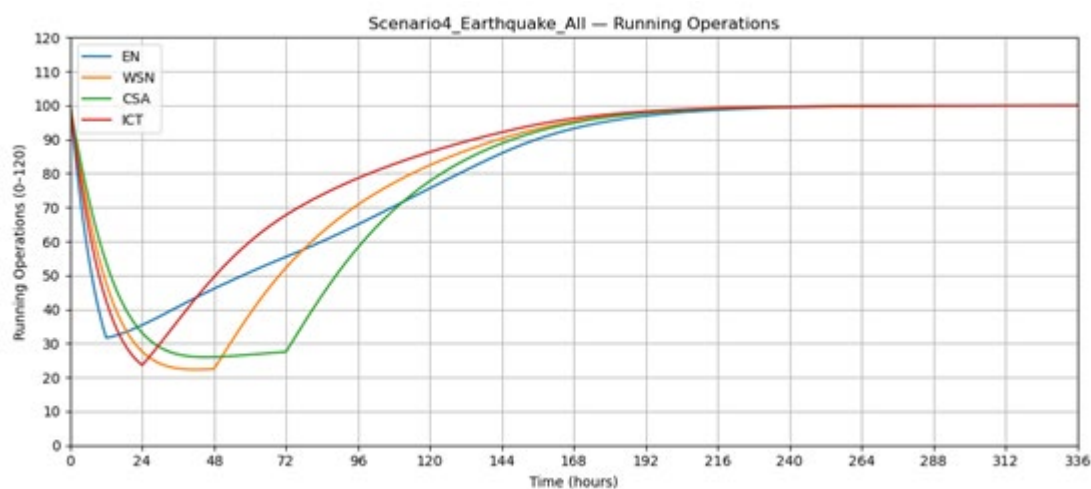


Figure 32 Scenario 4 - running operations.

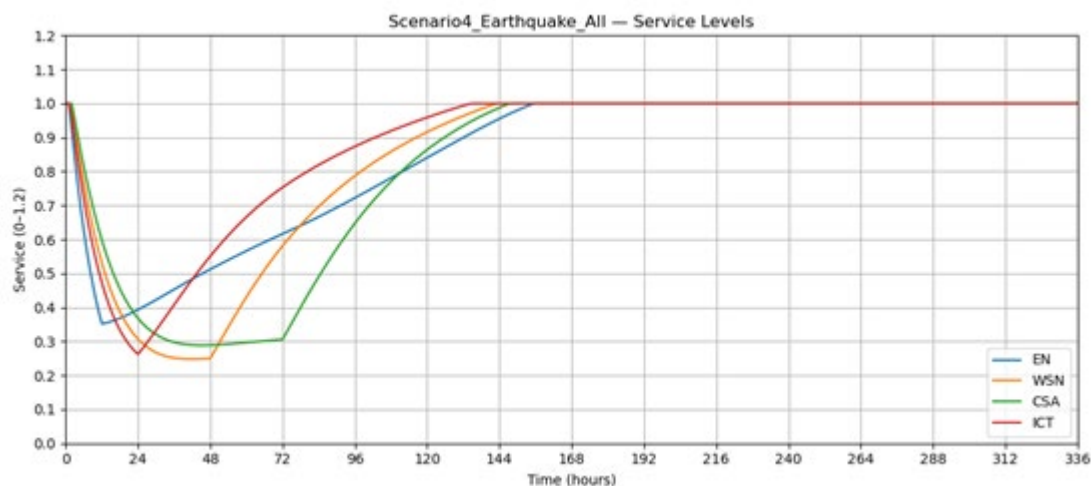


Figure 33 Scenario 4 - service levels.

Scenario 5 – Multiple Sequential Disruptions (ICT → EN)

A two-phase disturbance begins with a small ICT outage ($t_0 = 0$, $\Delta T = 24$ h, $m = 2$), followed by a severe EN failure ($t_0 = 96$ h, $\Delta T = 36$ h, $m = 8$). Despite the initial ICT disruption being minor, it delays detection and control actions for the subsequent energy event. As a result, the EN outage cascades to WSN and CSA, and the overall system recovery extends by nearly 30% compared to isolated events.

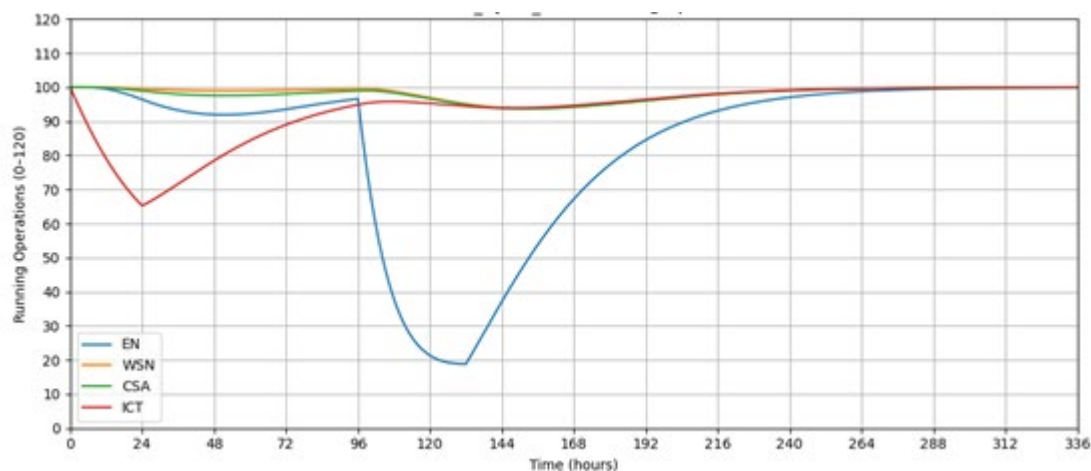


Figure 34 Scenario 5 - running operations.

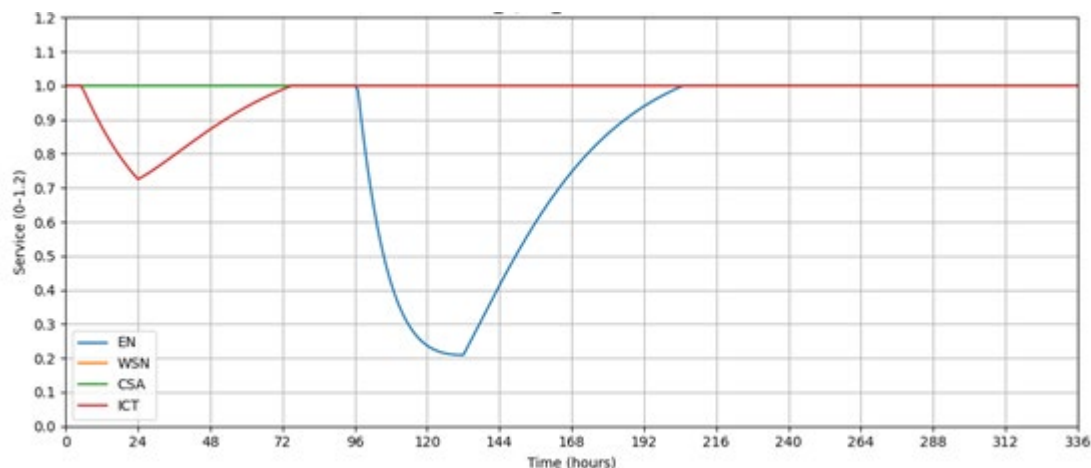


Figure 35 Scenario 5- Service levels.

Multiple scenario results

To better understand the behaviour and resilience of the city's critical infrastructure network, a series of simulation experiments were conducted focusing exclusively on EN disruption scenarios. In these tests, the Energy infrastructure was subjected to disturbances of varying duration (12, 24, 48, and 72 hours) and magnitude (5, 7, and 9), while all other infrastructures—WSN, CSA, and ICT—remained unaffected initially. This targeted approach allows for a detailed assessment of how the Energy system responds to escalating stress conditions and how its degradation and recovery dynamics influence the broader interdependent network.

In this case, the system exhibits the most pronounced decline across all simulated scenarios. The severity of degradation increases systematically with both the duration and magnitude of the event.

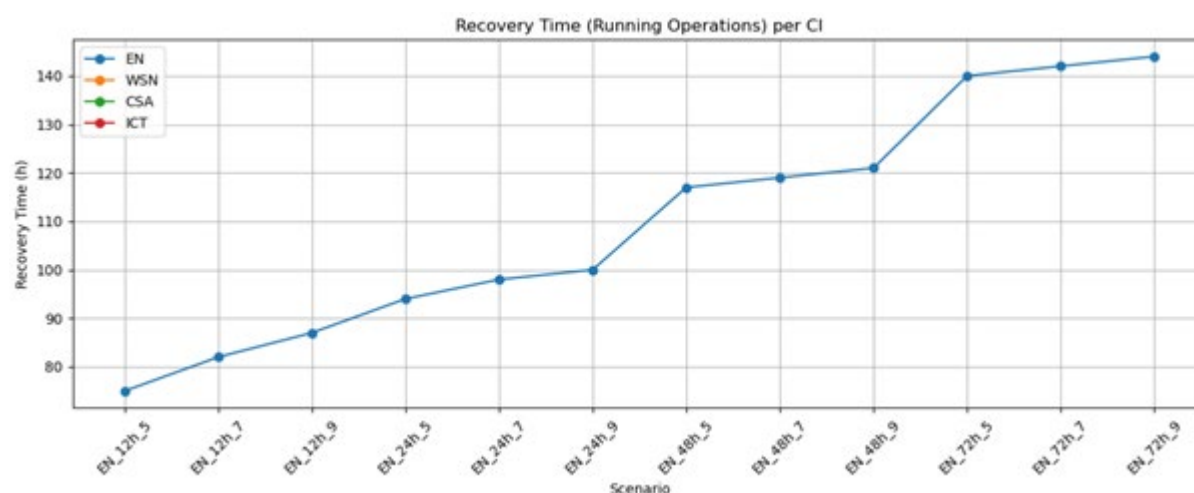


Figure 36 Recovery Time (Running Operations) per Critical Infrastructure under Energy disruption scenarios.

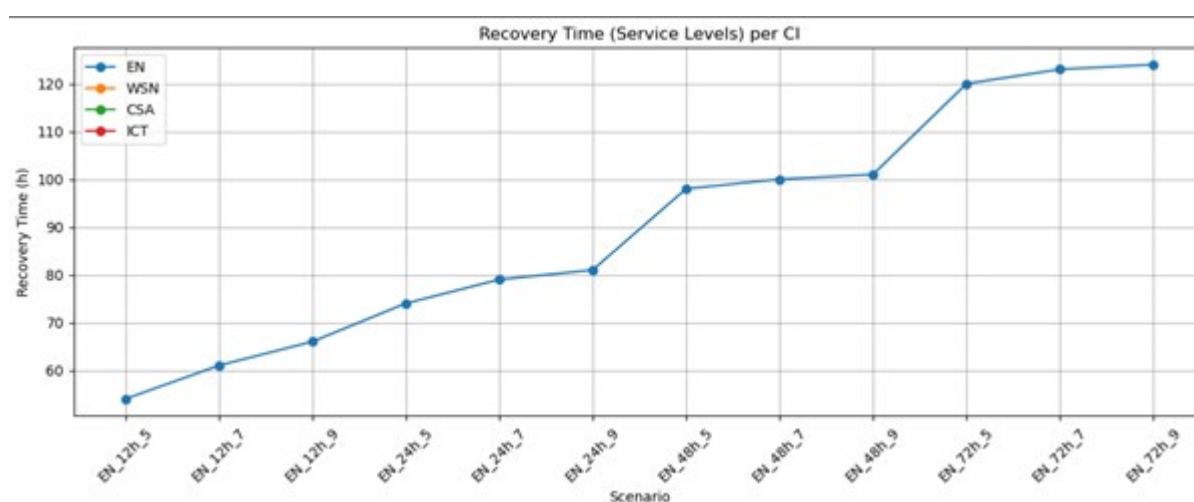


Figure 37 Recovery Time (Service Levels) per Critical Infrastructure under Energy disruption scenarios.

Figure 39 shows the recovery time for the running operation results for all CIs, under the EN disruption scenario, while Figure 40 shows the recovery time for the service levels. The simulation results show that that the EN infrastructure is the only system experiencing significant degradation and recovery behaviour across all disruption scenarios. In contrast, the WSN, CSA, and ICT infrastructures maintain

stable performance above the 90% demand threshold, resulting in effectively zero recovery times, as no operational or service-level decline occurs. For the Energy system, recovery patterns in both metrics exhibit a clear nonlinear relationship with disruption duration and magnitude. Short and mild events (12 hours, magnitude 5–7) are typically resolved within 75–85 hours for running operations and 70–80 hours for service levels. As disruptions intensify (24 hours, magnitude 7–9), recovery extends to approximately 95–100 hours, while prolonged and severe events (48–72 hours, magnitude 7–9) require between 120 and 145 hours to fully restore functionality and service provision. The close alignment between operational and service recovery curves indicates that service restoration occurs only slightly ahead of full operational recovery, reflecting the Energy network’s heavy dependence on physical repair and system stabilization processes. Overall, these results highlight the Energy infrastructure’s dominant vulnerability and nonlinear recovery dynamics, underscoring its critical role in sustaining urban resilience and the importance of strengthening its redundancy and response capacity to mitigate cascading effects on other infrastructures.

3.2.5 Conclusions

This study presented a Python-based SD simulation model for analysing cascading disruptions and resilience in interdependent CIs. We adopt a block building process based on SD methods to get a better understanding of interdependent dynamics within and across CIs, introduced by Canzani (2016), extending it with new computational capabilities and hazard scenarios relevant to the Greek context. By reproducing the essential structure of the three functional blocks (disruptive event modelling, single infrastructure dynamics, and interdependency representation) the work demonstrates that the existing approaches can be successfully implemented in an open, flexible simulation environment.

Simulation results across the six presented scenarios confirmed the model’s ability to capture nonlinear propagation, cascading failures, and delayed recovery behaviours. In particular, the multiple sequential disruption scenario highlighted how even a minor initial disturbance can significantly exacerbate later failures due to interdependency feedback. Similarly, multi-hazard events such as earthquakes and wildfires demonstrated system-wide degradation patterns, emphasizing the importance of considering temporal overlap and sectoral coupling when assessing infrastructure resilience. From a methodological perspective, the present implementation introduces several advancements to the original framework. It employs Python-based numerical solvers to build a SD model for continuous-time integration of interdependent differential equations, ensuring reproducibility and allowing parameter experimentation. The model is further extended to cover multiple hazard types and context-specific scenarios instead of generic failures, while also enabling visualization of dynamic resilience indicators, such as performance loss and recovery rate, over time. These extensions make the framework more adaptable for urban resilience planning, emergency preparedness, and CIP studies. Furthermore, the modular code structure allows additional modelling blocks to be incorporated, for instance components representing cyber-attack and defence dynamics or policy intervention layers that simulate recovery resource allocation.

The practical value of this modelling approach lies in its ability to present dynamic simulations and visual results in a form easily interpretable by decision-makers without advanced mathematical expertise. It also enables a clearer understanding of complex system behaviour during crises, even with limited data. However, a key limitation remains the lack of real-world information for validating CI scenarios and model parameters, using survey-based estimates. Overall, this work confirms that the System Dynamics paradigm is a powerful and interpretable framework for studying complex interdependent systems. The presented model offers a practical foundation for ongoing research in critical infrastructure resilience assessment and simulation-based crisis management.

3.3 Wellington, New Zealand

3.3.1 Introduction

Located on the North Island of New Zealand, the capital city of Wellington is exposed to a wide range of natural hazards both climate and seismic driven. Within the region the most common climate driven hazard is that of flooding with approximately 31% of the population at potential risk during a 1-in-100-year event (GWRC, 2025). In contrast to flooding, during the drier months between November and March the region is exposed to increased risks of wildfires, with about 20% of the land being at high or extreme risk during this period (GWRC, 2005). With the risks of both of these hazards predicted to increase in the future due to climate change, there is a growing need to understand these risks more and plan for means to mitigate against them.

Within the scope of the Wellington case study, detailed hazard modelling is being undertaken both in the flooding and wildfire domains for both current and future climate scenarios. By opting for the development of hazard models as part of the risk assessment process a greater range of mitigation measures can be explored such as those that can reduce the magnitude of the hazard and those that can reduce the impact through changing the vulnerability and/or fragility of exposed infrastructures.

3.3.2 Flood Model

Flood risk management is one of the most pressing challenges in New Zealand, where flooding is the most frequently occurring natural hazard (Ministry for the Environment, 2015). According to the National Institute of Water and Atmospheric Research (NIWA), most of the country is predicted to experience an increase in “extreme” rainfall events, which is defined as the 99th percentile daily rainfall based on historical records (NIWA, 2023). This trend has led to, and is expected to result in a growing number of storms that exceed the design capacity of the existing stormwater infrastructures. In Wellington City, the flood hazard is further intensified by the complexity of the urban environment and its densely populated metropolitan characteristics. Therefore, accurate and high-resolution flood modelling is essential for understanding flood risk, supporting informed decision-making for urban planning, infrastructure investments and emergency management.

To simulate urban flooding for hazard mapping in the Wellington Central Business District (CBD), the Personal Computer-Storm Water Management Model (PCSWMM) developed by Computational Hydraulics Inc. was initially employed. PCSWMM is a widely used flood modelling tool capable of simulating surface and sub-surface interactions, making it suitable in representing accurate urban flooding scenarios. However, following further consultation with the Wellington City Council (WCC) and Wellington Water, the decision was made to adopt InfoWorks ICM (Integrated Catchment Management) model was implemented. The shift was due to the availability of detailed stormwater network and subcatchment survey data. InfoWorks ICM, developed by Autodesk, is an integrated hydrologic and hydraulic model that can incorporate coastal level information (tide fluctuations and sea level rise) and simulate time increment and maximum flood depth, flow velocity and hazard levels, making it particularly advantageous for complex coastal urban catchments [1].

The input data used for the flood simulation and their corresponding sources can be found in Table 34. The historical and climate projected rainfall intensity data were obtained from the National Institute of Water and Atmospheric Research (NIWA) High Intensity Rainfall Design System Version 4 [2] (Figure 41). The historical and climate projected tide fluctuation and sea level rise projection data were obtained from the NIWA Tide Forecaster [3] and NIWA Sea level App [4], respectively (Figure 42). A comprehensive surveyed stormwater data and catchment models were provided by Wellington Water

(Figure 43). The most recent data for building outlines and elevation model were gathered from the Land Information New Zealand (LINZ).

Table 32. Input data and data source for the Wellington case study flood simulation

Data / Method	Source	Reference
Historical rainfall data	NIWA	High Intensity Rainfall System
Climate projected rainfall data		
Storm rainfall profile	Wellington Water	Reference Guide for Design Storm Hydrology
Tide profile	NIWA Tide Forecaster	Wellington - ferry building : NIWA Tides
Sea level rise data	NIWA Sea level App	NZ NIWA Sea Level App
Hydraulic Models	Wellington Water	c/o Wellington City Council and Drainage Modelling Team, Wellington Water
Stormwater network		
Elevation data (1m 2019-2020)	LINZ	Wellington City LiDAR 1m DEM (2019-2020) LINZ Data Service
Building outlines (2019)	LINZ	NZ Building Outlines LINZ Data Service
Hydraulic model	Infoworks ICM	Autodesk InfoWorks ICM

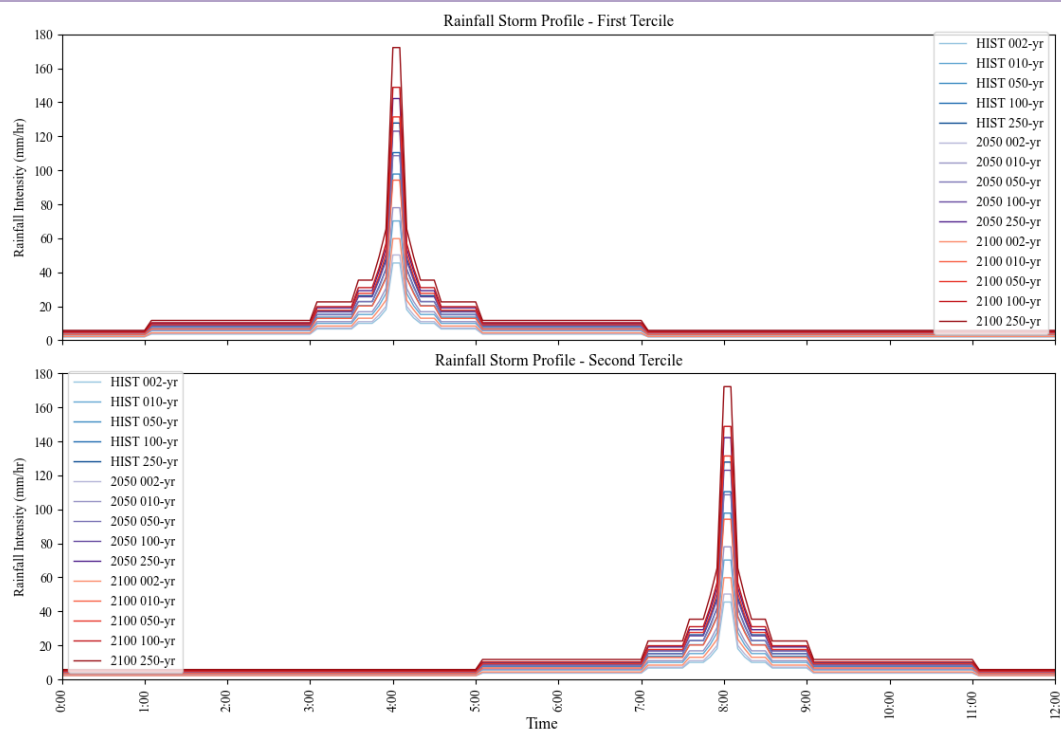


Figure 38. Rainfall profile with historical and climate projected rainfall intensities for Wellington City

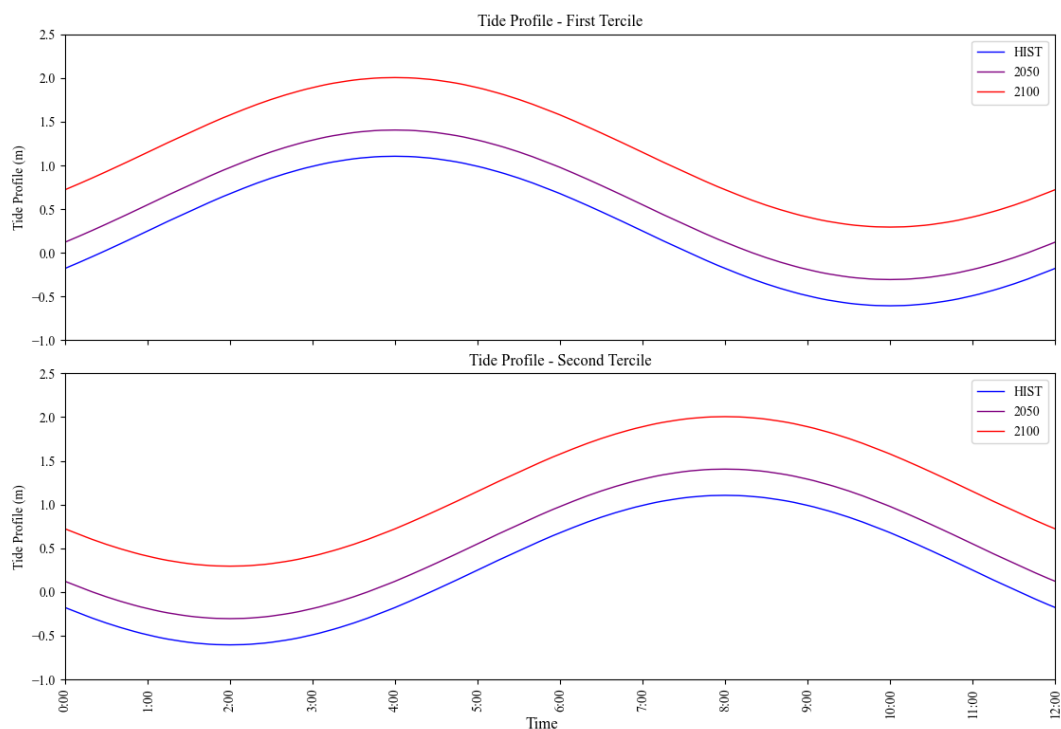


Figure 39. Coastal tide fluctuations with climate projected sea level rise projection for Wellington City

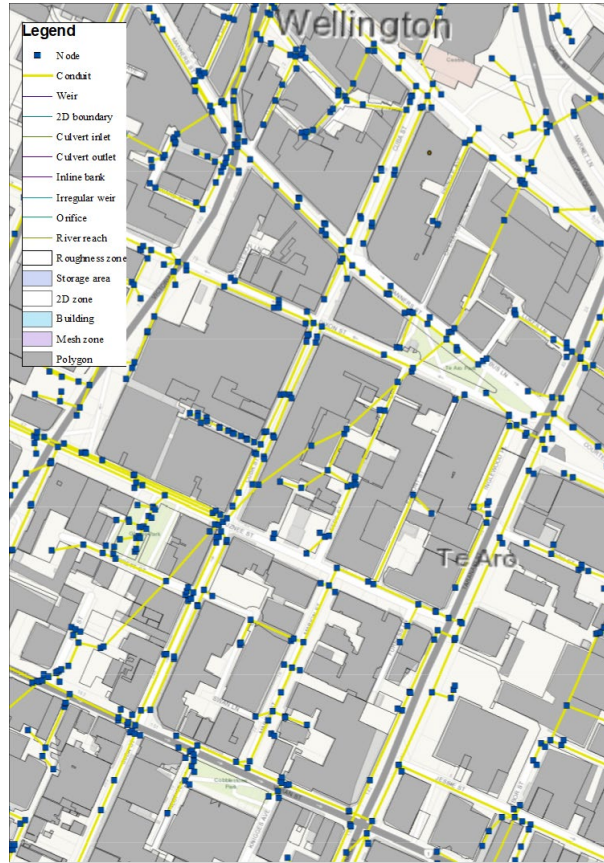


Figure 40 Infoworks ICM stormwater network and building void data

The governing equations used in Infoworks ICM to calculate the flood parameters are based on shallow water equations, in mathematically representing the overland flow. The conservative form of the equations used in the model is shown as [5]:

$$\frac{\partial h}{\partial t} + \frac{\partial(hu)}{\partial x} + \frac{\partial(hv)}{\partial y} = \sum_{i=1}^n q_i$$

$$\frac{\partial(hu)}{\partial t} + \frac{\partial}{\partial x} \left(hu^2 + \frac{gh^2}{2} \right) + \frac{\partial(huv)}{\partial y} - \frac{\partial}{\partial x} \left(\epsilon h \frac{\partial u}{\partial x} \right) - \frac{\partial}{\partial y} \left(\epsilon h \frac{\partial u}{\partial y} \right) = gh(S_{0,x} - S_{f,x}) + \sum_{i=1}^n q_i u_i$$

$$\frac{\partial(hv)}{\partial t} + \frac{\partial}{\partial y} \left(hv^2 + \frac{gh^2}{2} \right) + \frac{\partial(huv)}{\partial x} - \frac{\partial}{\partial x} \left(\epsilon h \frac{\partial v}{\partial x} \right) - \frac{\partial}{\partial y} \left(\epsilon h \frac{\partial v}{\partial y} \right) = gh(S_{0,y} - S_{f,y}) + \sum_{i=1}^n q_i v_i$$

Where h describes the flood depth (m), u and v are x- and y-directional velocities (m/s), q_i is the net source discharge per unit area (m/s), u_i and v_i are the net source discharge x- and y-directional velocities, g is the acceleration due to gravity (m/s²), ϵ is the eddy viscosity (m²/s), n is the number of source discharge, and $S_{0,x}$, $S_{0,y}$, $S_{f,x}$ and $S_{f,y}$ are the bed and friction slopes in x- and y-direction, respectively.

The model can define assets, such as buildings and structures, as damage receptors within the 2-Dimensional mesh, and are characterised by their location, property types, values, etc. A set of pre-defined damage functions, which relate to the flood duration, maximum flood depth and velocity, is used to determine the flood vulnerability and economic damage for each receptor. Flood scenarios based on different return periods, alongside with the implementation of flood mitigation measures, including structural and green infrastructures, are also simulated to assess the corresponding

vulnerability function values. An example of the flood depth output data using Infoworks ICM can be seen in Figure 44.

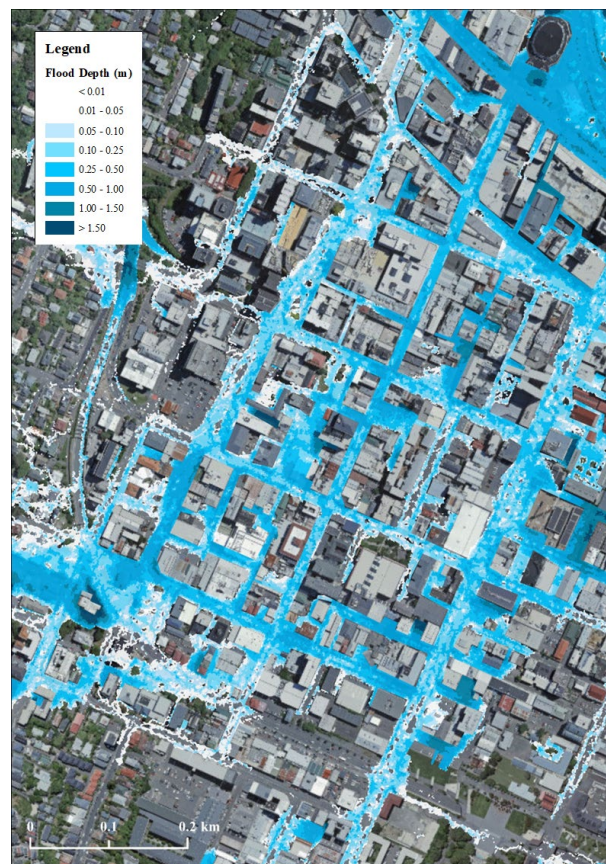


Figure 41 Sample flood depth output using Infoworks ICM

3.3.3 Wildfire Model

The severity and duration of fire seasons are expected to increase in the future due to the consequences of climate change (FENZ, 2023). This increase coupled with population growth and expanding cities are escalating wildfire risks at the Wildland-Urban Interface (WUI) (Vacca et al. 2023). Therefore, there is a growing need for a more complete understanding of the risk's wildfires pose to communities.

The wildfire model seeks to simulate the propagation of wildfire events over time for different modelled climate scenarios and ignition points and quantify risks posed to buildings at the WUI. For quantifying the risks wildfire poses to regions, a commonly adopted approach is the implementation of semi-empirical models such as Spark, WISE, WUI-nity, FlamMap, and Inferno. Using real world empirical data behavioural characteristics governed by landuse/fuel type, topology, along with climate and weather conditions, are defined for determining the rate of spread (RoS) of a wildfire and its intensity.

For calculating risks that properties, infrastructure and people are exposed to within the Wellington study area the semi-empirical wildfire model Inferno is used. This model allows for inputs relating to climate and weather conditions, topology, land cover and fuel characteristics to simulate the intensity, rate of spread, and radiant heat flux (RHF) (Cedaryn, 2025). Based on these inputted datasets we can define parameters for defining how they influence the rate of spread (RoS) of a fire and the radiative energy (Radiant Heat Flux (RHF)) being emitted from the fire. Through modelling these parameters, we can define the time of arrival, the magnitude, and duration of risks that assets are exposed to.

Theoretical equations and associated indices for defining the RoS of wildfire across various fuel types in New Zealand, based on distinct vegetation classes and characteristics, are detailed in Pearce (2005). The generalised equation for defining RoS is shown in Equation 1, where p_{ij} are indices relating to fuel characteristics, $pp\%$ (vegetation mix component), $DoC\%$ (degree of curing) relate to the fuel characteristics and ISI (Initial Spread Index), BUI (Buildup Index) are external parameters. Table 35 outlines example indices relating to two specific fuel characteristics of fuels present within the New Zealand case study.

$$RoS_g = \left[\frac{pp\%}{100} \times p_{1_1} \times (1 - EXP(p_{2_1} \times ISI))^{p_{3_1}} + 0.2 \times \left(1 - \frac{pp\%}{100} \right) \times p_{1_2} \times (1 - EXP(p_{2_2} \times ISI))^{p_{3_2}} \right] \times EXP \left(50 \times LN(p_4) \times \left(\frac{1}{BUI} - \frac{1}{p_5} \right) \right) \times [0.2 \times DoC\% - 1] \quad \text{Eq. 1}$$

Table 33 Example parameters for defining RoS (Pearce 2005)

Land Class	PP%	p_{1_1}	p_{1_2}	p_{2_1}	p_{2_2}	p_{3_1}	p_{3_2}	p_4	p_5	DoC%
Low Producing Grassland	100	11400	0	-0.0310	1	1.4	0	1	1	80
Gorse	100	4920	0	-0.1000	1	1.5	0	1	1	100

The head fire intensity (HFI) that relates to the rate of heat energy being released at the flame front per meter is influenced by the Fuel Load (FL) that relates to the amount of combustible material within an area and the RoS. Like that of the RoS, the FL parameters depend on the fuel characteristics and the preceding climate conditions. The generalised formula used within New Zealand for defining FL is given by equation 2. Table 36 outlines the fuel-based indices for the same fuel types outlined in Table 35.

$$FL_g = p_{1_1} \times [1 - EXP(p_{2_1} \times BUI)]^{p_{3_1}} + p_{1_2} \times [1 - EXP(p_{2_2} \times BUI)]^{p_{3_2}} \quad \text{Eq. 2}$$

Table 34 Example parameters for defining FL (Pearce 2005)

Land Class	p_{1_1}	p_{1_2}	p_{2_1}	p_{2_2}	p_{3_1}	p_{3_2}
Low Producing Grassland	3	0	1	1	0	0
Gorse	30	0	1	1	0	0

For defining the risk posed from a wildfire to a building we assess the likelihood of the building igniting as a result of its proximity to the wildfire. Whilst there are a number of pathways that can result in building ignition including firebrands, convection heating, flame contact, and radiant heat flux (RHF) the approach analysed within this study utilises RHF with including of flame contact for its assessment. Equation 3 shows how RHF (q'') is derived for a given flame temperature where:

- T = Flame temperature in Kelvin (K)
- ϵ = Flame emissivity (assumed to be 0.95kW/m²)
- σ = Stefan Boltzman constant (5.67x10⁻¹¹kW/m²K⁴)

- F = View factor that defines how much of energy radiated from the flame surface reaches the target surface (ranges from 0.0 – to 1.0).

$$q'' = F\sigma\epsilon T^4 \quad \text{Eq. 3}$$

Two key outputs generated from Inferno for use in risk assessment process are:

1. Maximum RHF Raster, and
2. Maximum RHF Polylines

The “Maximum RHF Raster” provides a regular rasterised grid at regular time-intervals depicting the maximum recorded RHF value at each timestep. By having a raw rasterised output infrastructures can be manually added to the domain and their subsequent risk exposure be assessed. The second “Maximum RHF Polylines” output maps the maximum recorded RHF values at each time-step to user defined polylines that can be, road segments, building outlines, and powerline transmissions as a few examples. By calculating this directly within the software we have readily available outputs highlighting hazard exposure to current assets within the model domain. Figure 45 shows an example of how the mapping of maximum recorded RHF values during a simulation has been derived at the building level along the WUI.

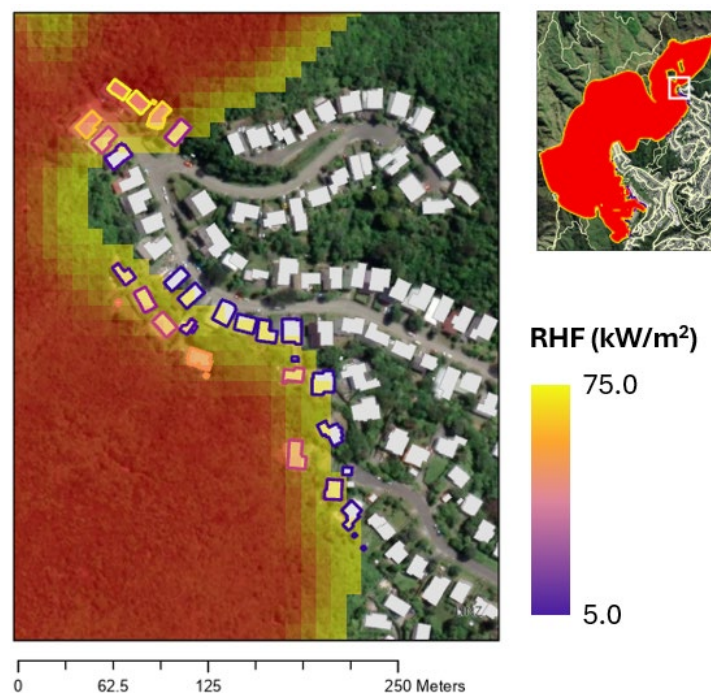


Figure 42 Example scenario of 6-hour wildfire spread and corresponding RHF values experienced at the property level.

With the hazard levels defined at the building level the next step is to define the associated risk values that are specific to exposure and fragility or vulnerability of the respective asset classes. To depict this risk, we can assess the likelihood of ignition based on the building characteristics and the level of RHF exposure. One approach outlined in First Street Foundation (2023) defined the likelihood of ignition related to maximum RHFS values (Figure 46).

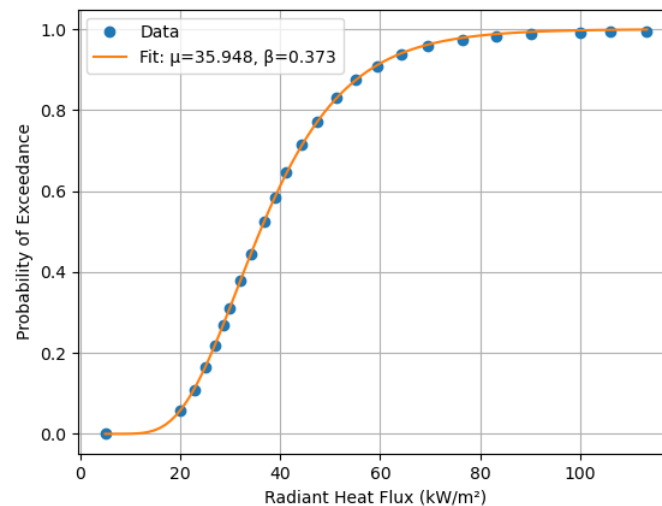


Figure 43 Example fragility curve derived from First Street Foundation (2023)

Applying the example fragility function in Figure 47 to the buildings outlined in Figure 45 we can derive a probabilistic depiction of ignition for this modelled scenario at the 6-hour time step.

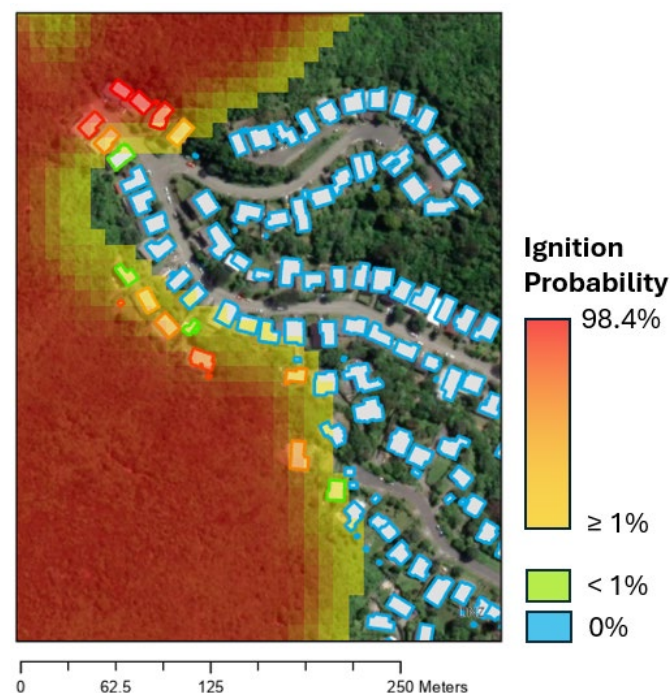


Figure 44 Example application of fragility curve to define ignition probability based off max RHF values.

3.3.4 Conclusions

This study outlines the approach of utilising hazard modelling software (Infoworks ICM, and Inferno) to create time-series hazard maps for flood and wildfire events respectively for use in risk assessment. By incorporating detailed hazard modelling into the Wellington case study, we can assess mitigation and adaptation strategies both at the catchment level (i.e. measures that facilitate hazard reduction) and property level (reduce vulnerability of assets).

4 Conclusions

D2.1 delivers a harmonised, scalable methodology to quantify physical vulnerability under multiple interacting hazards, grounded in a standardised asset taxonomy and a transparent scoring/selection process for impact models. Its application to Dublin, Patras, and Wellington shows that: (a) taxonomy-driven archotyping enables consistent linkage of exposure to vetted models; (b) physics-informed, component-level analysis improves the resolution of flood performance in timber housing and clarifies where mitigation yields the largest benefits; and (c) integrating time-series hazard modelling (flood and wildfire) supports practical assessment of adaptation options from catchment to property scale. These advances underpin the construction of dynamic multi-hazard vulnerability functions in WP2 and provide clear pathways for future integration with social vulnerability (T2.2 and T2.3), higher-fidelity data, and city-specific decision making.

5 References

- A. A. Abdelgawad and J. J. Gonzalez, "Reliability of expert estimates of cascading failures in Critical Infrastructure," 2019.
- A. Afsordegan, M. Sánchez, N. Agell, S. Zahedi, L. v. Cremades, *Decision making under uncertainty using a qualitative TOPSIS method for selecting sustainable energy alternatives*, *International Journal of Environmental Science and Technology*. 13 (2016) 1419–1432. <https://doi.org/10.1007/s13762-016-0982-7>.
- A. Ali, N. Raut, *Advances and Challenges in Flash Flood Risk Assessment: A Review*, *Article in Journal of Geography & Natural Disasters*. 7 (2017). <https://doi.org/10.4172/2167-0587.1000195>.
- A. Calderón, V. Silva, *Exposure forecasting for seismic risk estimation: Application to Costa Rica*, *Earthquake Spectra*. 37 (2021) 1806–1826. <https://doi.org/10.1177/8755293021989333>.
- A. Gravelsins et al., "Modelling energy production flexibility: system dynamics approach," *Energy Procedia*, vol. 147, pp. 503–509, Aug. 2018, doi: 10.1016/j.egypro.2018.07.060.
- A. Laugé, J. Hernantes, and J. M. Sarriegi, "Critical infrastructure dependencies: A holistic, dynamic and quantitative approach," *Int. J. Crit. Infrastruct. Prot.*, vol. 8, pp. 16–23, Jan. 2015, doi: 10.1016/j.ijcip.2014.12.004.
- A. Meslem, D. D'Ayala, I. Ioannu, T. Rossetto, D. Lang, *Uncertainty and Quality Rating in Analytical Vulnerability Assessment*, in: *Second European Conference on Earthquake Engineering and Seismology*, Istanbul, Turkey, 2014.
- A. Mignan, S. Wiemer, D. Giardini, *The quantification of low-probability–high-consequences events: part I. A generic multi-risk approach*, *Natural Hazards*. 73 (2014) 1999–2022. <https://doi.org/10.1007/s11069-014-1178-4>.
- A.C. Cornell, *Does Duration Really Matter?*, in: *FHWA/NCEER Workshop on the National Representation of Seismic Ground Motion for New and Existing Highway Facilities*, n.d.
- A.E. Zaghi, J.E. Padgett, M. Bruneau, M. Barbato, Y. Li, J. Mitrani-Reiser, A. McBride, *Establishing Common Nomenclature, Characterizing the Problem, and Identifying Future Opportunities in Multihazard Design*, *Journal of Structural Engineering*. 142 (2016). [https://doi.org/10.1061/\(ASCE\)ST.1943-541X.0001586](https://doi.org/10.1061/(ASCE)ST.1943-541X.0001586).
- AASHTO, 2013. *AASHTO LRFD Bridge Design Specification*, sixth ed. American Association of State Highway and Transportation Officials, Washington DC.
- American Society of Civil Engineers (ASCE). (2024). *Flood-resistant design and construction (ASCE/SEI 24-24)*. American Society of Civil Engineers. <https://doi.org/10.1061/9780784485781>

American Society of Civil Engineers. (2022). ASCE/SEI 7-22: Minimum design loads and associated criteria for buildings and other structures. <https://doi.org/10.1061/9780784415788>

American Society of Civil Engineers. (2023). ASCE/SEI 7-22 Supplement 2: Minimum design loads and associated criteria for buildings and other structures. <https://ascelibrary.org/doi/10.1061/9780784415788.sup2>

American Wood Council. (2018). National design specification for wood construction (ANSI/AWC NDS-2018).

American Wood Council. (2021). Special design provisions for wind and seismic (ANSI/AWC SDPWS-2021).

Applied Technology Council, Earthquake damage evaluation data for California, ATC-13., Redwood City, California, 1985.

ARUP. A Universal Taxonomy for Natural Hazard and Climate Risk and Resilience Assessments: Buildings Edition. ARUP: London, 2024.

ASTM International. (2006). Standard practice for establishing clear wood strength values (ASTM D2555-06).

Autodesk. (s. f.). One platform for every catchment: InfoWorks ICM. Recuperado el 10 de noviembre de 2025, de <https://www.autodesk.com/nz/campaigns/one-platform-for-every-catchment-infoworks-icm>.

B. Aygün, L. Dueñas-Osorio, J.E. Padgett, R. DesRoches, Efficient Longitudinal Seismic Fragility Assessment of a Multispan Continuous Steel Bridge on Liquefiable Soils, *Journal of Bridge Engineering*. 16 (2011) 93–107. [https://doi.org/10.1061/\(ASCE\)BE.1943-5592.0000131](https://doi.org/10.1061/(ASCE)BE.1943-5592.0000131).

B. Tang, X. Lu, L. Ye, W. Shi, Evaluation of collapse resistance of RC frame structures for Chinese schools in seismic design categories B and C, *Earthquake Engineering and Engineering Vibration*. 10 (2011) 369–377. <https://doi.org/10.1007/s11803-011-0073-1>.

Becker, A., Johnstone, W., & Lence, B. (2011). Wood frame building response to rapid-onset flooding. *Natural Hazards Review*, 12(2), 85–95. [https://doi.org/10.1061/\(ASCE\)NH.1527-6996.0000029](https://doi.org/10.1061/(ASCE)NH.1527-6996.0000029)

Botzen, W. J. W., Deschenes, O., & Sanders, M. (2019). The economic impacts of natural disasters: A review of models and empirical studies. *Review of Environmental Economics and Policy*, 13(2), 167–188.

C. Galasso, M. Pregnotato, F. Parisi, A model taxonomy for flood fragility and vulnerability assessment of buildings, *International Journal of Disaster Risk Reduction*. 53 (2021) 101985. <https://doi.org/10.1016/j.ijdr.2020.101985>.

C. Mesta, G. Cremen, C. Galasso, Urban growth modelling and social vulnerability assessment for a hazardous Kathmandu Valley, *Sci Rep*. 12 (2022) 6152. <https://doi.org/10.1038/s41598-022-09347-x>.

C. Petrone, T. Rossetto, M. Baiguera, C. De la Barra Bustamante, I. Ioannou, Fragility functions for a reinforced concrete structure subjected to earthquake and tsunami in sequence, *Eng Struct*. 205 (2020) 110120. <https://doi.org/10.1016/j.engstruct.2019.110120>.

C. Tarbotton, F. Dall’Osso, D. Dominey-Howes, J. Goff, The use of empirical vulnerability functions to assess the response of buildings to tsunami impact: Comparative review and summary of best practice, *Earth Sci Rev*. 142 (2015) 120–134. <https://doi.org/10.1016/j.earscirev.2015.01.002>.

C. Yepes-Estrada, V. Silva, T. Rossetto, D. D’Ayala, I. Ioannou, A. Meslem, H. Crowley, The Global Earthquake Model Physical Vulnerability Database, *Earthquake Spectra*. 32 (2016) 2567–2585. <https://doi.org/10.1193/011816EQS015DP>.

C.L. (Ching-L. Hwang, Kwangsun. Yoon, *Multiple Attribute Decision Making : Methods and Applications A State-of-the-Art Survey*, Springer Berlin Heidelberg, 1981.

CAPRA, *Integrating Disaster Risk Information Into Development Policies and Programs in Latin America and the Caribbean*, 2012.

Contreras, M. T., & Escauriaza, C. (2020). Modeling the effects of sediment concentration on the propagation of flash floods in an Andean watershed. *Natural Hazards and Earth System Sciences*, 20(1), 221-241.

Contreras, M. T., & Escauriaza, C. (2020). Modeling the effects of sediment concentration on the propagation of flash floods in an Andean watershed. *Natural Hazards and Earth System Sciences*, 20(1), 221-241.

Council of the European Union, Council Directive 2008/114/EC of 8 December 2008 on the Identification and Designation of European Critical Infrastructures and the Assessment of the Need to Improve their Protection, Brussels, Belgium, 2008.

Cremen, G., Galasso, C., & McCloskey, J. (2022). A simulation-based framework for earthquake risk-informed and people-centered decision making on future urban planning. *Earth's Future*, 10(1), e2021EF002388.

Custer, R., & Nishijima, K. (2015). Flood vulnerability assessment of residential buildings by explicit damage process modelling. *Natural Hazards*, 78, 461–496. <https://doi.org/10.1007/s11069-015-1721-3>

D. Asprone, F. Jalayer, A. Prota, G. Manfredi, Proposal of a probabilistic model for multi-hazard risk assessment of structures in seismic zones subjected to blast for the limit state of collapse, *Structural Safety*. 32 (2010) 25–34. <https://doi.org/10.1016/j.strusafe.2009.04.002>.

D. Asprone, F. Jalayer, A. Prota, G. Manfredi, Proposal of a probabilistic model for multi-hazard risk assessment of structures in seismic zones subjected to blast for the limit state of collapse, *Structural Safety*. 32 (2010) 25–34. <https://doi.org/10.1016/j.strusafe.2009.04.002>.

D. D'Ayala, A. Meslem, D. Vamvatsikos, K. Porter, T. Rossetto, H. Crowley, V. Silva, *Guidelines for Analytical Vulnerability Assessment - Low/Mid-Rise*, GEM Technical Report. (2013). <https://doi.org/10.13117/GEM.VULN-MOD.TR2014.12>.

D. Gautam, G. Fabbrocino, F. Santucci de Magistris, Derive empirical fragility functions for Nepali residential buildings, *Eng Struct*. 171 (2018) 617–628. <https://doi.org/10.1016/j.engstruct.2018.06.018>.

D. Lallemand, A. Kiremidjian, A Beta Distribution Model for Characterizing Earthquake Damage State Distribution, *Earthquake Spectra*. 31 (2015) 1337–1352. <https://doi.org/10.1193/012413EQS013M>.

D. Lallemand, A. Kiremidjian, H. Burton, Statistical procedures for developing earthquake damage fragility curves, *Earthq Eng Struct Dyn*. 44 (2015) 1373–1389. <https://doi.org/10.1002/eqe.2522>.

D. Molinari, K.M. de Bruijn, J.T. Castillo-Rodríguez, G.T. Aronica, L.M. Bouwer, Validation of flood risk models: Current practice and possible improvements, *International Journal of Disaster Risk Reduction*. 33 (2019) 441–448. <https://doi.org/10.1016/j.ijdrr.2018.10.022>.

D. Peduto, S. Ferlisi, G. Nicodemo, D. Reale, G. Pisciotta, G. Gullà, Empirical fragility and vulnerability curves for buildings exposed to slow-moving landslides at medium and large scales, *Landslides*. 14 (2017) 1993–2007. <https://doi.org/10.1007/S10346-017-0826-7/FIGURES/12>.

D. Shrestha, D.B. Basnyat, J. Gyawali, M. Creed, H. Sinclair, B. Golding, M. Manoranjan, S. Shrestha, D. Subedi, R. Haiju, Rainfall extremes under future climate change with implications for urban flood risk in Kathmandu, Nepal, *International Journal of Disaster Risk Reduction*. (2022).

- D. Sánchez-Muñoz, J.L. Domínguez-García, E. Martínez-Gomariz, B. Russo, J. Stevens, M. Pardo, *Electrical Grid Risk Assessment Against Flooding in Barcelona and Bristol Cities, Sustainability*. 12 (2020) 1527. <https://doi.org/10.3390/su12041527>.
- D. Vamvatsikos, A.C. Cornell, *Incremental dynamic analysis, Earthq Eng Struct Dyn*. 31 (2002) 491–514. <https://doi.org/10.1002/EQE.141>.
- D. Veneziano, A. Agarwal, E. Karaca, *Decision making with epistemic uncertainty under safety constraints: An application to seismic design, Probabilistic Engineering Mechanics*. 24 (2009) 426–437. <https://doi.org/10.1016/j.probengmech.2008.12.004>.
- D.A. Reed, C.J. Friedland, S. Wang, C.C. Massarra, *Multi-hazard system-level logit fragility functions, Eng Struct*. 122 (2016) 14–23. <https://doi.org/10.1016/j.engstruct.2016.05.006>.
- D.H. Peregrine, WATER-WAVE IMPACT ON WALLS, [Http://Dx.Doi.Org/10.1146/Annurev.Fluid.35.101101.161153](http://dx.doi.org/10.1146/annurev.fluid.35.101101.161153). 35 (2003) 23–43. <https://doi.org/10.1146/ANNUREV.FLUID.35.101101.161153>.
- D.M. Cruden, D.J. Varnes, *Landslides types and processes, Landslides: Investigation and Mitigation, Special Report, 247, Transportation Research Board, National Research Council, Washington DC, 1996*.
- D.N. Grant, *A mathematical form of probabilistic vulnerability model for loss and casualty ratios, Earthquake Spectra*. 36 (2020) 700–717. <https://doi.org/10.1177/8755293019891719>.
- de Ruiter, M. C., de Bruijn, J. A., Englhardt, J., Daniell, J. E., de Moel, H., & Ward, P. J. (2021). *The asynergies of structural disaster risk reduction measures: Comparing floods and earthquakes. Earth's Future*, 9(1), e2020EF001531.
- Department for Communities and Local Government (DCLG). (2007). *Improving the flood performance of new buildings: Flood resilient construction (Consortium managed by CIRIA)*. London: Department for Communities and Local Government.
- Donatti, C. I., Nicholas, K., Fedele, G., Delforge, D., Speybroeck, N., Moraga, P., et al. (2024). *Global hotspots of climate-related disasters. International Journal of Disaster Risk Reduction*, 108, 104488. <https://doi.org/10.1016/j.ijdr.2024.104488>
- Drakes, O., & Tate, E. (2022). *Social vulnerability in a multi-hazard context: a systematic review. Environmental research letters*, 17(3), 033001.
- Drdácký, M. F. (2010). *Flood damage to historic buildings and structures. Journal of Performance of Constructed Facilities*, 24(5), 439–445.
- E. Bastidas-Arteaga, M.G. Stewar, *Climate Adaptation Engineering, Elsevier, 2019*. <https://doi.org/10.1016/C2017-0-00942-4>.
- E. Canzani, *Modeling Dynamics of Disruptive Events for Impact Analysis in Networked Critical Infrastructures*. 2016.
- E. Fereshtehnejad, A. Shafieezadeh, *A multi-type multi-occurrence hazard lifecycle cost analysis framework for infrastructure management decision making, Eng Struct*. 167 (2018) 504–517. <https://doi.org/10.1016/j.engstruct.2018.04.049>.
- E. Martínez-Gomariz, E. Forero-Ortiz, M. Guerrero-Hidalga, S. Castán, M. Gómez, *Flood Depth–Damage Curves for Spanish Urban Areas, Sustainability*. 12 (2020) 2666. <https://doi.org/10.3390/su12072666>.
- E. Martínez-Gomariz, E. Forero-Ortiz, M. Guerrero-Hidalga, S. Castán, M. Gómez, *Flood Depth–Damage Curves for Spanish Urban Areas, Sustainability*. 12 (2020) 2666. <https://doi.org/10.3390/su12072666>.
- E.D. Haugen, A.M. Kaynia, *Vulnerability of structures impacted by debris flow, (2008)*. <https://doi.org/10.1201/9780203885284-c37>.

E.D. Haugen, A.M. Kaynia, *Vulnerability of structures impacted by debris flow*, (2008). <https://doi.org/10.1201/9780203885284-c37>.

E.Y. Mentese, G. Cremen, R. Gentile, M.E. Filippi, C. Galasso, J. McCloskey, *Risk-Informed Urbanisation Scenario Development through Interdisciplinary and GIS-Based Processes*, *International Journal of Disaster Risk Reduction*. under rev (2022).

E.Y. Mentese, G. Cremen, R. Gentile, M.E. Filippi, C. Galasso, J. McCloskey, *Risk-Informed Urbanisation Scenario Development through Interdisciplinary and GIS-Based Processes*, *International Journal of Disaster Risk Reduction*. under rev (2022).

E.Y. Mentese, G. Cremen, R. Gentile, M.E. Filippi, C. Galasso, J. McCloskey, *Risk-Informed Urbanisation Scenario Development through Interdisciplinary and GIS-Based Processes*, *International Journal of Disaster Risk Reduction*. under rev (2022).

Englhardt, J., de Moel, H., Huyck, C. K., de Ruiter, M. C., Aerts, J. C. J. H., & Ward, P. J. (2019). Enhancement of large-scale flood risk assessments using building-material-based vulnerability curves for an object-based approach in urban and rural areas. *Natural Hazards and Earth System Sciences*, 19(8), 1703–1722. <https://doi.org/10.5194/nhess-19-1703-2019>

Ermagun, A., Smith, V., & Janatabadi, F. (2024). High urban flood risk and no shelter access disproportionately impacts vulnerable communities in the USA. *Communications Earth & Environment*, 5(1), Article 2. <https://doi.org/10.1038/s43247-023-01165-x>

European Commission, *Green Paper on a European Programme for Critical Infrastructure Protection*, COM(2005) 576 Final, Brussels, Belgium, 2005

F. Brauer, P. Van Den Driessche, and J. Wu, Eds., *Mathematical Epidemiology*, vol. 1945. in *Lecture Notes in Mathematics*, vol. 1945. Berlin, Heidelberg: Springer Berlin Heidelberg, 2008. doi: 10.1007/978-3-540-78911-6.

F. Carisi, K. Schröter, A. Domeneghetti, H. Kreibich, A. Castellarin, *Development and assessment of uni- and multivariable flood loss models for Emilia-Romagna (Italy)*, *Natural Hazards and Earth System Sciences*. 18 (2018) 2057–2079. <https://doi.org/10.5194/nhess-18-2057-2018>.

F. Dottori, R. Figueiredo, M.L. v. Martina, D. Molinari, A.R. Scorzini, *INSYDE: a synthetic, probabilistic flood damage model based on explicit cost analysis*, *Natural Hazards and Earth System Sciences*. 16 (2016) 2577–2591. <https://doi.org/10.5194/nhess-16-2577-2016>.

F. Elmer, A.H. Thieken, I. Pech, H. Kreibich, *Influence of flood frequency on residential building losses*, *Natural Hazards and Earth System Sciences*. 10 (2010) 2145–2159. <https://doi.org/10.5194/nhess-10-2145-2010>.

F. Jalayer, *Direct Probabilistic Seismic Analysis: Implementation Non-Linear Dynamic Assessments*, Stanford University, 2003.

F. Jalayer, R. de Risi, G. Manfredi, *Bayesian Cloud Analysis: efficient structural fragility assessment using linear regression*, *Bulletin of Earthquake Engineering*. 13 (2015) 1183–1203.

F. Parisi, G. Sabella, *Flow-type landslide fragility of reinforced concrete framed buildings*, *Eng Struct*. 131 (2017) 28–43. <https://doi.org/10.1016/J.ENGSTRUCT.2016.10.013>.

F. Parisi, G. Sabella, *Flow-type landslide fragility of reinforced concrete framed buildings*, *Eng Struct*. 131 (2017) 28–43. <https://doi.org/10.1016/J.ENGSTRUCT.2016.10.013>.

F.M. Al-Nammari, M.K. Lindell, *Earthquake recovery of historic buildings: exploring cost and time needs*, *Disasters*. 33 (2009) 457–481. <https://doi.org/10.1111/j.1467-7717.2008.01083.x>.

Federal Emergency Management Agency, *HAZUS - MH MR4 technical manual*, Washington DC, USA, 2003.

Federal Emergency Management Agency, HAZUS MH MR5. *Earthquake loss estimation methodology*, Washington DC, USA, 2021. <https://www.hSDL.org/?view&did=12756>.

Federal Emergency Management Agency, *Seismic Performance Assessment of Buildings. Volume 1 - Methodology*, Washington, DC, 2012.

FEMA (Federal Emergency Management Agency), HAZUS MH MR4 technical manual, Washington DC, USA, 2003.

FEMA, 2011. *Coastal Construction Manual: Principles and Practices of Planning, Siting, Designing, Constructing, and Maintaining Residential Buildings in Coastal Areas*, FEMA P-55. Federal Emergency Management Association, Washington DC, USA.

Fire Emergency New Zealand (2023). *Climate and Wildfire Risk - Evidence Brief #205 – 2023*. ISBN 978-1-92-728770-5. Accessed January 2025.

First Street Foundation. (2023, September). *First Street Foundation - Arup Climate Risk and Losses Methodology Version 1.0*.

G. Cremen, C. Galasso, J. McCloskey, *A Simulation-Based Framework for Earthquake Risk-Informed and People-Centered Decision Making on Future Urban Planning*, *Earth's Future*. 10 (2022). <https://doi.org/10.1029/2021EF002388>.

G. Cremen, E.Y. Mentese, M.E. Filippi, R. Gentile, C. Galasso, J. McCloskey, *A State-of-the-Art Environment for Supporting Risk-Sensitive Decisions on Urbanisation in Tomorrow's Cities*, *International Journal of Disaster Risk Reduction*. under rev (2022).

G. Cremen, E.Y. Mentese, M.E. Filippi, R. Gentile, C. Galasso, J. McCloskey, *A State-of-the-Art Environment for Supporting Risk-Sensitive Decisions on Urbanisation in Tomorrow's Cities*, *International Journal of Disaster Risk Reduction*. under rev (2022).

G. Cremen, E.Y. Mentese, M.E. Filippi, R. Gentile, C. Galasso, J. McCloskey, *A State-of-the-Art Environment for Supporting Risk-Sensitive Decisions on Urbanisation in Tomorrow's Cities*, *International Journal of Disaster Risk Reduction*. under rev (2022).

G. Cremen, J.W. Baker, *Improving FEMA P-58 non-structural component fragility functions and loss predictions*, *Bulletin of Earthquake Engineering*. 17 (2019) 1941–1960. <https://doi.org/10.1007/s10518-018-00535-7>.

G. Di Pasquale, G. Orsini, R.W. Romeo, *New developments in seismic risk assessment in Italy*, *Bulletin of Earthquake Engineering*. 3 (2005) 101–128. <https://doi.org/10.1007/s10518-005-0202-1>.

G. Ganesh Prasad, S. Banerjee, *The Impact of Flood-Induced Scour on Seismic Fragility Characteristics of Bridges*, *Journal of Earthquake Engineering*. 17 (2013) 803–828. <https://doi.org/10.1080/13632469.2013.771593>.

G. Grünthal, *European Macroseismic Scale 1998*, European Seismological Commission, Subcommittee on Engineering Seismology. Working Group Macroseismic scales, 1998.

G. Liek Yeo, A.C. Cornell, *Building life-cycle cost analysis due to mainshock and aftershock occurrences*, *Structural Safety*. 31 (2009) 396–408. <https://doi.org/10.1016/j.strusafe.2009.01.002>.

G. Limongi, A. Galderisi, *Twenty years of European and international research on vulnerability: A multi-faceted concept for better dealing with evolving risk landscapes*, *International Journal of Disaster Risk Reduction*. 63 (2021) 102451. <https://doi.org/10.1016/j.ijdrr.2021.102451>.

G. Mavrommati, K. Bithas, and P. Panayiotidis, *“Operationalizing sustainability in urban coastal systems: A system dynamics analysis,”* *Water Res.*, vol. 47, no. 20, pp. 7235–7250, Dec. 2013, doi: 10.1016/j.watres.2013.10.041.

G. Miluccio, R. Gentile, C. Galasso, F. Parisi, *Fragility Modelling of Buildings subjected to Earthquake-Induced Landslides through Gaussian Process Regression*, in: *ICOSSAR 2021, International Conference on Structural Safety & Reliability*, Shanghai, Cina, 2021.

G. Pescaroli and D. Alexander, "Critical infrastructure, panarchies and the vulnerability paths of cascading disasters," *Nat. Hazards*, vol. 82, no. 1, pp. 175–192, May 2016, doi: 10.1007/s11069-016-2186-3.

G. Sevieri, C. Galasso, D. D'Ayala, R. de Jesus, A. Oreta, M.E.D.A. Grio, R. Ibabao, *A multi-hazard risk prioritisation framework for cultural heritage assets*, *Natural Hazards and Earth System Sciences*. 20 (2020) 1391–1414. <https://doi.org/https://doi.org/10.5194/nhess-20-1391-2020>.

G. Zuccaro, F. Cacace, R.J.S. Spence, P.J. Baxter, *Impact of explosive eruption scenarios at Vesuvius*, *Journal of Volcanology and Geothermal Research*. 178 (2008) 416–453. <https://doi.org/10.1016/j.jvolgeores.2008.01.005>.

G.A. Riddell, H. van Delden, H.R. Maier, A.C. Zecchin, *Tomorrow's disasters – Embedding foresight principles into disaster risk assessment and treatment*, *International Journal of Disaster Risk Reduction*. 45 (2020) 101437. <https://doi.org/10.1016/j.ijdr.2019.101437>.

G.M. Calvi, R. Pinho, G. Magenes, J.J. Bommer, L.F. Restrepo-Velez, H. Crowley, *Development of seismic vulnerability assessment methodologies over the past 30 years*, *Journal of Earthquake Technology*. 43 (2006) 75–104.

Gentile, R. (2025). *OpenVulnerability: An interactive web platform to select and score physical impact models*. In M. Papadrakakis & M. Fragiadakis (Eds.), *COMPDYN 2025: 10th ECCOMAS Thematic Conference on Computational Methods in Structural Dynamics and Earthquake Engineering* (June 15–18, Rhodes Island, Greece).

Gentile, R., Cremen, G., Galasso, C., Jenkins, L. T., Manandhar, V., Menteşe, E. Y., Guragain, R., & McCloskey, J. (2022). *Scoring, selecting, and developing physical impact models for multi-hazard risk assessment*. *International Journal of Disaster Risk Reduction*, 82, 103365.

Gentile, R., Cremen, G., Galasso, C., Jenkins, L. T., Manandhar, V., Menteşe, E. Y., Guragain, R., & McCloskey, J. (2022). *Scoring, selecting, and developing physical impact models for multi-hazard risk assessment*. *International Journal of Disaster Risk Reduction*, 82, 103365. <https://doi.org/10.1016/j.ijdr.2022.103365>

Goldwyn, B., Velasquez, C., Liel, A. B., Javernick-Will, A., & Koschmann, M. (2023). *Capacity-building to support safer housing through appropriate hurricane strap use*. *Natural Hazards Review*, 24(3), 04023026. <https://doi.org/10.1061/NHREFO.NHENG-1708>

Greater Wellington Regional Council. (2005). *Natural hazards. En Measuring up 2005: State of the Environment Report* (Cap. 8). https://www.gw.govt.nz/assets/Documents/2009/07/2511_MeasuringUpCh8lo_s4732.pdf. (Informe completo: https://www.gw.govt.nz/assets/Documents/2022/03/2515_MeasuringUpFull_s4736.pdf).

Greater Wellington Regional Council. (2025, octubre 31). *Know your flood risk*. <https://www.gw.govt.nz/your-region/emergency-and-hazard-management/flood-protection/know-your-flood-risk/>

Görüm, T., Bozkurt, D., Korup, O., İstanbulluoğlu, E., Şen, Ö. L., Yılmaz, A., Karabacak, F., Lombardo, L., & Tanyas, H. (2025). *The 2023 Türkiye-Syria earthquake disaster was exacerbated by an atmospheric river*. *Communications Earth & Environment*, 6(1), 151.

H. Crowley, J. Dabbeek, V. Despotaki, D. Rodrigues, L. Martins, V. Silva, X. Romão, N. Pereira, G. Weatherill, L. Danciu, *European Seismic Risk Model (ESRM20)*. EFEHR Technical Report 002 V1.0.0, 2021. <https://doi.org/10.7414/EUC-EFEHR-TR002-ESRM20>.

- H. Ebrahimian, F. Jalayer, *Selection of seismic intensity measures for prescribed limit states using alternative nonlinear dynamic analysis methods*, *Earthq Eng Struct Dyn.* 50 (2021) 1235–1250. <https://doi.org/10.1002/eqe.3393>.
- H. Li, L. Li, G. Zhou, L. Xu, *Time-dependent Seismic Fragility Assessment for Aging Highway Bridges Subject to Non-uniform Chloride-induced Corrosion*, *Journal of Earthquake Engineering.* (2020) 1–31. <https://doi.org/10.1080/13632469.2020.1809561>.
- H. Li, Y. Liu, C. Li, X.W. Zheng, *Multihazard fragility assessment of steel-concrete composite frame structures with buckling-restrained braces subjected to combined earthquake and wind*, *The Structural Design of Tall and Special Buildings.* 29 (2020). <https://doi.org/10.1002/tal.1746>.
- H. Luo, L. Zhang, H. Wang, J. He, *Multi-hazard vulnerability of buildings to debris flows*, *Eng Geol.* 279 (2020) 105859. <https://doi.org/10.1016/j.enggeo.2020.105859>.
- H. Maiwald, J. Schwarz, *Vereinheitlichte Schadensbeschreibung und Risikobewertung von Bauwerken unter extremen Naturgefahren*, *Bautechnik.* 95 (2018) 743–755. <https://doi.org/10.1002/bate.201800009>.
- H. Motamed, A. Calderon, V. Silva, C. Costa, *Development of a probabilistic earthquake loss model for Iran*, *Bulletin of Earthquake Engineering.* 17 (2019) 1795–1823. <https://doi.org/10.1007/s10518-018-0515-5>.
- H.-Y. Noh, A. Kiremidjian, L. Ceferino, E. So, *Bayesian Updating of Earthquake Vulnerability Functions with Application to Mortality Rates*, *Earthquake Spectra.* 33 (2017) 1173–1189. <https://doi.org/10.1193/081216eqs133m>.
- H.Y. Luo, R.L. Fan, H.J. Wang, L.M. Zhang, *Physics of building vulnerability to debris flows, floods and earth flows*, *Eng Geol.* 271 (2020) 105611. <https://doi.org/10.1016/J.ENGGEOL.2020.105611>.
- Hogan, J., Almufti, I., & Ackerson, M. (2023). REDi™: Resilience-Based Design Guidelines for Floods. Arup.
- Huizinga, J., Moel, H. de, Szewczyk, W. (2017). *Global flood depth-damage functions. Methodology and the database with guidelines.* EUR 28552 EN. doi: 10.2760/16510
- I. Bombelli, D. Molinari, P. Asaridis, F. Ballio, *The “Flood Damage Models” repository*, in: *Science and Practice for an Uncertain Future*, Budapest University of Technology and Economics, Online, 2021: p. null-null. <https://doi.org/10.3311/FloodRisk2020.11.3>.
- I. Zentner, *A general framework for the estimation of analytical fragility functions based on multivariate probability distributions*, *Structural Safety.* 64 (2017) 54–61. <https://doi.org/10.1016/j.strusafe.2016.09.003>.
- I. Zentner, M. Gündel, N. Bonfils, *Fragility analysis methods: Review of existing approaches and application*, *Nuclear Engineering and Design.* 323 (2017) 245–258. <https://doi.org/10.1016/j.nucengdes.2016.12.021>.
- Iannacone, L., Otárola, K., Gentile, R., & Galasso, C. (2024). *Simulating multi-hazard event sets for life cycle consequence analysis*. *Natural Hazards and Earth System Sciences*, 24(5), 1721-1740.
- Institut Wohnen und Umwelt (IWU). (2011). *TABULA WebTool*. Retrieved October 24, 2025, from <https://webtool.building-typology.eu/>
- J. Baker, *Probabilistic Seismic Hazard Analysis*, 2.0.1, 2013.
- J. Dabbeek, V. Silva, C. Galasso, A. Smith, *Probabilistic earthquake and flood loss assessment in the Middle East*, *International Journal of Disaster Risk Reduction.* 49 (2020) 101662. <https://doi.org/10.1016/J.IJDRR.2020.101662>.

- J. Douvinet, D. Delahaye, P. Langlois, *Measuring surface flow concentrations using a cellular automaton metric: a new way of detecting potential impacts of flash floods in sedimentary context*, *Http://Journals.Openedition.Org/Geomorphologie*. (2013) 27–46. <https://doi.org/10.4000/GEOMORPHOLOGIE.10112>.
- J. Fan, Q. Li, Y. Zhang, *Collapse analysis of wind turbine tower under the coupled effects of wind and near-field earthquake*, *Wind Energy*. 22 (2019) 407–419. <https://doi.org/10.1002/we.2294>.
- J. Ghosh, J.E. Padgett, *Aging Considerations in the Development of Time-Dependent Seismic Fragility Curves*, *Journal of Structural Engineering*. 136 (2010) 1497–1511. [https://doi.org/10.1061/\(ASCE\)ST.1943-541X.0000260](https://doi.org/10.1061/(ASCE)ST.1943-541X.0000260).
- J. Ghosh, J.E. Padgett, M. Sánchez-Silva, *Seismic Damage Accumulation in Highway Bridges in Earthquake-Prone Regions*, *Earthquake Spectra*. 31 (2015) 115–135. <https://doi.org/10.1193/120812EQS347M>.
- J. Han, S. Wu, H. Wang, *Preliminary Study on Geological Hazard Chains*, *Earth Science Frontiers*. 14 (2007) 11–20. [https://doi.org/10.1016/S1872-5791\(08\)60001-9](https://doi.org/10.1016/S1872-5791(08)60001-9).
- J. Huizinga, H. de Moel, W. Szewczyk, *Global flood depth-damage functions: methodology and the database with guidelines*, EUR 28552 EN, Ispra, Italy, 2017. <https://doi.org/https://doi.org/10.2760/16510>.
- J. Schwarz, H. Maiwald, *Empirical vulnerability assessment and damage description for natural hazards following the principles of modern macroseismic scales*, in: *15th World Conference on Earthquake Engineering*, Lisbon, Portugal, 2012. <https://doi.org/10.13140/2.1.3455.4565>.
- J. Stermann, “System Dynamics: Systems Thinking and Modeling for a Complex World,” Massachusetts Institute of Technology. Engineering Systems Division, Working Paper, May 2002. Accessed: Oct. 22, 2025. [Online]. Available: <https://dspace.mit.edu/handle/1721.1/102741>
- J.-G. Xu, G. Wu, D.-C. Feng, J.-J. Fan, *Probabilistic multi-hazard fragility analysis of RC bridges under earthquake-tsunami sequential events*, *Eng Struct*. 238 (2021) 112250. <https://doi.org/10.1016/j.engstruct.2021.112250>.
- J.-S. Jeon, R. DesRoches, L.N. Lowes, I. Brilakis, *Framework of aftershock fragility assessment-case studies: older California reinforced concrete building frames*, *Earthq Eng Struct Dyn*. 44 (2015) 2617–2636. <https://doi.org/10.1002/eqe.2599>.
- J.A. Prieto, M. Journeay, A.B. Acevedo, J.D. Arbelaez, M. Ulmi, *Development of structural debris flow fragility curves (debris flow buildings resistance) using momentum flux rate as a hazard parameter*, *Eng Geol*. 239 (2018) 144–157. <https://doi.org/10.1016/j.enggeo.2018.03.014>.
- J.A. Prieto, M. Journeay, A.B. Acevedo, J.D. Arbelaez, M. Ulmi, *Development of structural debris flow fragility curves (debris flow buildings resistance) using momentum flux rate as a hazard parameter*, *Eng Geol*. 239 (2018) 144–157. <https://doi.org/10.1016/j.enggeo.2018.03.014>.
- J.C. Gill, B.D. Malamud, *Reviewing and visualizing the interactions of natural hazards*, *Reviews of Geophysics*. 52 (2014) 680–722. <https://doi.org/10.1002/2013RG000445>.
- J.C.S. Tang, S. Vongvisessomjai, K. Sahasakmontri, *Estimation of flood damage cost for Bangkok*, *Water Resources Management*. 6 (1992) 47–56. <https://doi.org/10.1007/BF00872187>.
- J.W. Baker, *Efficient analytical fragility function fitting using dynamic structural analysis*, *Earthquake Spectra*. 31 (2015) 579–599. <https://doi.org/10.1193/021113EQS025M>.
- J.W. van de Lindt, M. Taggart, *Fragility Analysis Methodology for Performance-Based Analysis of Wood-Frame Buildings for Flood*, *Nat Hazards Rev*. 10 (2009) 113–123. [https://doi.org/10.1061/\(ASCE\)1527-6988\(2009\)10:3\(113\)](https://doi.org/10.1061/(ASCE)1527-6988(2009)10:3(113)).

- Jalayer, F., Carozza, S., De Risi, R., Manfredi, G., & Mbuya, E. (2016). Performance-based flood safety-checking for non-engineered masonry structures. *Engineering Structures*, 106, 109-123.
- Joint Committee on Housing, Local Government and Heritage (JCHLGH). (2023). *Modern methods of construction. Houses of the Oireachtas*.
- K. Aljawhari, R. Gentile, F. Freddi, C. Galasso, Effects of ground-motion sequences on fragility and vulnerability of case-study reinforced concrete frames, *Bulletin of Earthquake Engineering*. 19 (2021) 6329–6359. <https://doi.org/10.1007/s10518-020-01006-8>.
- K. Aljawhari, R. Gentile, F. Freddi, C. Galasso, Effects of ground-motion sequences on fragility and vulnerability of case-study reinforced concrete frames, *Bulletin of Earthquake Engineering*. 19 (2021) 6329–6359. <https://doi.org/10.1007/s10518-020-01006-8>.
- K. Otárola, J. Fayaz, C. Galasso, Fragility and vulnerability analysis of deteriorating ordinary bridges using simulated ground-motion sequences, *Earthq Eng Struct Dyn*. under rev (2022).
- K. Pitilakis, P. Franchin, B. Khazai, H. Wenzel, eds., *SYNER-G: Systemic Seismic Vulnerability and Risk Assessment of Complex Urban, Utility, Lifeline Systems and Critical Facilities*, Springer Netherlands, Dordrecht, 2014. <https://doi.org/10.1007/978-94-017-8835-9>.
- K. Porter, *A Beginner's Guide to Fragility, Vulnerability, and Risk*, 2021.
- K. Porter, GEM Vulnerability Rating System, GEM Global Vulnerability Estimation Methods Consortium, 2011.
- K. Porter, R. Kennedy, R. Bachman, Creating fragility functions for performance-based earthquake engineering, *Earthquake Spectra*. 23 (2007) 471–489. <https://doi.org/10.1193/1.2720892>.
- K. Schröter, H. Kreibich, K. Vogel, C. Riggelsen, F. Scherbaum, B. Merz, How useful are complex flood damage models?, *Water Resour Res*. 50 (2014) 3378–3395. <https://doi.org/10.1002/2013WR014396>.
- K.H. Lee, D. v. Rosowsky, Fragility analysis of woodframe buildings considering combined snow and earthquake loading, *Structural Safety*. 28 (2006) 289–303. <https://doi.org/10.1016/j.strusafe.2005.08.002>.
- K.S. Jaiswal, D.J. Wald, *Creating a global building inventory for earthquake loss assessment and risk management*. U.S. Geological Survey Open-File Report 2008-1160., Washington DC, USA, 2008.
- Kelman, I. (2003). *Physical flood vulnerability of residential properties in coastal, eastern England* (Doctoral dissertation, University of Cambridge).
- Krawinkler, H., & Miranda, E. (2004). 9.1. A Perspective of Performance-Based Earthquake Engineering. *Earthquake Engineering: From Engineering Seismology to Performance-Based Engineering*; CRC Press: Boca Raton, FL, USA, 87.
- L. Di Sarno, F. Pugliese, Effects of mainshock-aftershock sequences on fragility analysis of RC buildings with ageing, *Eng Struct*. 232 (2021) 111837. <https://doi.org/10.1016/j.engstruct.2020.111837>.
- L. Halder, S. Chandra Dutta, R.P. Sharma, Damage study and seismic vulnerability assessment of existing masonry buildings in Northeast India, *Journal of Building Engineering*. 29 (2020) 101190. <https://doi.org/10.1016/j.jobbe.2020.101190>.
- L. Jenkins, M. Creed, K. Tarbali, M. Muthusamy, robert sakic Trogrlic, J. Philips, S. Watson, H. Sinclair, C. Galasso, J. McCloskey, Physics-based simulations of multiple natural hazards for risk sensitive land use planning in expanding urban regions undefined, *International Journal of Disaster Risk Reduction*. under rev (2022).
- L. Martins, V. Silva, Development of a fragility and vulnerability model for global seismic risk analyses, *Bulletin of Earthquake Engineering*. 19 (2021) 6719–6745. <https://doi.org/10.1007/s10518-020-00885-1>.

- L. Martins, V. Silva, *Development of a fragility and vulnerability model for global seismic risk analyses*, *Bulletin of Earthquake Engineering*. 19 (2021) 6719–6745. <https://doi.org/10.1007/s10518-020-00885-1>.
- L. Martins, V. Silva, M. Marques, H. Crowley, R. Delgado, *Development and assessment of damage-to-loss models for moment-frame reinforced concrete buildings*, *Earthq Eng Struct Dyn*. 45 (2016) 797–817. <https://doi.org/10.1002/eqe.2687> Development.
- L. Martins, V. Silva, M. Marques, H. Crowley, R. Delgado, *Development and assessment of damage-to-loss models for moment-frame reinforced concrete buildings*, *Earthq Eng Struct Dyn*. 45 (2016) 797–817. <https://doi.org/10.1002/eqe.2687>.
- L.T. Jenkins, M. Creed, K. Tarbali, M. Muthusamy, robert sakic Trogrlic, J. Philips, S. Watson, H. Sinclair, C. Galasso, J. McCloskey, *Physics-based simulations of multiple natural hazards for risk sensitive land use planning in expanding urban regions undefined*, *International Journal of Disaster Risk Reduction*. under rev (2022).
- Lee, R., White, C. J., Adnan, M. S. G., Douglas, J., Mahecha, M. D., O'Loughlin, F. E., Patelli, E., Ramos, A. M., Roberts, M. J., Martius, O., Tubaldi, E., van den Hurk, B., Ward, P. J., & Zscheischler, J. (2024). *Reclassifying historical disasters: From single to multi-hazards*. *Science of the Total Environment*, 912, 169120.
- Luglio, C. E. (2016). *Resilience of critical infrastructures: Dynamic modeling of disruptive events in a European scenario* (Master's thesis, Politecnico di Milano). Supervisors: D. Manca; J. Tixier; A. Bony-Dandrieux. POLITesi.
- Luo, H. Y., Fan, R. L., Wang, H. J., & Zhang, L. M. (2020). *Physics of building vulnerability to debris flows, floods and earth flows*. *Engineering Geology*, 271, 105611.
- Luo, H. Y., Fan, R. L., Wang, H. J., & Zhang, L. M. (2020). *Physics of building vulnerability to debris flows, floods and earth flows*. *Engineering Geology*, 271, 105611.
- M. Arattano, L. Marchi, *Systems and Sensors for Debris-flow Monitoring and Warning*, *Sensors* 2008, Vol. 8, Pages 2436–2452. 8 (2008) 2436–2452. <https://doi.org/10.3390/S8042436>.
- M. Bruneau, M. Barbato, J.E. Padgett, A.E. Zaghi, J. Mitrani-Reiser, Y. Li, *State of the Art of Multihazard Design*, *Journal of Structural Engineering*. 143 (2017) 03117002. [https://doi.org/10.1061/\(ASCE\)ST.1943-541X.0001893](https://doi.org/10.1061/(ASCE)ST.1943-541X.0001893).
- M. Caruso, R. Pinho, F. Bianchi, F. Cavalieri, M.T. Lemmo, *Integrated economic and environmental building classification and optimal seismic vulnerability/energy efficiency retrofitting*, *Bulletin of Earthquake Engineering*. 19 (2021) 3627–3670. <https://doi.org/10.1007/s10518-021-01101-4>.
- M. Eeten, A. Nieuwenhuijs, E. Luijff, M. Klaver, and E. Cruz, “The State and the Threat of Cascading Failure Across Critical Infrastructures: The Implications of Empirical Evidence from Media Incident Reports,” *Public Adm.*, vol. 89, p. 381, June 2011, doi: 10.1111/j.1467-9299.2011.01926.x.
- M. Jakob, D. Stein, M. Ulmi, *Vulnerability of buildings to debris flow impact*, *Natural Hazards*. 60 (2012) 241–261. <https://doi.org/10.1007/S11069-011-0007-2/FIGURES/5>.
- M. Kohrangi, D. Vamvatsikos, P. Bazzurro, *Site dependence and record selection schemes for building fragility and regional loss assessment*, *Earthq Eng Struct Dyn*. 46 (2017) 1625–1643. <https://doi.org/10.1002/eqe.2873>.
- M. Mylonakou, A. Chassiakos, S. Karatzas, and G. Liappi, “System Dynamics Analysis of the Relationship between Urban Transportation and Overall Citizen Satisfaction: A Case Study of Patras City, Greece,” *Systems*, vol. 11, no. 3, p. 112, Mar. 2023, doi: 10.3390/systems11030112.
- M. Nguyen, D. Lallemand, *Order Matters: The Benefits of Ordinal Fragility Curves for Damage and Loss Estimation*, *Risk Analysis*. (2021). <https://doi.org/10.1111/risa.13815>.

- M. Ouyang, "Review on modeling and simulation of interdependent critical infrastructure systems," *Reliab. Eng. Syst. Saf.*, vol. 121, pp. 43–60, Jan. 2014, doi: 10.1016/j.res.2013.06.040.
- M. Papathoma-Köhle, B. Gems, M. Sturm, S. Fuchs, *Matrices, curves and indicators: A review of approaches to assess physical vulnerability to debris flows*, *Earth Sci Rev.* 171 (2017) 272–288. <https://doi.org/10.1016/J.EARSCIREV.2017.06.007>.
- M. Raghunandan, A.B. Liel, N. Luco, *Aftershock collapse vulnerability assessment of reinforced concrete frame structures*, *Earthq Eng Struct Dyn.* 44 (2015) 419–439. <https://doi.org/10.1002/eqe.2478>.
- M. Zarghami and S. Akbariyeh, "System dynamics modeling for complex urban water systems: Application to the city of Tabriz, Iran," *Resour. Conserv. Recycl.*, vol. 60, pp. 99–106, Mar. 2012, doi: 10.1016/j.resconrec.2011.11.008.
- M.A. Erberik, *Fragility-based assessment of typical mid-rise and low-rise RC buildings in Turkey*, *Eng Struct.* 30 (2008) 1360–1374. <https://doi.org/10.1016/j.engstruct.2007.07.016>.
- M.C. de Ruiter, J.A. de Bruijn, J. Enghardt, J.E. Daniell, H. de Moel, P.J. Ward, *The Asynergies of Structural Disaster Risk Reduction Measures: Comparing Floods and Earthquakes*, *Earths Future.* 9 (2021). <https://doi.org/10.1029/2020EF001531>.
- M.E. Filippi, A. Barcena, R. Šakić Trogrlić, G. Cremen, E.Y. Mentese, R. Gentile, L. Jenkins, D.P. Poudel, M.J. Creed, V. Manandhar, J. McCloskey, M. Rai, S. Adhikari, M. Muthusamy, C. Galasso, *Interdisciplinarity in practice: reflections from early career researchers developing a risk-informed decision support environment for Tomorrow's Cities*, *International Journal of Disaster Risk Reduction*. under rev (2022).
- M.E.A. Budimir, P.M. Atkinson, H.G. Lewis, *Earthquake-and-landslide events are associated with more fatalities than earthquakes alone*, *Natural Hazards.* 72 (2014) 895–914. <https://doi.org/10.1007/s11069-014-1044-4>.
- M.S. Alam, B.G. Simpson, A.R. Barbosa, *Defining Appropriate Fragility Functions for Oregon. A report for the Cascadia Lifelines Program (CLiP)*, 2020.
- M.S. Kappes, M. Keiler, K. von Elverfeldt, T. Glade, *Challenges of analyzing multi-hazard risk: a review*, *Natural Hazards.* 64 (2012) 1925–1958. <https://doi.org/10.1007/s11069-012-0294-2>.
- McGetrick, P. (2024). *HOME GROWN C16 – Increasing the use of Irish home grown C16 timber in housing construction* (Report No. CI-AHARDD03-Galway-R-01.01). Construct Innovate, University of Galway.
- Mesta, C., Kerschbaum, D., Cremen, G., & Galasso, C. (2023). *Quantifying the potential benefits of risk-mitigation strategies on present and future seismic losses in Kathmandu Valley, Nepal*. *Earthquake Spectra*, 39(1), 377-401.
- Ministry for the Environment & Statistics New Zealand (2015). *New Zealand's Environmental Reporting Series: Environment Aotearoa 2015*. <https://environment.govt.nz/assets/Publications/Files/Environment-Aotearoa-2015.pdf>
- Ministry of Business, Innovation and Employment. (2023). *Acceptable solutions and verification methods for New Zealand Building Code Clause E1 surface water* (1st ed., Amdt. 12). Retrieved November, 2025
- Moehle, J., & Deierlein, G. G. (2004). *A framework methodology for performance-based earthquake engineering*. In *13th World Conference on Earthquake Engineering* (Vol. 679, p. 12). WCEE, Vancouver.
- Moreno, D. G., O'Toole, D., McGetrick, P. J., & Harte, A. M. (2022). *Timber construction in Ireland for the mitigation of climate change and the housing crisis in 2022. Assessment (LCA)*, 2, 3.

Munich Re. (2024). *Flood risks on the rise—Greater loss prevention is needed*. Retrieved April 29, 2025, from <https://www.munichre.com/en/risks/natural-disasters/floods.html>

N. Ahmad, A. Shahzad, Q. Ali, M. Rizwan, A.N. Khan, *Seismic fragility functions for code compliant and non-compliant RC SMRF structures in Pakistan*, *Bulletin of Earthquake Engineering*. 16 (2018) 4675–4703. <https://doi.org/10.1007/s10518-018-0377-x>.

N. Caterino, I. Iervolino, G. Manfredi, E. Cosenza, *Comparative analysis of multi-criteria decision-making methods for seismic structural retrofitting*, *Computer-Aided Civil and Infrastructure Engineering*. 24 (2009) 432–445. <https://doi.org/10.1111/j.1467-8667.2009.00599.x>.

N. Luco, C.A. Cornell, *Structure-Specific Scalar Intensity Measures for Near-Source and Ordinary Earthquake Ground Motions*, *Earthquake Spectra*. 23 (2007) 357–392. <https://doi.org/10.1193/1.2723158>.

N. Tarque, H. Crowley, R. Pinho, H. Varum, *Displacement-Based Fragility Curves for Seismic Assessment of Adobe Buildings in Cusco, Peru*, *Earthquake Spectra*. 28 (2012) 759–794. <https://doi.org/10.1193/1.4000001>.

N.C. Dalkey, *The Delphi Method: An Experimental Study of Group Opinion*, Santa Monica, USA, 1969.

National Institute of Water and Atmospheric Research (2023). *Climate change scenarios for New Zealand*. Accessed 14 Oct 2025..

National Institute of Water and Atmospheric Research (NIWA). (s. f.). *High Intensity Rainfall Design System (HIRDS)*. Recuperado el 10 de noviembre de 2025, de <https://hirds.niwa.co.nz/>. (Descripción del servicio: <https://niwa.co.nz/climate-and-weather/high-intensity-rainfall-design-system-hirds>).

National Institute of Water and Atmospheric Research (NIWA). (s. f.). *NIWA Tides (Tide Forecaster)*. Recuperado el 10 de noviembre de 2025, de <https://tides.niwa.co.nz/>. (Página informativa: <https://niwa.co.nz/coasts/tide-forecaster>).

National Institute of Water and Atmospheric Research. (n.d.). *NZ NIWA Sea Level App [ArcGIS Experience]*. Retrieved November 10, 2025, from

NBC: 201, *Nepal national building code*, Kathmandu, Nepal, 1994.

Nieto, N., Chamorro, A., Echaveguren, T., & Escauriaza, C. (2023). *Fragility curves for road embankments exposed to adjacent debris flow*. *Progress in Physical Geography: Earth and Environment*, 47(1), 105-122.

Noble, N., & Roy, D. C. (2010). *Flood resistant housing: Low-cost disaster-resistant housing in Bangladesh*. *Practical Action*. <http://practicalaction.org/practicalanswers/>

Nofal, O. M., & van de Lindt, J. W. (2020a). *High-resolution approach to quantify the impact of building-level flood risk mitigation and adaptation measures on flood losses at the community level*. *International Journal of Disaster Risk Reduction*, 51, 101903.

Nofal, O. M., van de Lindt, J. W., & Do, T. Q. (2020b). *Multi-variate and single-variable flood fragility and loss approaches for buildings*. *Reliability Engineering & System Safety*, 202, 106971. <https://doi.org/10.1016/j.ress.2020.106971>

Nofal, O. M., Van De Lindt, J. W., Yan, G. G., Hamideh, S., & Dietrich, C. (2021b). *Multi Hazard Hurricane Vulnerability Model to Enable Resilience Informed Decision*. In *Proceedings of the 11th International Structural Engineering and Construction Conference, ISEC21 (2021: Jul. 26-31, Cairo, Egypt)*, vol. 8, no. 1, pp. RAD - 1, ISEC Press, Jul 2021.

Nowak, A.S., & Collins, K.R. (2012). *Reliability of Structures (2nd ed.)*. CRC Press. <https://doi.org/10.1201/b12913>

O. Hungr, G.C. Morgan, R. Kellerhals, Quantitative analysis of debris torrent hazards for design of remedial measures, *https://doi.org/10.1139/T84-073*. 21 (1984) 663–677. <https://doi.org/10.1139/T84-073>.

O.M. Nofal, J.W. van de Lindt, Minimal Building Flood Fragility and Loss Function Portfolio for Resilience Analysis at the Community Level, *Water (Basel)*. 12 (2020) 2277. <https://doi.org/10.3390/w12082277>.

O.M. Nofal, J.W. van de Lindt, Minimal building flood fragility and loss function portfolio for resilience analysis at the community level, *Water (Switzerland)*. 12 (2020). <https://doi.org/10.3390/w12082277>.

O.M. Nofal, J.W. van de Lindt, T.Q. Do, G. Yan, S. Hamideh, D.T. Cox, J.C. Dietrich, Methodology for Regional Multihazard Hurricane Damage and Risk Assessment, *Journal of Structural Engineering*. 147 (2021) 04021185. [https://doi.org/10.1061/\(ASCE\)ST.1943-541X.0003144](https://doi.org/10.1061/(ASCE)ST.1943-541X.0003144).

O.M. Nofal, J.W. van de Lindt, T.Q. Do, Multi-variate and single-variable flood fragility and loss approaches for buildings, *Reliab Eng Syst Saf*. 202 (2020). <https://doi.org/10.1016/j.ress.2020.106971>.

O.M. Nofal, J.W. van de Lindt, Understanding flood risk in the context of community resilience modeling for the built environment: research needs and trends, *Sustain Resilient Infrastruct*. 7 (2022) 171–187. <https://doi.org/10.1080/23789689.2020.1722546>.

O.O. Thomas, L. Chouinard, S. Langlois, Probabilistic Fatigue Fragility Curves for Overhead Transmission Line Conductor-Clamp Assemblies, *Front Built Environ*. 8 (2022). <https://doi.org/10.3389/fbuil.2022.833167>.

Otey, D., Vielma, J. C., & Winckler, P. (2025). Structural failure modes of single-story timber houses under tsunami loads using ASCE 7's energy grade line analysis. *Journal of Marine Science and Engineering*, 13(3), 484. <https://doi.org/10.3390/jmse13030484>

P. Deckers, W. Kellens, J. Reyns, W. Vanneuville, P. de Maeyer, A GIS for Flood Risk Management in Flanders, in: *Geospatial Techniques in Urban Hazard and Disaster Analysis*, Springer Netherlands, Dordrecht, 2009: pp. 51–69. https://doi.org/10.1007/978-90-481-2238-7_4.

P. Gehl, D.M. Seyed, J. Douglas, Vector-valued fragility functions for seismic risk evaluation, *Bulletin of Earthquake Engineering*. 11 (2013) 365–384. <https://doi.org/10.1007/s10518-012-9402-7>.

P.A. Korswagen, S.N. Jonkman, K.C. Terwel, Probabilistic assessment of structural damage from coupled multi-hazards, *Structural Safety*. 76 (2019) 135–148. <https://doi.org/10.1016/j.strusafe.2018.08.001>.

Pandolfi, F., Baltzopoulos, G., & Iervolino, I. (2023). ERMES: extreme wind risk assessment for building portfolios. *Natural Hazards*, 116(2), 2717–2743.

Parammal, A. (2022). *Performance Assessment of Masonry School Buildings to Seismic and Flood Hazards Using Bayesian Networks* (Doctoral dissertation, UCL (University College London)).

Peacock, W. G., Dash, N., Zhang, Y., & Van Zandt, S. (2018). Post-disaster sheltering, temporary housing and permanent housing recovery. In *Handbook of disaster research* (pp. 569–594).

Pearce, H. G. (2005). *Fuel Load and Fire Behaviour Assessments for Vegetation within LCDB2 (Appendix 3: Sub-contracted Report)*. Scion, Forest Research Limited. Retrieved from

Quick, L., Creed, M.J., Sinclair, H.D. et al. Hyperconcentrated floods cause extreme gravel transport through the sandy rivers of the Gangetic Plains. *Commun Earth Environ* 4, 297 (2023). <https://doi.org/10.1038/s43247-023-00953-9>

Quick, L., Creed, M.J., Sinclair, H.D. et al. Hyperconcentrated floods cause extreme gravel transport through the sandy rivers of the Gangetic Plains. *Commun Earth Environ* 4, 297 (2023). <https://doi.org/10.1038/s43247-023-00953-9>

- R. Figueiredo, X. Romão, E. Paupério, *Component-based flood vulnerability modelling for cultural heritage buildings*, *International Journal of Disaster Risk Reduction*. 61 (2021) 102323. <https://doi.org/10.1016/j.ijdr.2021.102323>.
- R. Gentile, C. Galasso, *Hysteretic energy-based state-dependent fragility for ground-motion sequences*, *Earthq Eng Struct Dyn*. 50 (2021) 1187–1203. <https://doi.org/10.1002/eqe.3387>.
- R. Gentile, C. Galasso, *Simplicity versus accuracy trade-off in estimating seismic fragility of existing reinforced concrete buildings*, *Soil Dynamics and Earthquake Engineering*. 144 (2021) 106678. <https://doi.org/10.1016/j.soildyn.2021.106678>.
- R. Gentile, C. Galasso, *Simplicity versus accuracy trade-off in estimating seismic fragility of existing reinforced concrete buildings*, *Soil Dynamics and Earthquake Engineering*. 144 (2021) 106678. <https://doi.org/10.1016/j.soildyn.2021.106678>.
- R. Gentile, C. Galasso, *Simplified seismic loss assessment for optimal structural retrofit of RC buildings [Open Access]*, *Earthquake Spectra*. 37 (2020). <https://doi.org/10.1177/8755293020952441>.
- R. Gentile, C. Galasso, Y. Idris, I. Rusydy, E. Meilianda, *From rapid visual survey to multi-hazard risk prioritisation and numerical fragility of school buildings in Banda Aceh, Indonesia*, *Natural Hazards and Earth System Sciences*. 19 (2019) 1365–1386. <https://doi.org/10.5194/nhess-2018-397>.
- R. Gentile, S. Pampanin, C. Galasso, *A computational framework for selecting the optimal combination of seismic retrofit and insurance coverage*, *Computer-Aided Civil and Infrastructure Engineering*. in press (2021). <https://doi.org/10.1111/mice.12778>.
- R. Guragain, *Development of seismic risk assessment system for Nepal*, University of Tokyo, 2015. <https://doi.org/http://doi.org/10.15083/00007589>.
- R. Setola, S. Bologna, E. Casalicchio, and V. Masucci, “An Integrated Approach For Simulating Interdependencies,” in *Critical Infrastructure Protection II*, M. Papa and S. Shenoi, Eds., Boston, MA: Springer US, 2008, pp. 229–239. doi: 10.1007/978-0-387-88523-0_17.
- R.J. Murnane, G. Allegri, A. Bushi, J. Dabbeek, H. de Moel, M. Duncan, S. Fraser, C. Galasso, C. Giovando, P. Henshaw, K. Horsburgh, C. Huyck, S. Jenkins, C. Johnson, G. Kamihanda, J. Kijazi, W. Kikwasi, W. Kombe, S. Loughlin, F. Løvholt, A. Masanja, G. Mbongoni, S. Minas, M. Msabi, M. Msechu, H. Mtongori, F. Nadim, M. O’Hara, M. Pagani, E. Phillips, T. Rossetto, R. Rudari, P. Sangana, V. Silva, J. Twigg, G. UHINGA, E. Verrucci, *Data schemas for multiple hazards, exposure and vulnerability*, *Disaster Prevention and Management: An International Journal*. 28 (2019) 752–763. <https://doi.org/10.1108/DPM-09-2019-0293>.
- R.M. Iverson, *Landslide triggering by rain infiltration*, *Water Resour Res*. 36 (2000) 1897–1910. <https://doi.org/10.1029/2000WR900090>.
- R.M. Iverson, *The debris-flow rheology myth*, (2003).
- S. Akkar, H. Sucuoğlu, A. Yakut, *Displacement-Based Fragility Functions for Low- and Mid-rise Ordinary Concrete Buildings*, *Earthquake Spectra*. 21 (2005) 901–927. <https://doi.org/10.1193/1.2084232>.
- S. Armenia, R. Onori, C. Carlini, and G. Tsaples, *Interactive Learning Environments for Crisis Management through a System Dynamics Approach*. 2015.
- S. Bologna, G. Di Costanzo, E. Luijff, and R. Setola, “An Overview of R&D Activities in Europe on Critical Information Infrastructure Protection (CIIP),” in *Critical Information Infrastructures Security*, J. Lopez, Ed., Berlin, Heidelberg: Springer, 2006, pp. 91–102. doi: 10.1007/11962977_8.
- S. Brzev, C. Scawthorn, A.W. Charleson, L. Allen, M. Greene, K. Jaiswal, V. Silva., *GEM building taxonomy version 2.0. GEM Technical Report 2013-02 V1.0.0*, Pavia, Italy, 2013.

- S. Cavallini et al., "A system dynamics framework for modeling critical infrastructure resilience," *IFIP Adv. Inf. Commun. Technol.*, vol. 441, pp. 141–154, Jan. 2014.
- S. de Angeli, B.D. Malamud, L. Rossi, F.E. Taylor, E. Trasforini, R. Rudari, A multi-hazard framework for spatial-temporal impact analysis, *International Journal of Disaster Risk Reduction*. 73 (2022) 102829. <https://doi.org/10.1016/j.ijdrr.2022.102829>.
- S. Lagomarsino, S. Giovinazzi, Macroseismic and mechanical models for the vulnerability and damage assessment of current buildings, *Bulletin of Earthquake Engineering*. (2006). <https://doi.org/10.1007/s10518-006-9024-z>.
- S. M. Rinaldi, J. P. Peerenboom, and T. K. Kelly, "Identifying, understanding, and analyzing critical infrastructure interdependencies," *IEEE Control Syst. Mag.*, vol. 21, no. 6, pp. 11–25, Sept. 2001, doi: 10.1109/37.969131.
- S. Tesfamariam, K. Goda, G. Mondal, Seismic Vulnerability of Reinforced Concrete Frame with Unreinforced Masonry Infill Due to Main Shock–Aftershock Earthquake Sequences, *Earthquake Spectra*. 31 (2015) 1427–1449. <https://doi.org/10.1193/042313EQS111M>.
- S.A. Argyroudis, S.A. Mitoulis, M.G. Winter, A.M. Kaynia, Fragility of transport assets exposed to multiple hazards: State-of-the-art review toward infrastructural resilience, *Reliab Eng Syst Saf*. 191 (2019) 106567. <https://doi.org/10.1016/j.ress.2019.106567>.
- S.A. Argyroudis, S.A. Mitoulis, M.G. Winter, A.M. Kaynia, Fragility of transport assets exposed to multiple hazards: State-of-the-art review toward infrastructural resilience, *Reliab Eng Syst Saf*. 191 (2019) 106567. <https://doi.org/10.1016/j.ress.2019.106567>.
- S.J. Brandenberg, P. Kashighandi, J. Zhang, Y. Huo, M. Zhao, Fragility Functions for Bridges in Liquefaction-Induced Lateral Spreads, *Earthquake Spectra*. 27 (2011) 683–717. <https://doi.org/10.1193/1.3610248>.
- S.P. Stefanidou, E.A. Paraskevopoulos, V.K. Papanikolaou, A.J. Kappos, An online platform for bridge-specific fragility analysis of as-built and retrofitted bridges, *Bulletin of Earthquake Engineering*. 20 (2022) 1717–1737. <https://doi.org/10.1007/s10518-021-01299-3>.
- Silva, C. Yepes-Estrada, J. Dabbeek, L. Martins, S. Brzev (2018). GED4ALL - Global Exposure Database for Multi-Hazard Risk Analysis – Multi-Hazard Exposure Taxonomy. GEM Technical Report 2018-01, GEM Foundation, Pavia, Italy.
- Silva, V., Brzev, S., Scawthorn, C., Yepes, C., Dabbeek, J., & Crowley, H. (2022). A building classification system for multi-hazard risk assessment. *International Journal of Disaster Risk Science*, 13(2), 161-177.
- Simpson Strong-Tie. (2024). Wood construction connectors catalog (C-C-2024). <https://www.strongtie.com/resources/literature/wood-construction-connectors-catalog>
- T. Gerl, H. Kreibich, G. Franco, D. Marechal, K. Schröter, A Review of Flood Loss Models as Basis for Harmonization and Benchmarking, *PLoS One*. 11 (2016) e0159791. <https://doi.org/10.1371/journal.pone.0159791>.
- T. Rossetto, D. D'Ayala, I. Ioannou, A. Meslem, Evaluation of Existing Fragility Curves, in: 2014: pp. 47–93. https://doi.org/10.1007/978-94-007-7872-6_3.
- T. Rossetto, I. Ioannou, D. Grant, Existing Empirical Fragility and Vulnerability Functions: Compendium and Guide for Selection, GEM Technical Report 2015-1, 2015. <https://doi.org/10.13117>.
- T. Rossetto, I. Ioannou, D. Grant, Existing Empirical Fragility and Vulnerability Functions: Compendium and Guide for Selection, GEM Technical Report 2015-1, 2015. <https://doi.org/10.13117>.
- T. Rossetto, I. Ioannu, D. Grant, T. Maqsood, Guidelines for empirical vulnerability assessment, 2014.
- T.L. Saaty, *The analytical hierarchy process*, McGraw-Hill, New York, USA, 1980.

Toitū Te Whenua Land Information New Zealand. (n.d.). LINZ Data Service [Data portal]. Retrieved November 10, 2025, from <https://data.linz.govt.nz/>

Trogrlić, R. Š., Reiter, K., Ciurean, R. L., Gottardo, S., Torresan, S., Daloz, A. S., Ma, L., Padrón Fumero, N., Tatman, S., Hochrainer-Stigler, S., de Ruiter, M. C., Schlumberger, J., Harris, R., García-Gonzalez, S., García-Vaquero, M., Febles Arévalo, T. L., Hernandez-Martin, R., Mendoza-Jimenez, J., Ferrario, D. M., Geurts, D., & Ward, P. J. (2024). Challenges in assessing and managing multi-hazard risks: A European stakeholders perspective. *Environmental Science & Policy*, 157, 103774.

Tupenaite, L., Kanapeckiene, L., Naimaviciene, J., Kaklauskas, A., & Gecys, T. (2023). Timber construction as a solution to climate change: A systematic literature review. *Buildings*, 13(4), 976. <https://doi.org/10.3390/buildings13040976>

U.N. Secretary general, Report of the open-ended intergovernmental expert working group on indicators and terminology relating to disaster risk reduction. *Proceedings of the Seventy-First Session Agenda, Item 19*, 2016.

Ullal A., Estrella X. (2021). Project Survey Report. South Sudan: State-of-the-Art on Flood Resilient Shelters.

United Nations Conference on Environment and Development (UNCED). (1992). Agenda 21: Programme of action for sustainable development. United Nations. Retrieved March 3, 2025, from <https://sustainabledevelopment.un.org/content/documents/Agenda21.pdf>

United Nations International Strategy for Disaster Reduction (UNISDR). (2005). Hyogo Framework for Action 2005–2015: Building the resilience of nations and communities to disasters. United Nations. Retrieved March 3, 2025, from <https://www.unisdr.org/we/inform/publications/1037>

United Nations Office for Disaster Risk Reduction (UNDRR). (2015). Sendai Framework for Disaster Risk Reduction 2015–2030. United Nations. Retrieved March 3, 2025, from <https://www.undrr.org/publication/sendai-framework-disaster-risk-reduction-2015-2030>

V. Silva, H. Crowley, H. Varum, R. Pinho, L. Sousa, Investigation of the characteristics of Portuguese regular moment-frame RC buildings and development of a vulnerability model, *Bulletin of Earthquake Engineering*. 13 (2015) 1455–1490. <https://doi.org/10.1007/s10518-014-9669-y>.

V. Silva, H. Crowley, M. Colombi, Fragility Function Manager Tool, in: 2014: pp. 385–402. https://doi.org/10.1007/978-94-007-7872-6_13.

V. Silva, S. Akkar, J. Baker, P. Bazzurro, J.M. Castro, H. Crowley, M. Dolsek, C. Galasso, S. Lagomarsino, R. Monteiro, D. Perrone, K. Pitilakis, D. Vamvatsikos, Current challenges and future trends in analytical fragility and vulnerability modeling, *Earthquake Spectra*. 35 (2019) 1927–1952. <https://doi.org/10.1193/042418EQS1010>.

V. Silva, S. Brzev, C. Scawthorn, C. Yepes, J. Dabbeek, H. Crowley, A Building Classification System for Multi-hazard Risk Assessment, *International Journal of Disaster Risk Science*. (2022). <https://doi.org/10.1007/s13753-022-00400-x>.

Vacca, P., Àgueda, A., Planas, E., Caballero, D., Pastor, E. (2023). Methodology for the analysis of structural vulnerability of WUI settlements. *Fire Safety Journal*, vol 140. Elsevier. <https://doi.org/10.1016/j.firesaf.2023.103853>

Valdivieso, D., Goldwyn, B., Liel, A. B., Javernick-Will, A., Lopez-Garcia, D., & Guindos, P. (2024). Potential for mitigating hurricane wind impact on informally constructed homes in Puerto Rico under current and future climate scenarios. *International Journal of Disaster Risk Reduction*, 110, 104627. <https://doi.org/10.1016/j.ijdr.2024.104627>

Valdivieso, D., Guindos, P., Montaña, J., & Lopez-Garcia, D. (2023). Experimental investigation of multi-layered strong wood-frame shear walls with nonstructural Type X gypsum wallboard layers under cyclic load. *Engineering Structures*, 282, 115797.

Vázquez-Tarrió, D., Ruiz-Villanueva, V., Garrote, J., Benito, G., Calle, M., Lucía, A., & Díez-Herrero, A. (2024). Effects of sediment transport on flood hazards: Lessons learned and remaining challenges. *Geomorphology*, 446, 108976.

Vázquez-Tarrió, D., Ruiz-Villanueva, V., Garrote, J., Benito, G., Calle, M., Lucía, A., & Díez-Herrero, A. (2024). Effects of sediment transport on flood hazards: Lessons learned and remaining challenges. *Geomorphology*, 446, 108976.

W. Marzocchi, A. Garcia-Aristizabal, P. Gasparini, M.L. Mastellone, A. Di Ruocco, Basic principles of multi-risk assessment: a case study in Italy, *Natural Hazards*. 62 (2012) 551–573. <https://doi.org/10.1007/s11069-012-0092-x>.

Ward, P. J., Daniell, J., Duncan, M., Dunne, A., Hananel, C., Hochrainer-Stigler, S., Tijssen, A., Torresan, S., Ciurean, R., Gill, J. C., Sillmann, J., Couasnon, A., Koks, E., Padrón-Fumero, N., Tatman, S., Tronstad Lund, M., Adesiyun, A., Aerts, J. C. J. H., Alabaster, A., Bulder, B., Campillo Torres, C., Critto, A., Hernández-Martín, R., Machado, M., Mysiak, J., Orth, R., Palomino Antolín, I., Petrescu, E.-C., Reichstein, M., Tiggeloven, T., Van Loon, A. F., Vuong Pham, H., & de Ruiter, M. C. (2022). Invited perspectives: A research agenda towards disaster risk management pathways in multi-(hazard-) risk assessment. *Natural Hazards and Earth System Sciences*, 22(4), 1487–1497.

X. Li, L. Zhang, Y. Hao, P. Zhang, X. Xiong, and Z. Shi, “System dynamics modeling of food-energy-water resource security in a megacity of China: Insights from the case of Beijing,” *J. Clean. Prod.*, vol. 355, p. 131773, June 2022, doi: 10.1016/j.jclepro.2022.131773.

X. Ming, Q. Liang, R. Dawson, X. Xia, J. Hou, A quantitative multi-hazard risk assessment framework for compound flooding considering hazard inter-dependencies and interactions, *J Hydrol (Amst)*. 607 (2022) 127477. <https://doi.org/10.1016/j.jhydrol.2022.127477>.

X. Ming, W. Xu, Y. Li, J. Du, B. Liu, P. Shi, Quantitative multi-hazard risk assessment with vulnerability surface and hazard joint return period, *Stochastic Environmental Research and Risk Assessment*. 29 (2015) 35–44. <https://doi.org/10.1007/s00477-014-0935-y>.

X.-W. Zheng, H.-N. Li, Y.-B. Yang, G. Li, L.-S. Huo, Y. Liu, Damage risk assessment of a high-rise building against multihazard of earthquake and strong wind with recorded data, *Eng Struct*. 200 (2019) 109697. <https://doi.org/10.1016/j.engstruct.2019.109697>.

Y. Li, R. Song, J.W. van de Lindt, Collapse Fragility of Steel Structures Subjected to Earthquake Mainshock-Aftershock Sequences, *Journal of Structural Engineering*. 140 (2014) 04014095. [https://doi.org/10.1061/\(ASCE\)ST.1943-541X.0001019](https://doi.org/10.1061/(ASCE)ST.1943-541X.0001019).

Yepes-Estrada, C., Calderon, A., Costa, C., Crowley, H., Dabbeek, J., Hoyos, M., Martins, L., Paul, N., Rao, A., Silva, V. (2023). Global Building Exposure Model for Earthquake Risk Assessment. *Earthquake Spectra*. doi:10.1177/87552930231194048

Yi, S. R., Taflanidis, A. A., Movaghar, P. T., & Galasso, C. (2025). Impact of structural information fidelity on reduced-order model development for regional risk assessment. *Structural Safety*, 116, 102602.

Zaghi, A. E., Padgett, J. E., Bruneau, M., Barbato, M., Li, Y., Mitrani-Reiser, J., & McBride, A. (2016). Establishing common nomenclature, characterizing the problem, and identifying future opportunities in multihazard design. *Journal of Structural Engineering*, 142(12), H2516001.

“Critical infrastructure dependencies,” *Int J Crit Infrastruct Prot*, vol. 8, no. C, pp. 16–23, Jan. 2015, doi: 10.1016/j.ijcip.2014.12.004.

Mitigating environmental disruptive events using people-centric predictive digital technologies to improve disaster and climate resilience



www.minorityreport-project.eu/en/



@Minority Report



@EU_MinorityRep



@MinorityReport_EU



This project has received funding from the European Union's Horizon Europe research and innovation programme under the grant agreement number 101147385. Views and opinions expressed are however those of the author(s) only and do not necessarily reflect those of the European Union or CINEA. Neither the European Union nor the granting authority can be held responsible for them.

In Confidence